Synthesis of Ruthenium Complexes with "PNR" (R = H, Me) Ligands and Their Role in the Electrocatalytic and Photocatalytic Reactions

Randa Jaloul

Thesis submitted to the University of Ottawa

In partial fulfillment of the requirements

For the degree of

Master of Science in Chemistry

Department of Chemistry and Biomolecular Science

Faculty of Science

University of Ottawa

uOttawa

L'Université canadienne
Canada's university

Abstract

Repurposing CO_2 in the atmosphere is a key strategy to combat global warming and reduce fossil fuel capture conditions. Molecular catalysts (metal complex catalysts) can be precisely designed at the molecular level to accelerate CO_2 conversion reactions. Different classes of metal complexes catalyzed the reduction of CO_2 with astonishing efficiency and selectivity. Recently, numerous semiconductor photocatalysts were designed in heterostructure systems, which are composed of complex components of semiconductor and metal. Homogeneous metal complexes can be employed to study reaction processes more straightforwardly than the heterogeneous method.

This study focuses mainly on proposed mechanisms driving the photochemical reduction of CO_2 initiated by ruthenium complexes. Ruthenium complexes mainly produce HCOOH and H_2, and the product selectivity is highly dependent on the reaction conditions. This study investigated complexes of ruthenium with bidentate phosphino-aminopyridine ligands for their photocatalytic activity. Catalysis was carried out using as solvent, 4 mL of a solution of this complex in N, N-dimethylacetamide (DMA), with $[Ru(bpy)_3]^{2+}$ as a photosensitizer, and 1 mL of triethanolamine (TEOA) as a sacrificial agent in the presence of carbon dioxide. LEDs (1050 mW, 700 mA, 3.4 x 10^{-8} mol photons/sec) at 450 nm wavelength were used to irradiate the reaction mixture with visible light.

The results show that the photocatalytic activity is greatly enhanced by the presence of the ligand group. NMR spectroscopy and gas chromatography confirmed the generation of carbon monoxide (CO), hydrogen (H_2), and formic acid (HCOOH) via the photocatalytic reduction of CO_2 catalyzed by ruthenium complexes.

Graphical Abstract: Ru-based complexes synthesized with various substituents on the N-(diphenylphosphino)-2-aminopyridines ligand were investigated for their behaviour in photocatalytic CO_2 reduction.

Photocatalytic CO_2 Reduction

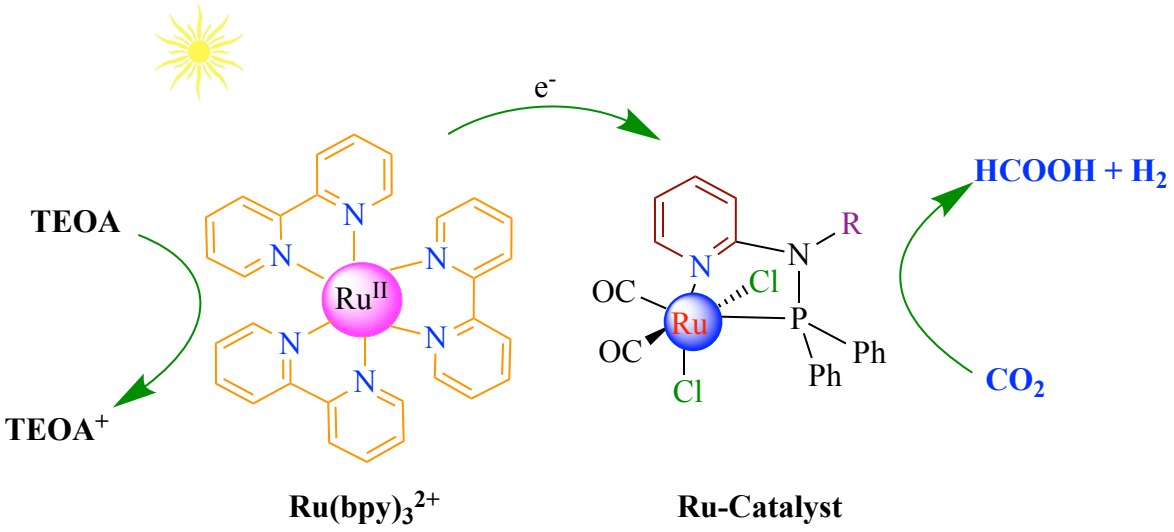

$Ru(bpy)_3^{2+}$ **Ru-Catalyst**

Acknowledgments

First of all, I render maximum respect and thanks to Allah, who has provided me with the strength, patience, and direction I ever needed in life and assisted me in confronting all the challenges I faced while acquiring my academic education.

I would like to express my greatest and sincerest thanks to my supervisor, Professor Darrin Richeson, who exhibited extraordinary support, perceptive direction, and boundless patience while working on the research and writing of the thesis. Your mentoring has been an enormous source of motivational drive and inspiration, for which I am truly appreciative of the knowledge, encouragement, and self-confidence transmitted to me through your mentorship. This work's completion wouldn't have been possible without your dedication and belief in me as an individual capable of developing research.

I am also sincerely thankful to all the members in the Richeson group (the previous and current members) for their friendship, collaboration, and helpful discussions, which made the journey more enjoyable and insightful, especially Dr. Yasmin Hameed, who is the person I cannot forget for her wonderful support when I needed it during my life in Canada. In addition, many thanks to Dr. Jeff for the help in the X-ray structure determination, Dr. Sharon for her help in the mass spectra and GC analysis, and Dr. Wendy for her help in the electrochemistry data and for their cooperation and beneficial deliberations, without which the journey would have been less pleasant and enriching. My special thanks go to the members of my thesis advisory committee for their able criticisms: Prof. Abdelhamid Sayari and Prof. Paul Mayer for sharing their knowledge and direction during the most critical phases of my research.

I am also interested in extending special appreciation to the Department of Chemistry and the Graduate Studies Administration of the University of Ottawa for granting me the privilege of pursuing my academic course and developing research capabilities. I also wish to thank the Petroleum Research Center in Libya sincerely for enabling me to continue with my academic work and also for their all-around help and support in all ways possible.

I present my deep appreciation to my respected friend Wesal Nabbal. Your encouragement, especially during rough times, in addition to the help and moral support of my honorable friend Eman Elmselati, was invaluable to me. The kindness, generosity, and confidence exhibited were the keys to the success of this work.

I am also very much indebted to my cherished family—indeed, to my parents—for their selfless affection, daily prayer, and sacrifices, without which my development to what I am would have been vastly influenced. I also wish to thank my honourable father in special appreciation for his continuous encouragement, and I wish with all honesty for his soul to find peace; Allah, God, grant him eternal rest. Lastly, I want to say my deepest appreciation to my wonderful siblings: Mohammad, Ahmed, Ghada, and Nouran. Being present in my life is the best appreciation, and their memory I'll take with me all through life. Years of encouragement and support have been invaluable. My devoted family is ever present with encouragement from a distance, always in spirit in my heart of mine.

My greatest thanks go to my true love, my life, my best friend ever, and my husband, Haitham, for patience, love, and encouragement, and to my daughters and son, Hedaya, Hadeer, Hatoon, and Omar, who are my best motivations and joys in life.

I would like to thank all those distant members of my family and friends who have ever encouraged me with affection from afar, always a strength.

This expedition has been through an infinite number of challenges and lessons learned, personal and otherwise. This great success wouldn't have been achieved without the encouragement, kindness, and help from the aforementioned people. I am willing to express all my gratitude to every one of them individually with all of my heart for their services to this venture and their help to achieve this dream.

Table of Contents

List of Figures

List of Schemes

List of Tables

List of Abbreviations

AA	Ascorbic acid
BNAH	1-Benzyl-1,4-dihydronicotinamide
Cat	Catalyst
CH_3CN	Acetonitrile
CS	Catalyst Selectivity
CV	Cyclic Voltammetry
DFT	Density Functional Theory
DMA	N, N′-dimethylacetamide
DMF	N, N′-dimethylformamide
E°	Standard potential
GC	Gas Chromatograph
GC-TCD	Gas Chromatograph with Thermal-Conductivity Detector
HOMO	Highest Occupied Molecular Orbital
IC	Internal Conversion
iPr	Isopropyl
ISC	Intersystem Crossing
LMCT	Ligand-to-Metal Charge Transfer
LUMO	Lowest Unoccupied Molecular Orbital
mM	Millimolar
Me	Methyl
MLCT	Metal-to-Ligand Charge Transfer
NMR	Nuclear Magnetic Resonance
pH	Potential of Hydrogen
PS	Photosensitizer
S	Solvent
SCE	Standard Calomel Electrode
SC-XRD	Single-Crystal X-ray Diffraction
SD	Sacrificial Electron Donor
SHE	Standard Hydrogen Electrode

t	Time
TEA	Triethylamine
TEOA	Triethanolamine
TON	Turnover Number
TOF	Turnover frequency
UV	Ultraviolet
V	Volt
XRD	X-ray Diffraction
Φ	Quantum yield

Chapter 1: Photochemical Techniques of Catalytic Carbon Dioxide Reduction with Homogeneous Transition-Metal Complexes

1.1 Introduction

A major global issue today is the simultaneous environmental degradation and energy supply scarcity crisis. Energy from fossil fuels still provides the dominant percentage of the world's energy supply, but its expanded use to provide for growing energy needs has detrimental environmental effects. Rising levels of the greenhouse gas carbon dioxide in the world's atmosphere are to blame for global warming and have consequently elicited various means of lowering emissions.[1,2]

Global warming refers to the gradual increase in Earth's average surface temperature, largely driven by human activities, particularly the emission of greenhouse gases such as carbon dioxide, methane, and nitrous oxide. A boost to global warming results from the trapping of heat within the atmosphere due to such emissions. Ways to cut down on greenhouse gas emissions include reforestation, making buildings and industries energy-efficient, investing in renewable energy, and signing on to global accords such as the Paris Agreement to mitigate the impact of climate change and slow rising temperatures.[1, 2-4]

Photocatalytic CO_2 reduction reactions, based on an artificial photosynthetic system, involve a photosensitizer that absorbs sunlight and excites a high-energy electron to a catalyst site for CO_2 reduction and converts it to useful chemical fuels, mostly hydrogen or other fuels, to make the processes environmentally friendly. Such approaches include the development of photocatalysts for the splitting of water to give hydrogen and oxygen or the conversion of CO_2 to organometallic species to be used as electron donors. Chapter 1 of the thesis provides an introduction to the study object and provides the necessary background information. In Chapter 2, the details and characterization of all the ligands and complexes used in the present work will be discussed. In Chapter 3, the experimental results, along with the respective photochemical processes, will be discussed.

A relevant methodology for reaching a carbon-neutral world is renewable energy utilization and the creation of useful commodities from CO_2 as substitutes for fossil fuels. A number of approaches have emerged for converting CO_2 to renewable commodities, and they are of three major categories: chemical, electrochemical, and photochemical processes. In chemical processes,

if hydrogen gas reacts with CO_2 under appropriate experimental conditions, different commodities like CO, CH_4, and HCOOH are formed. Some of the commodities, however, require an active suitable catalyst to form quickly. A serious shortcoming of the chemical process is its requirement for high temperatures of approximately 150°C to effectively drive the reaction, a condition that is bound to destroy the catalyst's structure, for example, in the synthesis of methanol.[5-9]

The reduction of carbon dioxide (CO_2) is of great importance for environmental and energy applications. The different avenues to convert CO_2 to value-added products employing electrochemical and photochemical means are, for example, ethylene and methanol, as shown in Fig. 1.1.[10]. Electrochemical reduction utilizes an electric current to reduce the CO_2 to chemical commodities in the form of carbon monoxide, methane, or methanol.

When we do a photochemical reduction of CO_2, we employ light to assist the reaction to attain the same outcome.[2,11]

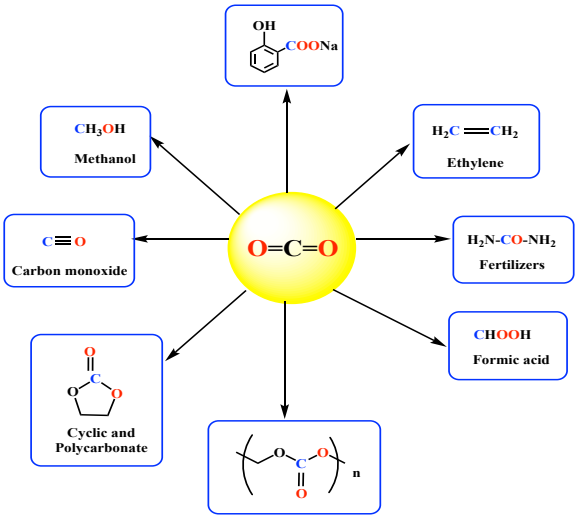

Figure 1.1. *Conversion of CO_2 into valuable commodity chemicals.*[10]

Formic acid (HCOOH) is a very important chemical with extensive applications in the chemical industry as well as the renewable energy sector.[5] In industrial applications, formic acid is used as a preservative and antibacterial agent in livestock feed, in leather processing, textile dyeing, and rubber coagulation. Formic acid serves as a chemical intermediate for ester formation and formamide formation. In renewable energy, formic acid also finds use as a material for storing hydrogen. Owing to its non-toxicity, being simpler to biodegrade, and being less harmful to the environment than other acids, formic acid may also be used as a premium fuel for formic acid fuel

cell technology. Formic acid also finds use as a major end-product material for photocatalytic and/or electrocatalytic CO_2 reduction for carbon-neutral energy generation.[7,11,12]

This work, in particular, deals with successful efforts at carbon dioxide reduction. The goal is to design efficient, highly selective, sustainable carbon dioxide conversion systems. This will be realized by improvements in catalyst design, reaction optimization, and light-harvesting methods. It describes the photochemistry behind it and looks into improving the performance and stability of catalysts.

1.2. Thermodynamics of CO_2 Reduction

Over the last couple of decades, several groups in the clean energy community have been studying electrocatalytic CO_2 reduction methods.[13,14] The strong thermodynamic stability of CO_2 leads to high barriers to reductive transformation due to its two strong C=O double bonds and fully oxidized carbon (+4), making electron addition thermodynamically unfavorable. Thus, very stable molecules (CO, formate, formaldehyde, methanol, methane, etc.) are usually produced via proton-coupled multielectron cascades (Equations (1–6), Table 1.1).[15,16]

In contrast, the single electron reduction of CO_2 requires relatively higher potential energy (approximately -1.9 V vs. NHE) due to the large transformation of energy from linear to the best radical anion state (Equation (7), Table 1.1). Additionally, the kinetics of the CO_2 reduction reaction is complex, having a multi-step mechanism, and often give a mixture of the products; see Table 1.1. The reaction rates are still very low, even in the presence of electrocatalysts. The low catalytic activity, selectivity, and stability of the widely used electrocatalysts hinder the practical application and technological commercialization of the electrocatalytic CO_2 conversion systems.[15, 17]

Figure 1.2 and Table 1.1 show the C1 compounds obtainable from the conversion of carbon dioxide. Accordingly, various products can be synthesized based on the quantity of electrons transferred to carbon dioxide: 2, 4, 6, and 8, giving carbon monoxide (CO) or formic acid (HCOOH), formaldehyde (H_2CO), methanol (CH_3OH), or methane (CH_4), respectively.

Table 1.1. Selected standard potentials of CO_2 reduction in aqueous solutions.[3,15]

Equation Number	Thermodynamic Reactions	$E°$ (V)
Equation (1)	$CO_2 + 2H^+ + 2e^- \rightleftharpoons CO(g) + H_2O$	−0.53
Equation (2)	$CO_2 + 2H^+ + 2e^- \rightleftharpoons HCOOH$	−0.61
Equation (3)	$CO_2 + 4H^+ + 4e^- \rightleftharpoons H_2CO + H_2O$	−0.48
Equation (4)	$CO_2 + 6H^+ + 6e^- \rightleftharpoons CH_3OH + H_2O$	−0.38
Equation (5)	$CO_2 + 8H^+ + 8e^- \rightleftharpoons CH_4 + 2H_2O$	−0.24
Equation (6)	$2CO_2 + 12H^+ + 12e^- \rightleftharpoons C_2H_4 + 4H_2O$	−0.34
Equation (7)	$CO_2 + e^- \rightleftharpoons CO_2^{\bullet -}$	−1.90

[15] pH = 7 in aqueous solution vs. standard hydrogen electrode (SHE), 25 °C, 1 atmosphere gas pressure, and 1 M for other solutes.

The carbon atom of CO_2 is already in the fully oxidized state and cannot be further oxidized. The reduction of carbon dioxide is possible for a variety of products, because adding electrons and protons can convert it into lower-oxidation-state carbon products such as CO, formate, methanol, or methane, as shown in Figure 1.2. These reductions are energetically uphill and require significant input of energy to overcome the strong C=O bonds and the high activation barrier, but they are chemically possible when sufficient reducing power, catalysts, or light energy is provided.[3]

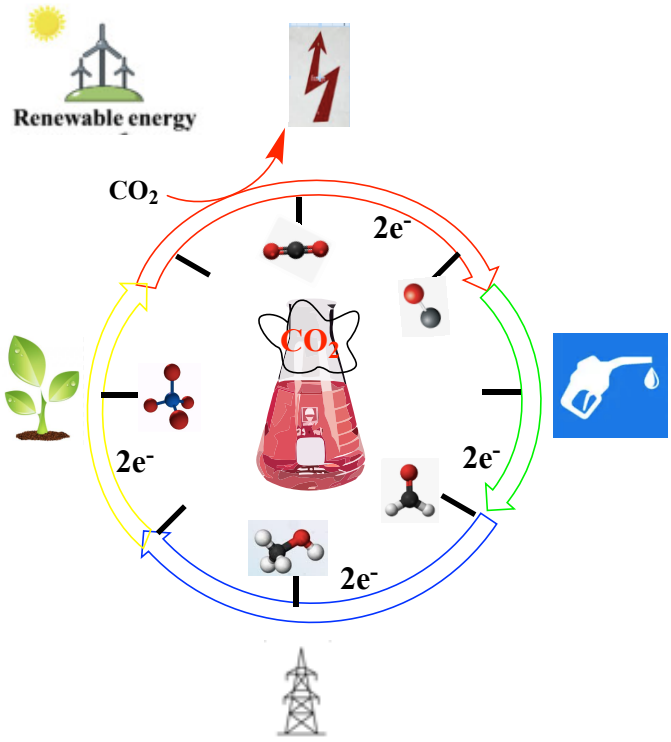

Figure 1.2. *C1 reduction products from CO_2 depending on the number of electrons transferred ("the CO_2 clock").*[3]

Transition metal complexes that have partially filled d-orbitals are supposed to take part in the coupling of CO_2 via the generation of reactive intermediates. Aresta and Nobile presented a crystal structure in 1975, where CO_2 was coordinated to a transition metal complex.[15] It was useful in illustrating the positive features of the expansion into transition elements as electrocatalysts to provide CO_2 reduction, adding to the diversity of the η^2-bidentate series, such as the carbon and one of the oxygen atoms of the CO_2 molecule, where the greatest buckling of the CO_2 structure occurred. Fewer transition elements and compounds are representative of mainstream thought as electrocatalysts.[15,16] One-electron reduction of CO_2 to $CO_2^{\bullet-}$ is a thermodynamically uphill process owing to the stability of CO_2 in the oxidized state and the fact that it requires a lot of energy, hence large input energy, usually from photochemical reactions.

1.3 Reduction of CO_2 by Photochemistry

Over the past decades, photochemical reduction of carbon dioxide has attracted research interest, further motivated by the general call for a sustainable energy approach and the oil crises that raised people's attention to energy security and environmental concerns.[18] The interest in researching the reduction of carbon dioxide comes from the importance of trying to alleviate the effects of global

warming due to the environmental factors of CO_2. This approach transforms CO_2 from a greenhouse gas into valuable fuels and chemicals through sunlight exposure to establish a sustainable carbon reduction method while generating renewable energy resources. The system operates under mild conditions while drawing upon renewable energy sources to replicate natural photosynthesis and adhere to green chemistry principles. The scientific quest of CO_2 catalyzing and selective reduction triggers continued developments in both basic and catalyst research. The exploration into this area started with early experiments during the 1970s and 1980s and has developed tremendously over the decades. The continuous quest for effective carbon conversion techniques has broadened this research area to involve diverse catalysts and their respective applications.[18,19]

Photocatalytic CO_2 reduction is one of the most important tasks in developing artificial photosynthetic apparatus and solar fuel devices, which can reduce the consumption of fossil fuels and slow down global warming.

Researchers have carried out extensive studies into the carbon dioxide mechanisms with homogeneous catalysts of transition metal complexes. Extensive research has documented general knowledge about how the carbon dioxide reduction mechanism functions. The process requires four essential stages, which include photon absorption by a photosensitizer, followed by charge separation to generate electron-hole pairs and then transferring electrons to the catalyst that initiates product conversion. The majority of photocatalytic carbon dioxide reduction systems contain three main components: a sacrificial electron donor (SD), a photosensitizer for light absorption and electron transfer facilitation, and a catalyst (Cat) which activates CO_2 to start the reduction reaction.

1.3.1 Photocatalytic Systems in CO_2 Reduction

The term "photocatalysis" has two words: "photo" and "catalysis." A photo refers to light, which is the primary required energy input of the reaction. Catalysis refers to the action of a substance during the chemical transformation of the reactants to alter the rate of the reaction without being used up in the process.[23]

Photocatalytic carbon dioxide reduction is an effective solar-powered method that necessitates no supplementary energy and has no ecological repercussions, as the gas may be transformed into

high-value goods. Solar radiation supplies the substantial activation energy required to decrease the very stable carbon dioxide.[2]

In the CO_2 photoreduction system, the reaction mixture will typically include a catalyst, a photosensitizer, a sacrificial electron donor, and a solvent. The reaction mixture will then be irradiated using a light source defined by its emission wavelength and photon flux/intensity.

The two significant components of the CO_2 photoreduction reaction are the photosensitizer and the catalyst. The photosensitizer absorbs a photon, increasing to an excited state, then using this energy to facilitate a reaction. The Ru complex, $[Ru(bpy)_3]^{2+}$, is extensively used as a photosensitizer since its structural and electronic features provide an ideal balance of photophysical and redox properties and prolonged excited-state lifespan.

A fundamental mechanism of the photocatalytic reaction describes the character of such reactions and how they occur. The sections to follow will thus briefly sketch the overall processes of the established photocatalytic reduction of CO_2.[23,24] The catalyst component is the centrepiece of the findings and research presented in this thesis.

The generic mechanism of the CO_2 reduction reaction using molecular catalysts:

In standard photocatalytic procedures, there is a sequence of important phases following one another, as explained below:

$$PS + h\nu \rightarrow PS^* \quad (8)$$

$$PS^* + D \rightarrow PS^{\bullet -} + D^{\bullet +} \quad (9)$$

$$PS^{\bullet -} + Cat \rightarrow PS + Cat^{-} \quad (10)$$

$$Cat^{-} + CO_2 \rightarrow Cat + products \quad (11)$$

In photochemistry, the transfer of electrons is an indirect phenomenon induced by light absorption. As the radiation is absorbed by the photosensitizer (PS), the electron is promoted from the ground state to an excited state of higher energy, thereby forming the excited state (PS*), (eq. 8), which is different in nature from the ground state. It has a higher electron affinity and lower electron potential and hence can function as a more effective oxidizing and reducing agent than the ground state (PS). The photosensitizer in its excited state (PS*) must have a long enough lifetime to enable

the occurrence of subsequent electron transfer reactions, as electron transfer requires time for the excited PS* to meet and interact with an appropriate electron acceptor or donor. It is required that the excited state does not revert quickly to the ground state via fluorescence or non-radiative relaxation, as this would inhibit electron transfer. Excited-state long lifetimes increase the possibility that PS* can undergo electron transfer, which is a requirement for photocatalytic reactions like CO_2 reduction and hydrogen evolution. This is usually done through intersystem crossing (ISC), which facilitates conversion from the initially formed singlet excited state, following photon absorption, into a comparatively stable triplet excited state. From this triplet state, several deactivation processes can occur, such as energy transfer, oxidative quenching, or reductive quenching, as shown in Scheme 1.1. In reductive quenching (Scheme 1.1a), PS* is a strong oxidant that abstracts one electron from the sacrificial donor (D) and thereby oxidizes (D). This results in the formation of reduced photosensitizer ($PS^{\bullet -}$), which is a stronger reducing agent than either PS or PS*. If the redox potential of PS^- is more negative (lower) than that of the catalyst, then PS^- can reduce the catalyst and regenerate the ground state of the photosensitizer.

The reduced catalyst is then able to reduce CO_2. Conversely, in oxidative quenching (Scheme 1.1.b), PS* must be a sufficiently good reductant to reduce the catalyst directly. The oxidized photosensitizer (PS^+) is then regenerated by accepting electrons from the sacrificial donor (SD) to close the cycle.[14,21,25]

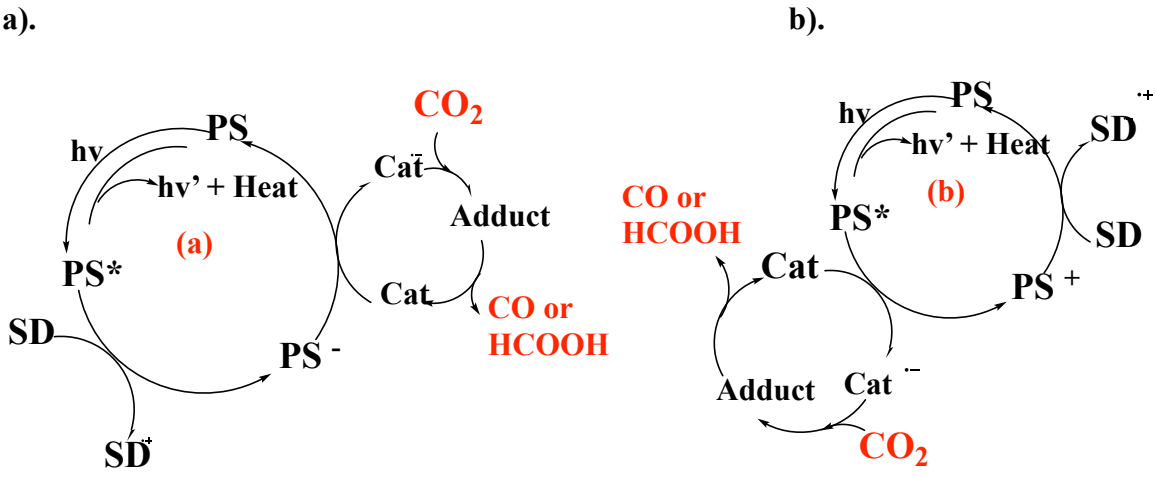

Scheme 1.1. *Two possible mechanisms of deactivation of the photosensitizer are: (a) by reducing deactivation and (b) by oxidizing deactivation.[21] Produced from reference number 21 with permission by the European Journal of Inorganic Chemistry*

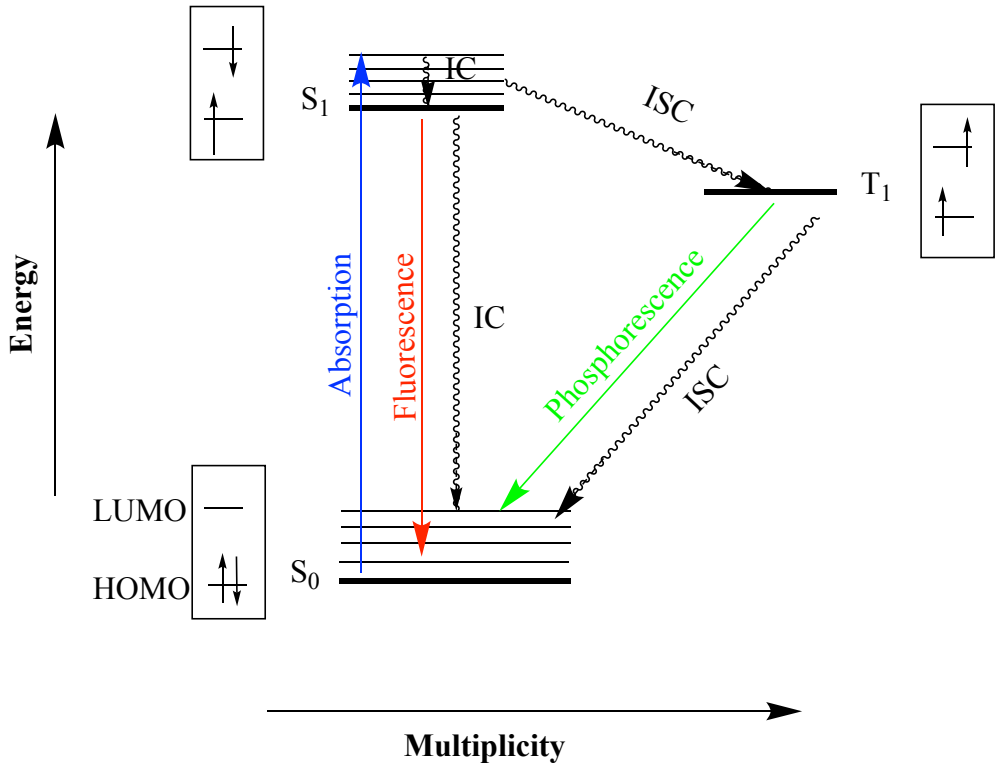

Figure 1.3. *Jablonski diagram alongside the orbital occupancy and energy levels.*[26]

Figure 1.3. A Jablonski diagram shows the electronic and vibrational energy levels of molecules (especially photosensitizers) in photochemistry and photophysics. It explains emission, absorption, and other non-radiative transitions. The Jablonski diagram shows that the lowest energy level of a molecule (HOMO) corresponds to the singlet ground state (S_0). Upon absorption of a photon by a photosensitizer, the molecule is excited to the first excited singlet state (S_1). Higher singlet states like (S_2) may be accessed in the very early stages of excitation, but molecules tend to settle in (S_1) via internal conversion (IC). Spin-orbit coupling can relocate molecules from the excited singlet state (S_1) to the triplet state (T_1) during intersystem crossing (ISC). In the triplet state, the lifetime is orders of magnitude longer than that of a singlet one, approximately 0.6-1.0 μs in solution at room temperature, depending on solvent and conditions; this has less energy than the singlet state. After relaxing non-radiatively to the lowest vibration level (S_1), the molecule can produce a photon (fluorescence), where the downward arrow indicates the step back to vibration (S_0). Another downward arrow, showing the triplet state (T_1) returning to the ground state (S_0), indicates phosphorescence, a process that takes comparatively lower energy and frequently occurs over intervals longer than the fluorescent return transfer. Horizontal or slightly bent internal conversion (IC) and intersystem crossing (ISC) arrows indicate energy loss and non-photonic emission.[27-29]

For instance, longer lifetime excited states (e.g., triplet states) tend to exhibit higher reactivity in photocatalysis. This aspect enables longer interaction time with substrates or other reactants and therefore enables a vast array of reactions similarly recognized to be initiated through energy or electron transfer processes. This property is essential in the context of the design of effective photocatalytic systems because it helps to optimize the conditions in which the energy is absorbed by the target material, transferred, and then used for chemical transformations.[30,31]

1.3.2 Types of Catalysts for Photocatalytic CO_2 Reduction

As explained above, a homogeneous photocatalytic system typically comprises a photosensitizer and a catalyst. Through these two components, it is classified into type I and type II systems. In the type I system, the photosensitizer and catalyst are two separate entities and mixed in solution to form the photocatalytic system. In contrast, type II systems consist of a single molecular entity that performs both the light absorption and catalytic functions. The following section will provide a comprehensive comparison of these two systems.

1.3.2.1 Type I Photocatalyst System (Multi-Component System)

Type I photocatalytic CO_2 reduction entails a catalyst and a photosensitizer that cooperate in light energy to induce the reductive transformation of CO_2 into valuable products. This system enhances the reaction's efficacy and selectivity by separating the photosensitizer's roles from the catalyst. The excited state catalyst directly transfers charge to the reactants, and as a result, there is no extra need to add an electron source or acceptor, sometimes called a hole scavenger, when it is a type I photocatalyst.[6,15, 32-35]

As discussed above, effective photocatalysts for the two-electron reduction of CO_2 need to involve the inclusion of a photosensitizing unit that promotes photoinduced one-electron transfer, along with a catalytic unit that activates CO_2 and allows two electrons to be passed on. Scheme 1.2 illustrates chemical structures and abbreviations for the two-component systems, in which the two functions are achieved by separate molecules.[36]

Ruthenium (II) Diimine Photosensitizers

The photosensitizers must also possess long-lived excited states and stability in both the oxidized and reduced forms. Photosensitizers need to have a long-lived excited state and be stable under oxidation and reduction conditions. The most common photosensitizer, $[Ru(bpy)_3]^{2+}$, has strong visible-light absorption and a long excited-state lifetime of the ^{3}MLCT pf of approximately 1 μs. Moreover, the one-electron reduced and oxidized forms $[Ru^{III}(bpy)_3]^{3+}$ and $[(bpy)Ru^{II}(bpy)_2]^{2+}$ are comparatively stable. As noted earlier, effective photocatalysts for the two-electron reduction of CO_2 need to be made up of a component that enhances light absorption in order to enable one-electron transfer and another component that facilitates the activation of CO_2 to enable two-electron transfer.[36] Several photosensitizers can be employed in photocatalysis reactions. They range from transition metal complexes, i.e., iridium and ruthenium complexes, organic dyes, as indicated in Scheme 1.2, and ruthenium catalysts, as indicated in Scheme 1.3. Their capacity to transfer electrons or energy and their capacity to absorb specific wavelengths to trigger the catalysis reaction is the ground on which they are classified.[6]

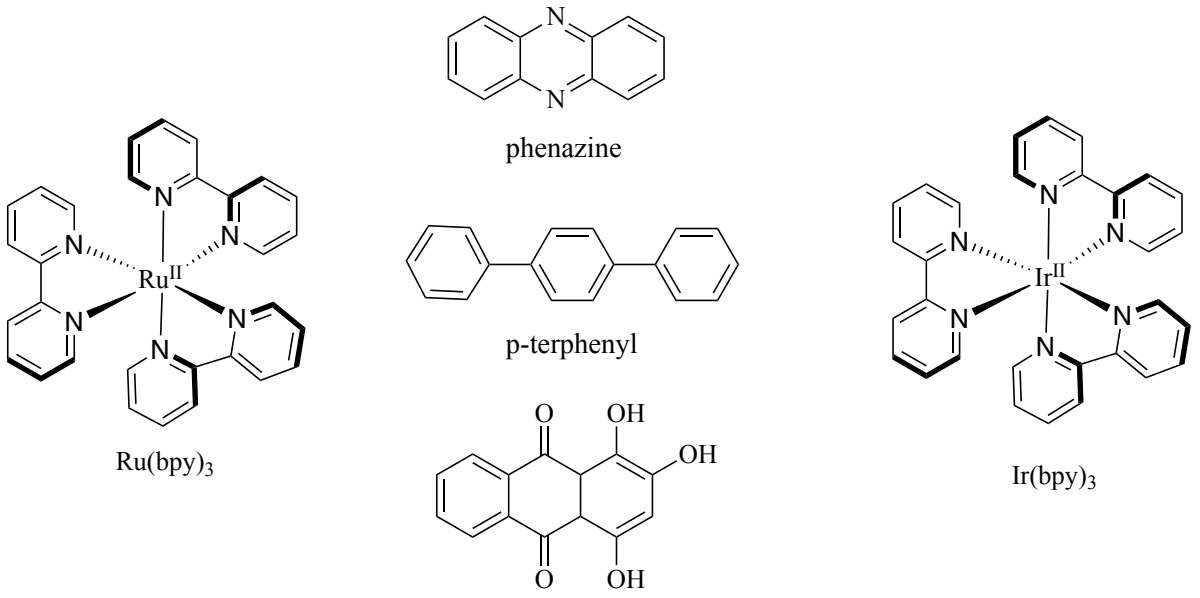

Scheme 1.2. *Various inorganic complexes and organic molecules are used as photosensitizers in multi-component systems.*[36,43]

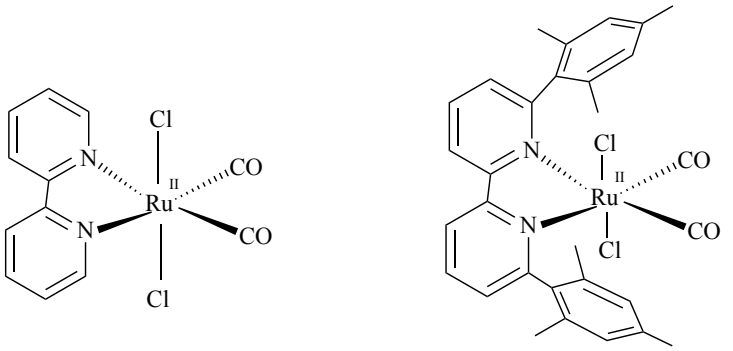

$[Ru(bpy)(CO)_2Cl]_2$ trans(Cl)–$Ru(6Mes\text{-}bpy)(CO)_2Cl_2$

Scheme 1.3. *The structure of some of the Ru(II) catalysts.*[20]

1.3.2.2 Type II Photocatalyst System (Single-Component Systems)

A Type II system occurs when light is absorbed by one compound that acts as a photosensitizer and as a homogeneous catalyst. This photocatalytic PScat absorbs light and produces an excited state PScat*, which will generally result in an electron transition from the highest occupied molecular orbital (HOMO) to the lowest unoccupied molecular orbital (LUMO).[37] The active state of the photocatalytic $PScat^-$ will thereafter be generated by reductively quenching the excited state (D). Subsequently, it is able to directly react with CO_2 and convert it to the respective products. The general type II catalytic photocatalytic process is shown in the following equations and **Scheme 1.4**. [6,15,32,33,34,37]

$$PScat + h\nu \rightarrow PScat^* \quad (12)$$

$$PScat^* + D \rightarrow PScat^- + D^{\bullet+} \quad (13)$$

$$PScat^- + CO_2 \rightarrow \rightarrow PScat + Products \quad (14)$$

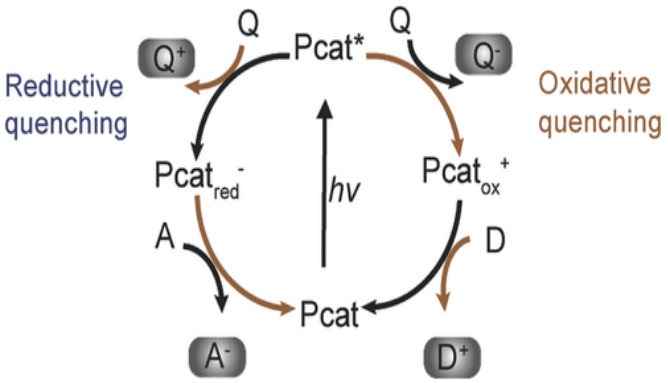

Scheme 1.4. *Photoredox catalysis by a homogeneous photocatalyst. The oxidation steps are depicted on the right; the reduction steps are shown on the left. Pcat: photocatalyst, Q: quencher, D: donor, A: acceptor.*[37] *Reproduced from reference number 37 with permission by Advanced Energy Materials*

.

The first report of the use of a rhenium complex as a photocatalyst for CO_2 reduction was made by Lehn et al.[33] A solution containing fac-Re(bpy)$(CO)_3$Cl and a sacrificial donor, triethanolamine (TEOA), was irradiated using > 400-nm light to produce CO efficiently and selectively. Furthermore, this Re(I) complex can function as a Type II system by acting as both a catalyst and a photosensitizer for CO_2. The product selectivity was very high, and little HCOOH and H_2 were detected. The quantum yield for CO formation was 0.14, the highest efficiency for CO_2 reduction at the time. The chemical structure of the Re(bpy)$(CO)_3$Cl complex is shown below in **Scheme 1.5**.[35,38,39]

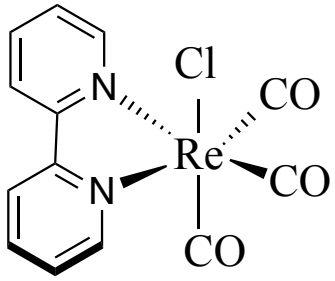

Scheme 1.5. *The structure of [ReI(bpy)$(CO)_3$Cl] complex.*[33] *Reproduced from reference number 33 with permission by the Accounts of Chemical Research.*

1.4 The Components Typically Used in Photocatalytic CO_2 Reduction Systems and Performance Parameters

Typically, a photocatalytic CO_2 reduction process comprises a photosensitizer (PS), which is required to harvest solar light and convert it into chemical potential, i.e., reductive or oxidative potential. A catalyst (Cat) facilitates a photochemical reaction without being consumed or irreversibly changed by the reaction. A sacrificial electron donor (SD) reagent supplies electrons as needed by PS. The reaction mixture is consequently irradiated by light from a light source, characterized by emission wavelength and photon flux/intensity.[40]

Parameters like catalytic selectivity (CS), quantum yield (Φ), turnover number (TON), and turnover frequency (TOF) have been studied. The results and observations of these components and parameters will be further discussed in this thesis.

1.4.1 Redox Photosensitizer (PS)

Photosensitizers are molecules capable of strongly absorbing light of chosen wavelengths, enabling the conversion of this light energy into useful products.

While, in the photosensitized reaction, there exist two disparate mechanisms of initiating the reactions, i.e., reductive quenching, where the excited photosensitizer (PS*) is reduced by the donor (D), thereby functioning as a one-electron reductant (OERS), and oxidative quenching, in which PS* gets oxidatively quenched by Cat or a mediator, which further transfers electrons to Cat, as seen in Scheme 1.6.[6,23,41,42]

The majority of the reported photocatalytic reactions employ transition metal complexes having coupled systems involving a redox photosensitizer (PS) system, transferring one electron after light absorption from a reductant (D) to a catalyst (Cat), and Cat receives the electron from the PS, "accumulating" two electrons to bring them to an oxidized CO_2 molecule to produce CO and/or HCOOH.[6]

Either process can effectively achieve continuous electron flow to sustain photocatalytic activity. Reductive and oxidative quenching are distinct processes involving specific redox potentials of the component involved. The design of effective electronic structures in photocatalysts is important for maximizing potential in CO_2 reduction and other photo-driven processes, and understanding these quenching pathways can provide unique insights. **Scheme 1.6** displays both oxidative and reductive quenching pathways.[41,42]

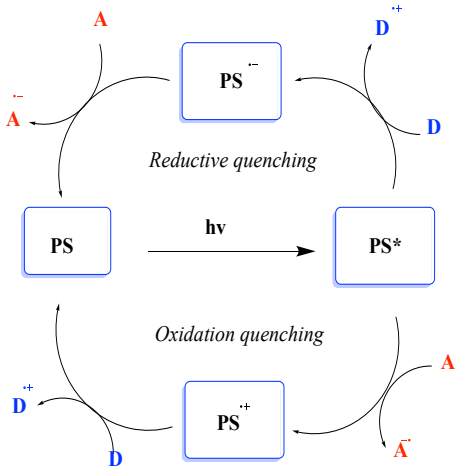

Scheme 1.6. *Photoinduced Electron Transfer Reactions of Photosensitizers.*[42]

Choosing a suitable photosensitizer requires some careful thought to make sure it absorbs light properly and initiates the required chemical changes. Some important factors deserve attention in this endeavor:

1. The photosensitizer must efficiently absorb light in the region of the electromagnetic spectrum required, preferably in the visible region.
2. High quantum yield implies efficient use of absorbed photons as chemical energy or reactions.
3. An ideally timed duration of an excited state allows enough time for the photosensitizer to pass on energy or electrons to nearby molecules.
4. The photosensitizer must be resistant to photobleaching and retain its structure and function throughout numerous cycles of excitation and reaction.
5. The redox potentials should be appropriate for electron transfer to the desired catalysts or substrates without causing decomposition or undesirable side reactions.
6. The photosensitizer must be capable of returning to its ground state with minimal or no loss of activity or alteration of its characteristics.[23,41,42]

Tris(2,2′-bipyridine) ruthenium (II) complex, abbreviated as $[Ru(bpy)_3]^{2+}$, is perhaps the most used photosensitizer in homogeneous photocatalytic reactions, particularly in the reduction of CO_2.

In this thesis, $[Ru(bpy)_3]^{2+}$ is employed as a photosensitizer, and that is the most common species used in such systems. $[Ru(bpy)_3]^{2+}$ has acceptable stability toward light irradiation and with various solvents and can be reused over multiple reaction cycles with minimal degradation. The excited state of $[Ru(bpy)_3]^{2+}$ has a relatively long lifetime, providing ample time for the complex

to interact with electron donors and catalysts. The tris(2,2′-bipyridine) ruthenium (II) photosensitizer structure is presented in the following **Scheme 1.7**.[32]

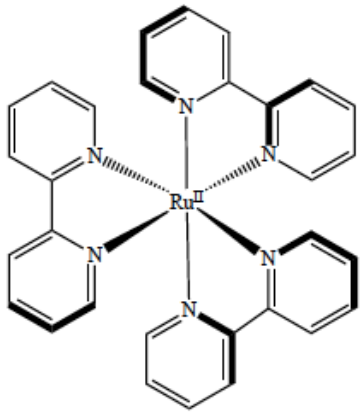

Scheme 1.7. *The structure of* $[Ru(bpy)_3]^{2+}$ *complex.*[32,43]

1.4.2 Electron Donor (D)

An essential step for initiating catalytic cycles in a photocatalytic CO_2 reduction system is a reductive quenching process. The steps involved in the process are detailed below:

Reductive Quenching Mechanism

1- Photoexcitation

A photosensitizer (PS) absorbs light energy, then goes to a high-energy state (PS*).

2- Electronic Transition in Donor (D)

In reductive quenching, the excited photosensitizer (PS *) is quenched by an electron donor (D) that donates an electron to the photosensitizer.

$$(PS^*) + (D) \rightarrow (PS^{\bullet -}) + (D^{\bullet +})$$

3- Electron transfer to the catalyst (Cat)

This generates the reduced photosensitizer ($PS^{\bullet -}$), which then transfers one electron to the catalyst (Cat), allowing for CO_2 reduction.

$$(PS^{\bullet -}) + Cat \rightarrow (PS) + (Cat^{-})$$

4- CO_2 Reduction

The reduced catalyst (Cat^-) catalyzes CO_2 reduction with the generation of desired products such as CO, formate, or hydrocarbons. Within a CO_2 photocatalytic reduction setup, the electron donor (sacrificial reductant) needs to fulfill multiple essential requirements to guarantee effective, selective, and reliable performance. The primary considerations include:

1. The donor must be sufficiently negative oxidation potential to quench the excited photosensitizer (i.e., donate an electron to PS*).
2. The donor must also be stable under reaction conditions and should not degrade into toxic by-products.
3. The donor ought to respond easily, donating electrons with minimal kinetic obstacles.
4. The electron donor must be available and inexpensive for practical applications.

The donor should not only be environmentally benign but must also not introduce toxicity or pollution. To facilitate its interaction with the photocatalyst, it is also essential that the chosen electron donor be soluble in the reaction medium.

Most photocatalytic systems for CO_2 reduction have adopted some electron donors extensively. They are triethanolamine (TEOA), triethylamine (TEA), 1-benzyl-1,4-dihydronicotinamide (BNAH), ascorbic acid (AA), and 1,3-dimethyl-2-phenylbenzimidazoline (BIH). All of these electron donor structures are shown in **Scheme 1.8**.[23,43] The reactivity of these electron donors is demonstrated in the reported literature.[6,40,44] Also, **Scheme 1.9** shows the possible mechanism of how TEA works during the photocatalytic cycle.

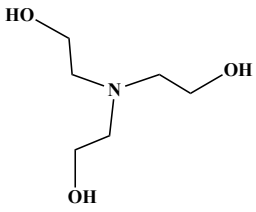

Triethanolamine (**TEOA**)

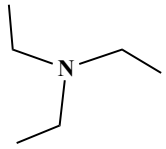

Triethylamine **(TEA)**

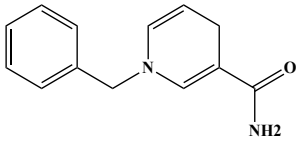

1-Benzyl-1,4-dihydronicotinamide (**BNAH)**

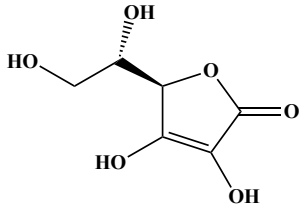

Ascorbic acid (**AA)**

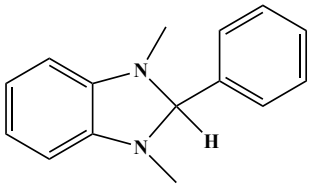

1,3-dimethyl-2-phenyl-2,3-dihydro-1H-benzo[d]-imidazole (**BIH**)

Scheme 1.8. *The structures of some electron donor complexes.*[6,40,44]

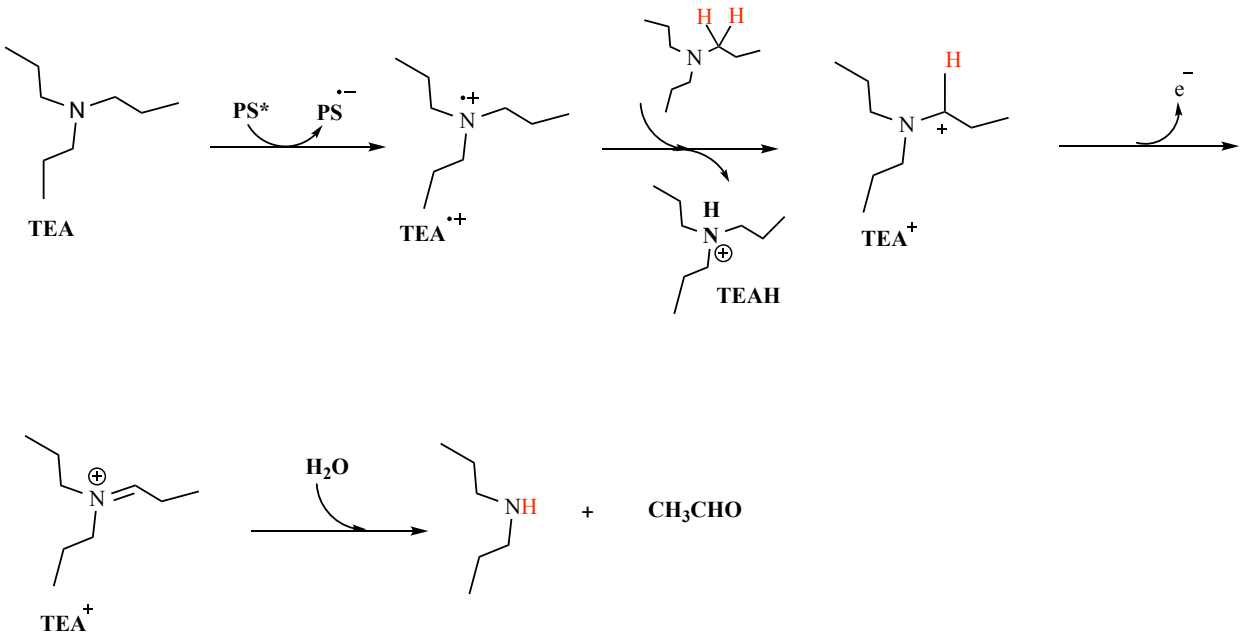

Scheme 1.9. *Reaction sequence for the oxidation of TEA.*[30]

1.4.3 Catalyst (Cat)

The elevated atmospheric carbon dioxide (CO_2) concentration due to human activities has heightened the demand for viable climate change mitigation measures. Catalytic CO_2 reduction has been regarded as a bright prospect in which CO_2 is transformed into valuable chemicals and fuels. Catalysts are employed to promote the process by reducing energy barriers in reactions and enhancing product selectivity and yield. The catalysts used for the reduction of CO_2, mechanisms, and recent advances in the area are reviewed in this article.[31, 45-47]

The two broad approaches to CO_2 reduction are homogeneous and heterogeneous catalysis. Either method may be used either electro-catalytically or photo-catalytically. Heterogeneous electrocatalytic CO_2 reduction largely uses electrolysis, typically assisted by nanostructured materials. Additionally, heterogeneous photocatalytic CO_2 reduction relies on various semiconductor photocatalysts.[47-49] However, whether it is photochemical or electrochemical, transition metal complexes play a key role in homogeneous CO_2 reduction. For this purpose, coordination complexes of a number of metals have been explored as catalysts, including first-row

metals Mn, Fe, Co, Ni, and Cu; second-row metals Ru, Rh, and Pd; and third-row metals W, Re, Os, and Ir.[39,49,50]

A catalyst in the photochemical reduction of CO_2 is used to activate and convert CO_2 into reduced forms, including CO, HCOOH and hydrocarbons. Photoexcitation of a sensitizer leads to electron transfer to a catalyst, changing the oxidation state of the catalyst, which helps facilitate the binding, activation and multiple electron/proton transfer processes of CO_2. At the end of each cycle of catalysis, the catalyst is restored.

For photochemical systems using ruthenium as a catalyst, the catalytic component is typically a metal complex that has distinctive coordination sites and redox characteristics enabling it to support electron transfer with a high level of control and product specificity. The catalytic component also plays a significant role in controlling the efficiency, selectivity and stability of CO_2 photoreduction reactions.[51]

1.4.3.1 Types of Catalysts

a. Homogeneous Catalysts:

Catalysts in the same phase as reactants are metal complexes, which can be adjusted to modify their properties. A few examples are:

• Transition metal complexes, i.e., ruthenium, rhodium, and iridium. They are normally assisted in achieving coordinative saturation through chelating ligands, for example, bipyridine or phenanthroline, to bind and reduce CO_2.

• Organic catalysts: CO_2 reduction mechanisms by non-metal-based systems via a wide range of organic structures.[31, 45-47]

b. Heterogeneous Catalysts:

In photochemistry, heterogeneous catalysts are solids that absorb light and promote photochemical reactions at their surfaces while remaining in a different phase from that of the reactants.

- Metal Nanoparticles: The substrate material is decorated with metal nanoparticles like gold, palladium, and copper to improve the active surface area along with catalytic activity.

- Metal Oxides: They are titanium dioxide (TiO_2) and ZnO, respectively. They are highly recognized for thermochemical and photochemical stability.
- Carbon-based Catalysts: Catalytic sites are functionalized on graphene and carbon nanotubes for better interaction with CO_2 molecules.[31,45-47]

1.4.4 Solvent

The solvent in a photochemical reaction is one of the main factors in controlling both the nature and the effectiveness of the reaction; as such, the choice of solvent is a very serious photochemical concern. Here, the solvent not only acts to solubilize the reactant but also influences the absorptive capacity and potential reaction mechanisms accountable for the effectiveness of photochemical processes. Selection of the solvent is a relevant aspect of the photocatalytic process of the reduction of CO_2 and, to a large degree, defines the reaction's efficacy, selectivity, and kinetics. There have been different works on photochemical reactions performed using different solvents, such as dimethylformamide (DMF), acetonitrile (ACN), dimethylacetamide (DMA), and methanol (MeOH). The unique benefits and functions of each solvent during the photocatalytic reaction for CO_2 reduction are discussed along with the mechanisms by which they enable CO_2 utilization. Solvent can influence the reaction kinetics.[52] The polarity of the solvent can have a significant effect on the photophysical properties of the molecules and their absorption and emission spectra. The polar solvent can stabilize polar excited states with changes in energy levels and subsequently determine fluorescence or phosphorescence.[52]

1.4.4.1 Roles of Solvents in Photochemistry:

1. Solvent polarity, rate of reaction, and the stabilization of reactive intermediates: The polarity of the solvent can have a significant effect on the photophysical properties of the molecules, their absorption and emission spectra. The polar solvent can stabilize polar excited states with changes in energy levels and subsequently determine fluorescence or phosphorescence.[52] The reaction kinetics can be influenced by the solvent due to the stabilization or destabilization of transition states and intermediates. Certain reactions may occur faster in polar solvents because solute-solvent interactions are enhanced in such, and others may favour a nonpolar environment.[53] Specific solvents can stabilize radical species or ion pairs and influence

mechanistic pathways. In this context, solvent polarity and the presence of specific functional groups impart stability.[54]

2. Solvent Selection: The process of selecting a suitable solvent for photoreduction reactions involves a close familiarity with the photochemical system and with the objective. Considerations are the polarity of the solvent relative to the reactants and products, its transparency at the wavelengths used to ensure it does not interfere with light absorption, and its capacity to solubilize the reactants sufficiently without becoming involved in or modifying the chemical reaction.[55-57]

For catalytic CO_2 reduction, the process efficiency is generally defined by the following four terms:

1.4.5 Turnover Number (TON)

The turnover number demonstrates catalytic efficiency, quantifying how much time the catalyst operates by determining how many reduction reactions occur per cycle during the active lifecycle of the catalyst. The metric is formally defined as the molar ratio of product formed from CO_2 reduction relative to the catalyst, and its specific definition is given in Equation (15).[2,15,33,34,58]

$$\text{Turnover Number (TON)} = \frac{\text{moles of } CO_2 \text{ reduction product formed}}{\text{moles of catalyst used}} \qquad (15)$$

1.4.6 Turnover Frequency (TOF)

This metric describes the rate at which a catalyst can process reactants to products. It is most expressed as the number of catalytic cycles per time unit (e.g., hr) and per mole of catalyst.[15,33,34,58] The turnover frequency can be defined by Equation (16):

$$\text{TOF} = \frac{\text{TON}}{\text{Time}} \qquad (16)$$

1.4.7 Catalytic Selectivity (CS)

In photochemistry, catalytic selectivity is the capability of a catalyst to drive a photochemical reaction toward the production of a specific product from amongst several others. The selectivity

is critical to enhance the reaction efficiency with reduced production of unwanted side products. The intrinsic selectivity of photochemical processes can be modulated by different factors, including the nature of the photocatalyst used, the reaction conditions employed, and the presence of co-catalysts or auxiliary reagents. Especially in the case of photochemical reduction of CO_2, the control of reaction conditions becomes a very important factor in achieving selectivity towards C_1 products.

The selectivity shown by a catalyst is largely determined by the particular experimental conditions utilized, and improvements in the formation of one product over another can be made by adjusting these conditions. For example, in a homogeneous photochemical reaction, for a given catalyst/sensitizer couple, the reaction products depend on the type of sacrificial electron donor used.[3]

However, in this thesis, the attention is on formic acid/formate (HCOOH, $HCOO^-$) and carbon monoxide (CO). The catalysts used can have a selectivity for a specific reaction product (eq. 17).

$$\mathrm{CS}(\%) = \frac{\text{Amount of one specific product}}{\text{Total amount of all product}} \text{ x } 100 \qquad (17)$$

1.4.8 Photochemical Quantum Yield (Φ)

Quantum yield (Φ) of photocatalytic CO_2 reduction H_2 is a quantification of the efficiency with which light absorbed is used for the creation of chemical products from carbon dioxide. It may be expressed as the ratio of the number of product molecules (e.g., CO, HCOOH, or CH_4) produced to the number of photons absorbed by the photocatalytic system using the following equation (18):

$$\Phi = \frac{[CO_2 \text{ reduction products}]}{[\text{incident photons}]} \qquad (18)$$

Generally, the quantum yield for CO_2 reduction to HCOOH was calculated after irradiation for 1h at 450 nm using the following equation (19):[3,58]

$$\Phi\mathrm{HCOOH} = \frac{\#\text{ number of the HCOOH molecules}}{\#\text{ number of incident photons}} \text{ x } 100\% \qquad (19)$$

High quantum yields are indicative of an efficient energy conversion of absorbed light energy into useful chemical products, for example, carbon monoxide (CO), hydrocarbons, or formic acid. A large quantum yield also corresponds to a high fraction of absorbed photons for desirable reactions and thus an optimization of the efficiency of the catalytic process and its associated reaction parameters.[58,60]

1.5 Electrocatalytic Reduction of CO_2

The electrochemical reduction of carbon dioxide has attracted considerable attention as a possible carbon source for synthesizing organic molecules and as a possible means of energy storage. CO_2 is described as a low-energy molecule, and electrochemical reduction to its anionic radical requires a very negative potential.[61] The direct electrochemical reduction products depend on the electrode and the reaction medium.

Homogeneous catalysis electrochemical processes include the use of soluble molecular catalysts to facilitate redox reactions, as in the effective and controlled electrochemical conversion of carbon dioxide (CO_2). In this, the homogeneous catalyst is typically illustrated as the transition metal complex that is dissolved within the reaction phase and interacts with the substrate (e.g., CO_2) on the molecular level.

These systems are of significant interest because of the well-defined structures, physically tunable electronic properties, and the promise of a mechanistic understanding afforded by the application of spectroscopic and electrochemical techniques. One of the powerful features of homogeneous electrochemical catalysts is that they can be engineered at a molecular level with high specificity. Ligand design allows the chemist to precisely adjust redox potentials, electronic properties, and selectivity in catalytic reactions. Besides, the investigation of electrocatalytic reduction mechanisms is a supporting field to photocatalytic reduction that constitutes the heart of the thesis discussion. A summary of CO_2 reduction reactions and their reduction potentials is provided in Table 1.1.[2,10]

Metal complexes with bipyridine or phosphine ligands are a promising field of investigation regarding carbon dioxide reduction. Here, changes in the structure of the ligand framework may enhance the interaction of the intermediates or facilitate the stabilization of reactive intermediates. The primary challenges investigated within this field are achieving high turnover numbers (TONs)

and turnover frequencies (TOFs) with high product selectivity and long-term catalyst stability. Some significant challenges encountered are catalyst deactivation, side reactions, e.g., hydrogen evolution, and promoting efficient electron transfer.[60]

The electrochemical configuration typically includes a working electrode, where the catalytic cycle is triggered by the reduction or oxidation of the catalyst; a counter electrode for charge balancing; and a reference electrode for potential control. The reaction is normally operated in an electrolyte solution using standard methods, e.g., cyclic voltammetry, to investigate the redox behaviour of the catalyst.[2]

The experiments of cyclic voltammetry were conducted in a three-neck round-bottom flask; thus, the sample solution was prepared inside a glove box under a nitrogen atmosphere and sealed prior to its removal. Cyclic voltammetry experiments were carried out with a VersaSTAT 3 potentiostat (Princeton Applied Research) in a conventional three-electrode setup. The working electrode was a 0.2 cm diameter glassy carbon, and a platinum wire and an Ag wire served as the auxiliary and pseudo-reference electrodes, respectively. The ferrocene/ferrocenium couple as reference potential was added to the analysis mixture after purging with CO_2 and measured before and after the addition of water.[62]

Tetrabutylammonium hexafluorophosphate is the supporting electrolyte employed in this study. Before each experimental procedure, the electrolyte solution of 0.1 M $(n\text{-}Bu)_4N(PF_6)$ in anhydrous CH_3CN was saturated with N_2 or CO_2 by purging for 20 minutes. The concentration of the catalyst utilized during experiments was 0.02 mM (15 mL of acetonitrile). The amount of evolved carbon monoxide and hydrogen gases were analyzed using an Agilent 7820A gas chromatograph (GC), which is furnished with a thermal conductivity detector (TCD) and an Agilent Select permanent gases column.[63]

1.6 Summary of Content for The Body of The Thesis

Chapter **1**, "Introduction": In this chapter, a brief introduction to photochemistry and photocatalytic CO_2 reduction is given. The background and overview of the overall photocatalytic CO_2 reduction system were explained in this chapter. In addition, this chapter gives an overview of the experimental methods and conditions employed in the study of this thesis. In Chapter **2**, we

concentrate on the synthesis and characterization of ruthenium complexes containing a ligand with a phenyl group and different substituents on the amine part (hydrogen or methyl). We also discuss key factors affecting photochemical CO_2 reduction reactions, such as the solvent, proton source, electron donor, and photosensitizer. Chapter **3** proceeds to the synthesis and analysis of a third ruthenium complex, in which the phenyl group is substituted with an isopropyl group. In this chapter, we explore the reaction mechanisms of photocatalytic CO_2 reduction by Ru (II) catalysts since these systems are highly promising and have gained much attention. Getting a clearer picture of these processes is important for the design of more efficient photocatalysts and progress towards useful photosynthetic systems. The purpose of this review is to describe the extent of current knowledge on these processes and to point out gaps that exist in the case of these systems. Chapter **4** presents a newly synthesized cobalt complex, while experimental work continues. Chapter **5** then outlines our results and indicates possible avenues of future research.

1.7 Conclusion

The conversion of CO_2 to practical fuels using sunlight has the prospect of an essentially unlimited energy supply in the form of energy-rich chemical species. As much as photocatalytic CO_2 reduction to carbon fuels is an encouraging and emerging technology, it is faced with significant scientific and engineering hurdles. Homogeneous transition metal complex catalysis can be utilized in the production of products, i.e., formic acid and CO. Formic acid can indeed be considered as an interesting intermediate or, merely, energy storage. In most cases, it is thought that formate is generated via the reaction of a hydride donor intermediate and CO_2. In-depth investigations into the determinations of the factors affecting the generation of formate, carbon monoxide, and hydrogen would be useful. Polypyridine–metal complexes are the most dominant class of molecular catalysts used to bring about the electrochemical and photochemical reduction of CO_2.

The aims and objectives of this study are to explore new catalysts for the photocatalytic reduction of CO_2 to produce HCOOH, H_2 or CO. Therefore, there are different approaches with different ligand geometries, which are presented and explained here in this thesis to investigate and look for new catalysts for the reduction of CO_2.

1.8 References

1. Su, D.-J.; Xiang, S.-Q.; Gao, S.-T.; Jiang, Y.; Liu, X.; Zhang, W.; Zhao, L.-B.; Tian, Z.-Q. *Kinetic Understanding of Catalytic Selectivity and Product Distribution of Electrochemical Carbon Dioxide Reduction Reaction. JACS Au* **2023**, *3* (3), 905–918.

2. Ḥamīd, Y. *Exploring New Catalysts for Photocatalytic Carbon Dioxide Reduction Using Homogeneous Transition Metal Complexes*; Ph.D. Thesis, University of Ottawa, Department of Chemistry, Ottawa, 2019.

3. Kientz, M. *Renewable Methane Production from the Catalytic Reduction of CO_2 Using Sunlight*; Catalysis, Université Paris, Paris, 2022.

4. Takeda, H.; Koike, K.; Inoue, H.; Ishitani, O. *Development of an Efficient Photocatalytic System for CO_2 Reduction Using Rhenium(I) Complexes Based on Mechanistic Studies. J. Am. Chem. Soc.* **2008**, *130* (6), 2023–2031.

5. Duarah, P.; Haldar, D.; Yadav, V. S. K.; Purkait, M. K. *Progress in the Electrochemical Reduction of CO_2 to Formic Acid: A Review on Current Trends and Prospects. J. Environ. Chem. Eng.* **2021**, *9* (6), 106394.

6. Yang, J.; Goh, K. E. J.; Yu, Z. G.; Wong, R. E.; Zhang, Y.-W. *A First-Principles Study on Strain Engineering of Monolayer Stanene for Enhanced Catalysis of CO_2 Reduction*. *Chemosphere* **2021**, *268*, 129317.

7. Voyame, P.; Toghill, K. E.; Méndez, M. A.; Girault, H. H. *Photoreduction of CO_2 Using $[Ru(bpy)_2(CO)L]^{n+}$ Catalysts in Biphasic Solution/Supercritical CO_2 Systems*. *Inorg. Chem.* **2013**, *52* (19), 10949–10957.

8. Gao, Y.; Qian, K.; Xu, B.; Li, Z.; Zheng, J.; Zhao, S.; Ding, F.; Sun, Y.; Xu, Z. *Recent Advances in Visible-Light-Driven Conversion of CO_2 by Photocatalysts into Fuels or Value-Added Chemicals*. *Carbon Resour. Convers.* **2020**, *3*, 46–59.

9. Rasul, S.; Pugnant, A.; Xiang, H.; Fontmorin, J.-M.; Yu, E. H. *Low-Cost and Efficient Alloy Electrocatalysts for CO2 Reduction to Formate*. *J. CO_2 Util.* **2019**, *32*, 1–10.

10. Finn, C.; Schnittger, S.; Yellowlees, L. J.; Love, J. B. *Molecular Approaches to the Electrochemical Reduction of Carbon Dioxide*. *Chem. Commun.* **2012**, *48* (10), 1392–1399.

11. Mardini, N.; Bicer, Y. *Direct Synthesis of Formic Acid as Hydrogen Carrier from CO_2 for Cleaner Power Generation through Direct Formic Acid Fuel Cell. Int. J. Hydrogen Energy* **2021**, *46* (24), 13050–13060.

12. Wang, H.-H.; Zhang, S.-N.; Zhao, T.-J.; Liu, Y.-X.; Liu, X.; Su, J.; Li, X.-H.; Chen, J.-S. Mild and Selective Hydrogenation of CO_2 into Formic Acid over Electron-Rich MoC Nanocatalysts. *Sci. Bull.* **2020**, *65* (8), 651–657.

13. Qiao, J.; Liu, Y.; Hong, F.; Zhang, J. A Review of Catalysts for the Electroreduction of Carbon Dioxide to Produce Low-Carbon Fuels. *Chem. Soc. Rev.* **2014**, *43* (2), 631–675.

14. Kumar, B.; Llorente, M.; Froehlich, J.; Dang, T.; Sathrum, A.; Kubiak, C. P. Photochemical and Photoelectrochemical Reduction of CO_2. *Annu. Rev. Phys. Chem.* **2012**, *63*, 541–569.

15. Feng, D.-M.; Zhu, Y.-P.; Chen, P.; Ma, T.-Y. Recent Advances in Transition-Metal-Mediated Electrocatalytic CO_2 Reduction: From Homogeneous to Heterogeneous Systems. *Catalysts* **2017**, *7* (12), 373.

16. Schneider, J.; Jia, H. F.; Muckerman, J. T.; Fujita, E. Thermodynamics and Kinetics of CO_2, CO, and H^+ Binding to the Metal Centre of CO_2 Reduction Catalysts. *Chem. Soc. Rev.* **2012**, *41* (6), 2036–2051.

17. Genovese, C.; Ampelli, C.; Marepally, B. C.; Papanikolaou, G.; Perathoner, S.; Centi, G. Electrocatalytic Reduction of CO_2 for the Production of Fuels: A Comparison between Liquid and Gas Phase Conditions. *Chem. Eng. Trans.* **2015**, *43*, 2281–2286.

18. Yamazaki, Y.; Takeda, H.; Ishitani, O. Photocatalytic Reduction of CO_2 Using Metal Complexes. *J. Photochem. Photobiol. C: Photochem. Rev.* **2015**, *25*, 106–137.

19. Kavarnos, G. J.; Turro, N. J. Photosensitization by Reversible Electron Transfer: Theories, Experimental Evidence, and Examples. *Chem. Rev.* **1986**, *86* (2), 401–449.

20. Kuramochi, Y.; Itabashi, J.; Fukaya, K.; Enomoto, A.; Yoshida, M.; Ishida, H. Unexpected Effect of Catalyst Concentration on Photochemical CO_2 Reduction by trans(Cl)–$Ru(bpy)(CO)_2Cl_2$: New Mechanistic Insight into the $CO/HCOO^-$ Selectivity. *Chem. Sci.* **2015**, *6* (5), 3063–3074.

21. Masdeu-Bultó, A. M.; Reguero, M.; Claver, C. Mechanistic Insights of Photocatalytic CO_2 Reduction: Experimental versus Computational Studies. *Eur. J. Inorg. Chem.* **2022**, *2022* (14), 1–17.

22. Piumetti, M.; Fino, D.; Russo, N. Photocatalytic Reduction of CO_2 into Fuels: A Short Review. *J. Adv. Catal. Sci. Technol.* **2014**, *1* (2), 16–25.

23. Mohamad pour, F.; Amani, A. M. Photocatalytic Systems: Reactions, Mechanism and Applications. *RSC Adv.* **2024**, *14* (29), 20609–20641.

24. Nahar, S.; Zain, M. F. M.; Kadhum, A. A. H.; Hasan, H. A.; Hasan, M. R. Advances in Photocatalytic CO_2 Reduction with Water: A Review. *Materials* **2017**, *10* (6), 629.

25. Boutin, E.; Merakeb, L.; Ma, B.; Boudy, B.; Wang, M.; Bonin, J.; Anxolabéhère-Mallart, E.; Robert, M. Molecular Catalysis of CO_2 Reduction: Recent Advances and Perspectives

in Electrochemical and Light-Driven Processes with Selected Fe, Ni, and Co Aza Macrocyclic and Polypyridine Complexes. *Chem. Soc. Rev.* **2020**, *49* (15), 5772–5809.

26. Yaghmaei-Sabegh, M. *Advancements in Photochemistry and Flow Systems for Synthesis and Analysis*; Ph.D. Thesis, University of Ottawa, Department of Chemistry, Ottawa, 2024.

27. Lakowicz, J. R.; Masters, B. R. Principles of Fluorescence Spectroscopy, Third Edition. *J. Biomed. Opt.* **2008**, *13* (2), 029901.

28. Valeur, B. *Molecular Fluorescence: Principles and Applications*; Wiley-VCH: Weinheim, 2002.

29. Turro, N. J.; Ramamurthy, V.; Scaiano, J. C. *Principles of Molecular Photochemistry: An Introduction*; University Science Books: Sausalito, CA, 2010.

30. Reithmeier, R.; Bruckmeier, C.; Rieger, B. Conversion of CO_2 via Visible Light Promoted Homogeneous Redox Catalysis. *Catalysts* **2012**, *2* (4), 544–571.

31. Artz, J.; Müller, T. E.; Thenert, K.; Kleinekorte, J.; Meys, R.; Sternberg, A.; Bardow, A.; Leitner, W. Sustainable Conversion of Carbon Dioxide: An Integrated Review of Catalysis and Life Cycle Assessment. *Chem. Rev.* **2018**, *118* (2), 434–504.

32. Prier, C. K.; Rankic, D. A.; MacMillan, D. W. C. Visible Light Photoredox Catalysis with Transition Metal Complexes: Applications in Organic Synthesis. *Chem. Rev.* **2013**, *113* (7), 5322–5363.

33. Morris, A. J.; Meyer, G. J.; Fujita, E. Molecular Approaches to the Photocatalytic Reduction of Carbon Dioxide for Solar Fuels. *Acc. Chem. Res.* **2009**, *42* (12), 1983–1994.

34. Osterholm, S. *Photocatalytic CO_2 Reduction Using Manganese and Rhenium Catalysts Containing Bidentate Phosphinoaminopyridine Ligands*; Master's Thesis, University of Ottawa, 2021.

35. Hawecker, J.; Lehn, J.-M.; Ziessel, R. Efficient Photochemical Reduction of CO_2 to CO by Visible Light Irradiation of Systems Containing $Re(bipy)(CO)_3X$ or $Ru(bipy)_3^{2+}$–Co^{2+} Combinations as Homogeneous Catalysts. *J. Chem. Soc., Chem. Commun.* **1983**, 536–538.

36. Bignozzi, C. A. (Ed.). *Photocatalysis*; Topics in Current Chemistry, Vol. 303; Springer: Berlin, 2011.

37. Zhu, S.; Wang, D. Photocatalysis: Basic Principles, Diverse Forms of Implementations and Emerging Scientific Opportunities. *Adv. Energy Mater.* **2017**, *7* (23), 1701240.

38. Wang, Y.; He, D.; Chen, H.; Wang, D. Catalysts in Electro-, Photo-, and Photoelectrocatalytic CO_2 Reduction Reactions. *J. Photochem. Photobiol. C: Photochem. Rev.* **2019**, *40*, 117–149.

39. Hawecker, J.; Lehn, J.-M.; Ziessel, R. Photochemical and Electrochemical Reduction of Carbon Dioxide to Carbon Monoxide Mediated by (2,2′-Bipyridine) tricarbonylchlororhenium(I) and Related Complexes as Homogeneous Catalysts. *Helv. Chim. Acta* **1986**, *69* (1), 199–206.

40. Pellegrin, Y.; Odobel, F. Sacrificial Electron Donor Reagents for Solar Fuel Production. *C. R. Chim.* **2017**, *20* (3), 283–295.

41. Alves, J. *Advanced Photochemical Reaction Systems for Molecular Design*; Ph.D. Thesis, Queensland University of Technology, 2022.

42. Dadashi-Silab, S.; Doran, S.; Yagci, Y. Photoinduced Electron Transfer Reactions for Macromolecular Syntheses. *Chem. Rev.* **2016**, *116* (17), 10212–10275.

43. Xiao, P.; Zhang, J.; Dumur, F.; Tehfe, M. A.; Morlet-Savary, F.; Graff, B.; Gigmes, D.; Fouassier, J. P.; Lalevée, J. Visible Light Sensitive Photoinitiating Systems: Recent Progress in Cationic and Radical Photopolymerization Reactions under Soft Conditions. Prog. Polym. Sci. **2015**, 41, 32–66.

44. Elgrishi, N.; Chambers, M. B.; Wang, X.; Fontecave, M. Molecular Polypyridine-Based Metal Complexes as Catalysts for the Reduction of CO_2. Chem. Soc. Rev. **2017**, 46 (3), 761–796.

45. Kornienko, N.; Zhang, J. Z.; Reisner, E. Theoretical Insights into the Efficiency and Performance of Hybrid Biological–Inorganic Systems for Solar Fuel Synthesis. Nat. Nanotechnol. **2017**, 12 (8), 772–773.

46. Sun, Z.; Ma, T.; Tao, H.; Fan, Q.; Han, B. Fundamentals and Challenges of Electrochemical CO_2 Reduction Using Two-Dimensional Materials. Chem **2016**, 1 (4), 550–567.

47. Yang, C.; Wang, Y.; Qian, L.; Al-Enizi, A. M.; Zhang, L.; Zheng, G. Heterogeneous Electrocatalysts for CO_2 Reduction. ACS Appl. Energy Mater. **2021**, 4 (2), 1034–1044.

48. Li, K.; Peng, B.; Peng, T. Recent Advances in Heterogeneous Photocatalytic CO_2 Conversion to Solar Fuels. ACS Catal. **2016**, 6, 7485–7527.

49. Ishida, H. Electrochemical/Photochemical CO_2 Reduction Catalyzed by Transition Metal Complexes. In Carbon Dioxide Chemistry, Capture and Oil Recovery; Iyad, K., Shaya, J., Srour, H., Eds.; InTechOpen: London, 2018; pp 17–40.

50. Sarantou, A.; Tsipis, A. *Photocatalytic Reduction of CO_2 into CO with Cyclometalated Pt (II) Complexes of N^C^N Pincer Dipyridylbenzene Ligands*: A DFT Study. Molecules **2024**, 29 (2), 403.

51. Ncube, P.; Mochane, M. J. *Visible-Light-Driven CO_2 Photoreduction Using Ruthenium(II) Complexes: Mechanisms, Hybrid Systems, and Recent Advances.* **Catalysts 2025**, *15* (11), 1036.

52. Reichardt, C.; Welton, T. Solvents and Solvent Effects in Organic Chemistry, 4th ed.; Wiley-VCH: Weinheim, 2010.

53. Wöhrle, D. Chemistry and Light (Book Review of Chemistry and Light by P. Suppan). Angew. Chem. **1995**, 107 (6), 760.

54. Lakowicz, J. R. Principles of Fluorescence Spectroscopy, 3rd ed.; Springer: Boston, 2006.

55. Su, X.; Lu, X.; Li, Y.; Liu, B.; Xi, H.; Li, Y. Photocatalytic CO_2 Conversion Using Solvent-Enhanced Systems. J. CO_2 Util. **2015**, 11, 142–150.

56. Smith, P. J.; Lee, J. T. Role of Solvents in the Photocatalysis of Carbon Dioxide. Catal. Today. **2013**, 207, 28–36.

57. Kuramochi, Y.; Kamiya, M.; Ishida, H. *Photocatalytic CO_2 Reduction in N,N-Dimethylacetamide/Water as an Alternative Solvent System*. **Inorg. Chem. 2014**, *53* (7), 3326–3332.

58. Braslavsky, S. E.; Braun, A. M.; Cassano, A. E.; Emeline, A. V.; Litter, M. I.; Palmisano, L.; Parmon, V. N.; Serpone, N. Glossary of Terms Used in Photocatalysis and Radiation Catalysis (IUPAC Recommendations 2011). *Pure Appl. Chem.* **2011**, *83* (10), 2301–2312.

59. Zhang, L.; Müller, A. V.; Desai, S. P.; Grills, D. C.; Polyansky, D. E.; Sampaio, R. N.; Concepcion, J. J. Controlling Product Selectivity in Photochemical CO_2 Reduction with the Redox Potential of the Photosensitizer. ***ACS Catal.*** **2024**, *14* (24), 18477–18487.

60. Hammouche, M.; Lexa, D.; Momenteau, M.; Savéant, J.-M. Chem. Catal. Electrochem. Reactions. Homogeneous Catalysis of the Electrochemical Reduction of Carbon Dioxide by Iron (0) Porphyrins. Role of the Addition of Magnesium Cations. J. Am. Chem. Soc. 1991, 113 (22), 8455–8466.

61. Zhang, H.; Liang, Q.; Xie, K. *How to Rationally Design Homogeneous Catalysts for Efficient CO_2 Electroreduction?* ***iScience.*** **2024**, *27* (2), 108973.

62. Kim, B. Y.; Lee, D. H.; Lee, J.-Y.; Yun, J.-I. *Electrochemical and Spectroscopic Investigations of Tb (III) in Molten LiCl–KCl Eutectic at High Temperature*. **Electrochem. Commun. 2010**, *12* (8), 1005–1008.

63. Rao, G. K.; Pell, W.; Korobkov, I.; Richeson, D. *Electrocatalytic Reduction of CO_2 Using Mn Complexes with Unconventional Coordination Environments*. **Chem. Commun. 2016**, *52* (51), 8010–8013.

Chapter 2: Tuning Selectivity and Overcoming the α-Diimine Ligand Constraint in Group 8 Catalysts: Ruthenium Complexes with Phosphinoaminopyridine Ligands for Photocatalytic CO_2 Reduction

This chapter addresses one of the principal challenges in advancing CO_2 reduction research, namely the efficient catalytic cycling of CO_2 to generate energy-rich products. From a catalyst-design perspective. Most, if not all, catalytic systems used in CO_2 reduction employ α-diimine ligation, which has constrained how researchers can develop photocatalysts and their catalytic performance. New ruthenium-based photocatalysts were presented, [Ru{κ²-$(Ph_2P)NR(NC_5H_4)$}$(CO)_2Cl_2$], as shown in **Scheme 2.1**, which were supported by phosphinoaminopyridine ligands. The complexes exhibited tremendous product selectivity and were stable under visible-light irradiation for the reduction of CO_2. Of importance is the studied ligand substituent (R = H, Me) and its influence on catalytic performance from the same ruthenium center—specifically, when R = H, which formed more formic acid (HCOOH) relative to R = Me. This example nicely portrays how seemingly minor changes made to ligands could positively influence catalytic activity, and selectivity provides a potential avenue for advancing the design of improved photocatalysts for CO_2 reduction.

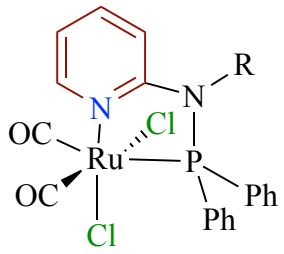

Scheme 2.1. Ru-catalyst structure.

2.1 Introduction

The process of reducing CO_2 is thermodynamically unfavorable and has a large activation barrier that must be overcome with suitable catalysts to allow the reaction to carry on at reasonable rates. An effective photocatalytic system for CO_2 reduction generally utilizes three distinct components: a photosensitizer, a sacrificial reducing agent, and a molecular catalyst.[1-3] To date, most of the systems that have been reported have utilized noble metal-based catalysts, especially Re[4-6] and Ru[7,8] complexes because of their greater catalytic activity and robustness. However, to promote greater economic feasibility and facilitate greater scalability of the development of photocatalytic

systems, further advancement toward developing systems that utilize earth-abundant metals such as Cu, Co, Ni, Mn, and Fe is essential. Although extensive research has demonstrated that the reduction of CO_2 can be achieved using Co-based complexes,[9-11] as well as related systems utilizing Ni,[10,12] Fe,[13,14] and Mn,[14,15] it is apparent that many of these catalysts still suffer from low efficiency and insufficient product selectivity, indicating an ongoing requirement for further advancement in the design of catalysts.

Transition metal complexes, which are made up of a central metal ion or atom with a coordination of organic ligands, have special properties including adjustable activity, diverse redox valence, and simple theoretical modelling. The reduction potentials of the metal complexes can be tuned systematically by intelligent selection of both the metal centers and the various organic ligands, aligning with the necessary potentials for CO_2 reduction. Various photocatalysts based on rare noble metal complexes have been established for CO_2 photocatalytic reduction, with the predominant participation of homogeneous and heterogeneous Ru, Re, and Ir complex-based photocatalysts.[16-20]

We outline herein the preparation of two homogeneous ruthenium complexes and their use as photocatalysts in the conversion of carbon dioxide to useful chemical products. Formic acid was the major reduction product with high product selectivity and confirmed the system's catalytic action through TON and quantum yields, along with H_2 as a byproduct. The description also goes further into the crucial factors involved while choosing the solvent, catalyst, and photosensitizer that can optimize photocatalytic efficiency. Supporting electrochemical studies were conducted and showed that structural optimization needs to be further improved for better catalytic efficiency.

2.2 Synthesis and Characterization of the Complexes

2.2.1 Experimental Procedures

All manipulations for air or moisture-sensitive materials were carried out under an inert atmosphere in a glovebox or using Schlenk techniques. Starting materials for ligand synthesis were obtained from Sigma-Aldrich and used as received without further purification. All NMR spectra (^{1}H, ^{13}C and ^{31}P) were recorded at 300 or 400 MHz spectrometers at 25 °C with chemical shifts

reported in ppm using the residual protons of the NMR solvent as internal standards. The photochemical techniques used in this chapter are already described in section 1.3.1 of Chapter 1. The direct reaction of $[Ru(CO)_3Cl_2]_2$ with two different N-(diphenylphosphino) -2-aminopyridines yielded the complexes $[Ru\{\kappa^2\text{-}(Ph_2P)NR(NC_5H_4)\}(CO)_2Cl_2]$ (R = Me, R = H), obtained in yields of 85% and 77%, respectively. Confirmation of the identities of $[Ru\{\kappa^2\text{-}(Ph_2P)NMe(NC_5H_4)\}(CO)_2Cl_2]$ (**1**) and $[Ru\{\kappa^2\text{-}(Ph_2P)NH(NC_5H_4)\}(CO)_2Cl_2]$ (**2**) was provided by matching the spectroscopic data with the literature and our independent single-crystal X-ray analyses (Figure 2.1).

2.2.2 Synthesis and characterization of N-(diphenylphosphino)-2-(methylamino) pyridine ligands $(Ph_2P)NMe(NC_5H_4)$

This ligand was synthesized following the procedure described in the literature (Scheme 2.2).[21] In the glovebox, a mixture of 1.08g (10.0 mmol, 1.026 ml) of 2-(methylamino) pyridine in 25 ml of diethyl ether was chilled to -78°C with a dry ice and acetone bath. n-BuLi (10 mmol, 1.6 M in hexane, 6.25 ml) was added dropwise. After 30 minutes of stirring, the reaction mixture was allowed to warm to room temperature and stirred for 3 hours. $PClPh_2$ (chlorodiphenylphosphine) (10 mmol, 1.8 ml) was then added dropwise at 0°C, and the reaction mixture was stirred overnight at room temperature. The reaction mixture was filtered twice using diethyl ether (2 × 15 ml), and the solvent was removed to give an off-white solid. Yield: 1.89 g (65%). ^{1}H NMR (400 MHz, CDCl3, 25ºC): δ= 8.25 (1H, d), 7.55 (1H, t), 7.38-7.25 (11H, m), 6.47 (1H, t), 2.95 (3H, d).

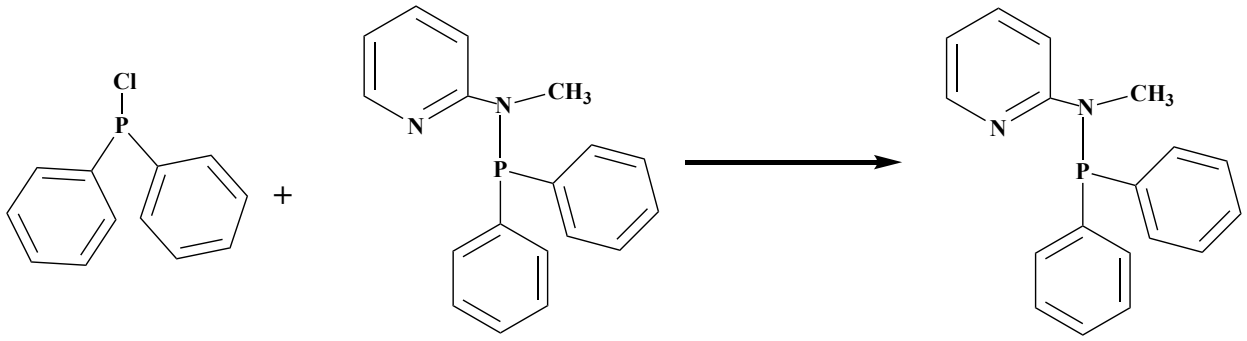

Scheme 2.2. Synthetic scheme for the preparation of phosphinoaminopyridine $(Ph_2P)NMe(NC_5H_4)$ ligand.

2.2.3 Synthesis and Characterization of [Ru{κ²-(Ph_2PNMe) NC_5H_4}$(CO)_2(Cl)_2$] (1)

This complex was synthesized following the procedure described in the literature (Scheme 2.3).[22] In a glove box, a mixture was made by dissolving (0.2334 g, 0.8 mmol) of the ligand (diphenylphosphino)-2-(methylamino) pyridine in 30 mL of toluene. To this solution was added $[Ru(CO)_3Cl_2]_2$ (0.204 g, 0.4 mmol). The flask was removed from the glovebox and connected to a Schlenk line via a reflux condenser. The reaction mixture was stirred and heated to 110 °C under N_2 for over 16 h. The solution was cooled to room temperature. The reaction mixture was filtered, and the precipitate was washed with hexane to give the complex (**1**). Yield 0.3471 g (85%). Single crystals were grown by slow diffusion of hexane and DCM, see Figure 2.1.

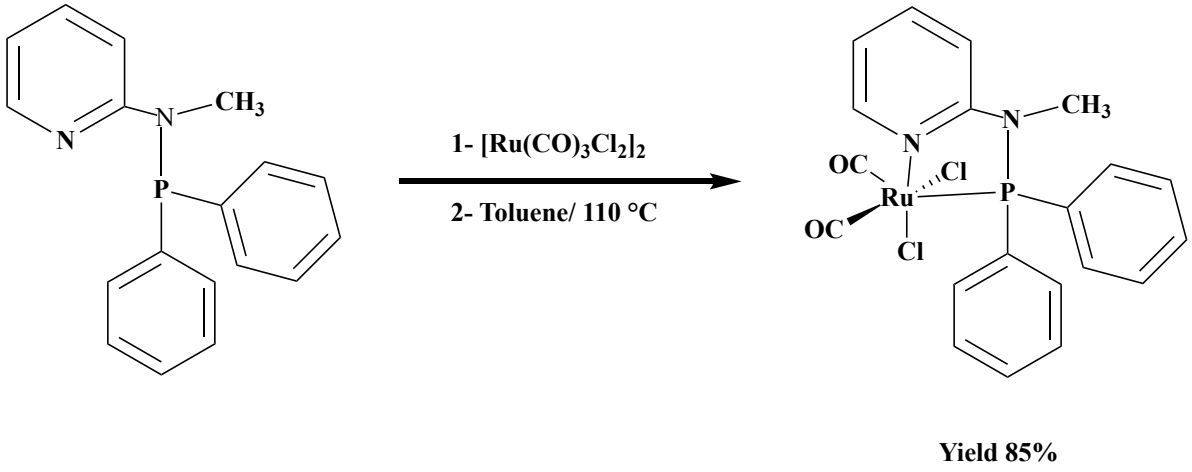

Scheme 2.3. The reaction scheme for the preparation of catalyst (**1**)

2.2.4 Synthesis and characterization of N-(diphenylphosphino)-2-aminopyridine ligand (Ph_2P)NH(NC_5H_4):

This ligand was synthesized following the procedure described in the literature (Scheme 2.4).[21] In the glovebox, a mixture of (0.941 g, 10 mmol, 0.884 ml) of 2-aminopyridine in 25 ml of diethyl ether was chilled to -78°C with a dry ice and acetone bath. n-BuLi (10 mmol, 1.6 M in hexane, 6.25 ml) was added dropwise. After 30 minutes of stirring, the reaction mixture was allowed to warm to room temperature and stirred for 3 hours. $PClPh_2$ (chlorodiphenylphosphine) (10 mmol, 1.8 ml) was then added dropwise at 0 °C, and the reaction mixture was stirred overnight at room temperature. The reaction mixture was filtered twice with diethyl ether (2 × 15 ml), and the solvent was removed to give a yellowish solid. Yield: (65%). ^{1}HNMR (400 MHz, $CDCl_3$, 25°C): δ= 8.20-8.30 (1H, d), 6.80-8.50 (2H, m), 6.75-6.79 (1H, t), 4.86 (1H, braod).

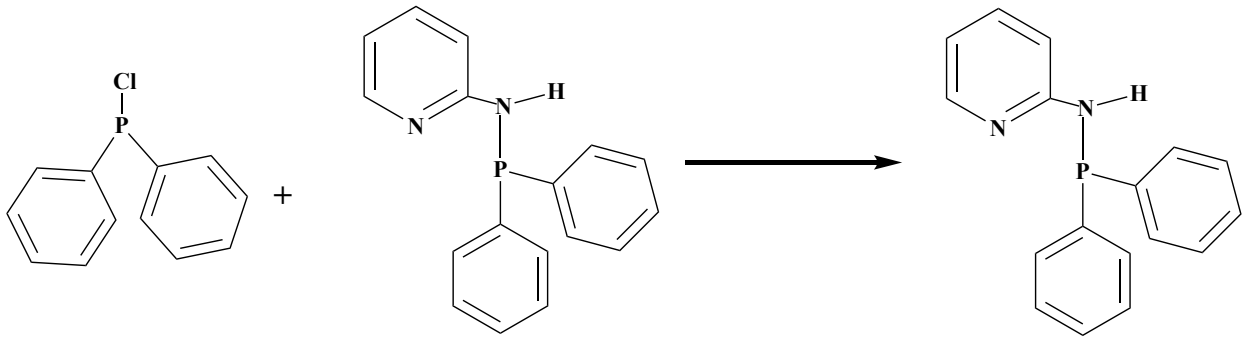

Scheme 2.4. Synthetic scheme for the preparation of phosphinoaminopyridine $(Ph_2P)NH(NC_5H_4)$ ligand

2.2.5 Synthesis and Characterization of $[Ru\{\kappa^2\text{-}(Ph_2PNH)\ NC_5H_4\}(CO)_2(Cl)_2]$ (2)

This complex was synthesized following the procedure described in the literature (Scheme 2.5).[22] In a glove box, a mixture was made by dissolving (0.1121 g, 0.4 mmol) of the ligand (diphenylphosphino)-2-(amino) pyridine in 30 mL of toluene. To this solution was added $[Ru(CO)_3Cl_2]_2$ (0.102 g, 0.2 mmol). The flask was removed from the glovebox and connected to a Schlenk line via a reflux condenser. The reaction mixture was stirred and heated to 110 °C under N_2 for over 16 h. The solution was cooled to room temperature. The reaction mixture was filtered, and the precipitate was washed with hexane to give the complex (**2**). Yield 0.1528 g (77%). Single crystals were grown by slow diffusion of hexane and DCM.

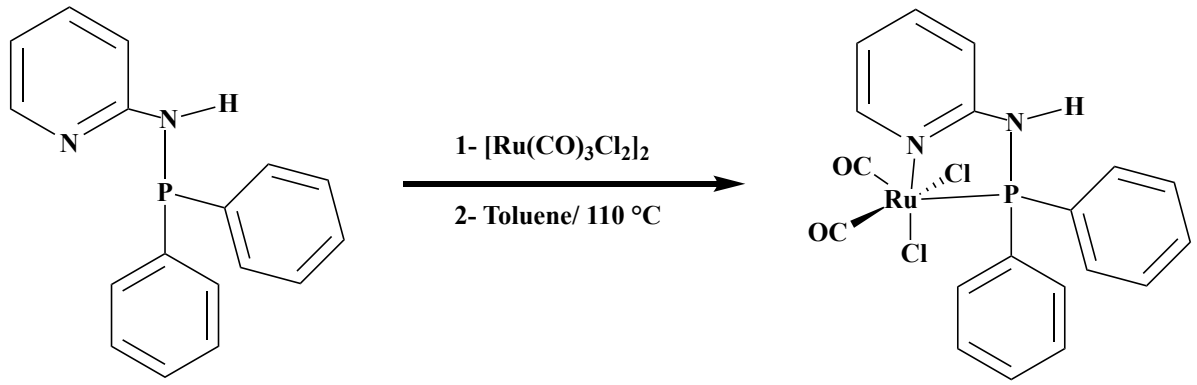

Yield 77%

Scheme 2.5. The reaction scheme for the preparation of catalyst (**2**)

2.2.6 Photocatalytic CO_2 Reduction Systems Experimental Environment

Reagents and solvents of analytical grade were purchased from either Sigma Aldrich or Strem Chemicals and employed without purification. CO_2 (>99.998%, CarbaGas, Switzerland) was used in all the experiments. All the experiments were conducted within the glove box under a nitrogen environment. Photochemically generated gases (H_2 and CO) were determined by gas chromatography (GC) at room temperature. The liquid products from the photocatalytic reactions were analyzed using ^1H NMR.

2.2.6.1 Experimental Details

This thesis utilized photocatalytic processes for CO_2 reduction, conducted in a 20 mL glass vial (i.d. = 10 mm) fitted with a magnetic stirrer bar. A mixed solution comprising DMF–TEOA (4:1, v/v, 4 mL) containing (0.02 mM) of photocatalyst and (0.02 mM) of $Ru(bpy)_3^{2+}$ as a photosensitizer was introduced into the vial, sealed, extracted from the nitrogen-filled glovebox, and purged with CO_2 for a minimum of 20 minutes. The vials were subsequently positioned on a magnetic stirrer, including a four-reaction vial sample holder and four blue-light LEDs (a 450 nm LED light, with a radiant flux of 1050 mW at 700 mA) for 24 hours, set around 10 cm from the reaction vials as the excitation source. The light intensity was quantified at $3.4x10^{-8}$ moles of photons per second utilizing a $[Ru(bpy)_3]^{2+}$ /1,9-diphenylanthracene (DPA) actinometer, as delineated in the existing literature.[23] **Scheme 2.6** below depicts an image of the irradiation apparatus utilized for the photocatalytic studies of this thesis. All experiments were performed in triplicate, and the results were reproducible within an experimental error of ± 3%.

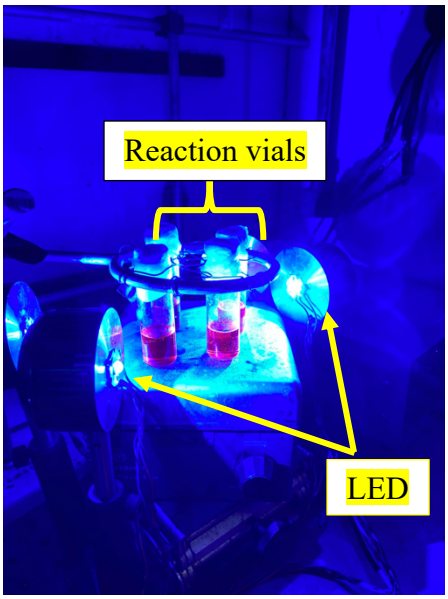

Scheme 2.6. *The photograph of the irradiation apparatus used for the photocatalytic experiments.*

2.2.6.2 Actinometer Experiment

In the actinometer experiment, the context is the reduction of CO_2 by photocatalysis. The photon flux is measured with the intention of calculating the quantum efficiency. The purpose of this calculation is to establish a framework for the comparison of the performance of different photocatalysts.

The photon flux from the experimental setup was determined using a literature-reported actinometric method.[23] The light intensity measured with a $Ru(bpy)_3(PF_6)_2$ / 1,9-diphenylanthracene (DPA) actinometer was 3.4×10^{-8} mol photons·s^{-1}. The corresponding experimental data are presented in Figure 2.5 below. The following are the steps on how to carry out this experiment:

1. Because of the visible light nature of the $Ru(bpy)_3(PF_6)_2$ actinometer, these experiments must be done in a dark room to avoid conversion due to ambient lighting. Before irradiation, a UV-Vis spectrum of the $Ru(bpy)_3(PF_6)_2$ and DPA solution was measured. The absorbance at "time zero" was at 372 nm; this was the initial absorbance (AINITIAL).

2. A $Ru(bpy)_3(PF_6)_2$ and DPA in acetonitrile solution was prepared, using the same concentration as the one used in the reaction of interest (0.19 mM) and (0.10 mM), respectively. As a way to

match lamp-sample spectral overlap, $Ru(bpy)_3(PF_6)_2$ acts as both the photocatalyst and actinometer. A critical note: the accuracy of the actinometer relies on this concentration match.

3. The sample was irradiated for a specific period of time (1 minute), a new UV-Vis Spectrum of the irradiated sample must be recorded and note the absorbance at 372 nm (AFINAL).

4. At the end of the irradiation, a residual absorption at 372 nm is expected; this occurs even after all DPA has been consumed. As a result, AFINAL will be larger than the absorbance found at 372 nm in the absence of DPA.

2.2.7 Electrocatalytic CO_2 Reduction Experiment

In order to further investigate the catalytic conduct of the catalysts, an analysis of the electrochemical study has also been carried out. The samples were initially prepared in a glovebox, then sealed, and finally removed from the glovebox. The electrochemical experiments were conducted in a 25 mL gas-impermeable three-neck flask containing a three-electrode assembly, including a glassy carbon working electrode (diameter = 0.3 cm), a platinum wire working as an auxiliary electrode, and a silver wire working as the pseudo-reference electrode. [24] The electrodes were contained in a supporting electrolyte solution of 0.1 mM tetrabutylammonium hexafluorophosphate $[(n\text{-}Bu)_4N]PF_6$ (TBAHFP) and 15 mL of CH_3CN. The solution was degassed for 20 minutes with CO_2 before each experiment started. Scanning speed was 100 mV s^{-1}. All potential results were referred against the internal standard of ferrocenium/ferrocene (Fc^+/Fc).[25]

2.3 Results and Discussion

2.3.1 X-ray Analysis

Single crystals of this complex (**1)** were grown by slow diffusion of hexane into the solution of the complex made in dichloromethane. The structural features of (**1)** were determined by single-crystal X-ray analysis as shown in Figure 2.1.

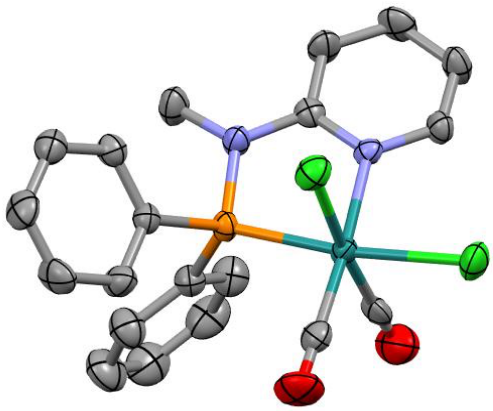

Figure 2.1. *The diagram shows the structure of the compound [Ru{κ²-(Ph₂PNMe) NC₅H₄} (CO)₂(Cl)₂] (Catalyst **1**) as determined by X-ray analysis. Chlorine atoms are shown in green, and carbonyl groups are in red. H atoms are omitted for clarity.*

2.3.2 UV-Vis Spectroscopy

To characterize the light absorption properties of each complex, UV-visible absorption spectra were collected of the complexes dissolved in acetonitrile (MeCN) and are shown in Figure 2.2. Complexes (**1** and **2)** are white and cannot function as a visible light photocatalyst without a photosensitizer. As shown in Figure 2.2, the UV-vis spectrum of the catalysts was obtained in CH_3CN, and it shows the ligand absorption below 400 nm.

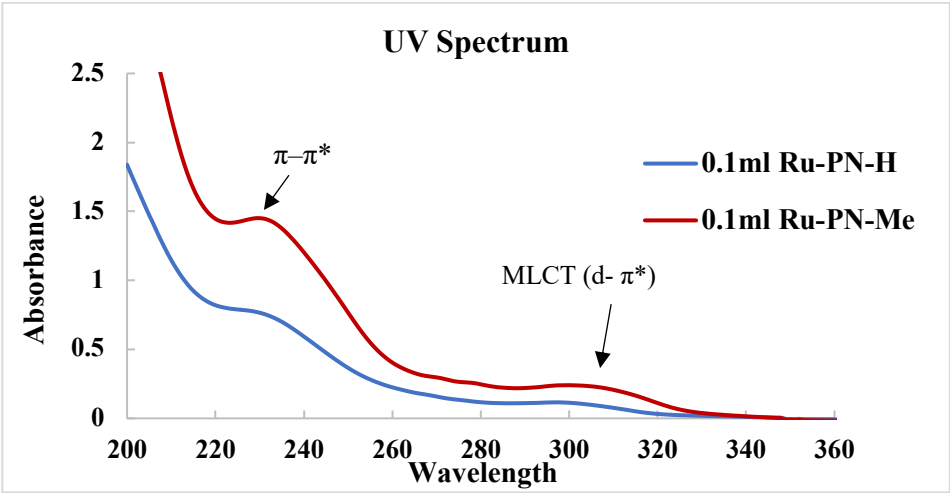

Figure 2.2. *UV-vis spectra in CH_3CN for catalysts **1** and **2***

The UV spectra of the Ru-PN-Me (**1**) and Ru-PN-H (**2**) complexes, both at 0.1 mL, show strong absorption in the UV region (200–360 nm), with Ru-PN-Me (red line) exhibiting consistently higher absorbance than Ru-PN-H (blue line) across all wavelengths. Both spectra exhibit intense

peaks below 250 nm, which are probably due to transitions in the ligand framework (π- π*), and broad bands of absorbance extending up to 300 nm, which are generally due to metal-to-ligand charge transfer transitions characteristic of Ru (II) complexes MLCT (d- π*). The increased absorbance at the Ru-PN-Me is indicative that the methyl group, being an electron-donating substituent on the ligand, is adding electron density and augmenting light-harvesting efficiency, with possibilities of modifying the photocatalytic activity of the complex.

2.3.3 Photochemistry Gaseous Product Analysis

In general, the chromatographic data is shown as a graph of detector response versus the retention time, and it gives a spectrum of peaks for the sample that will be injected to represent the substance analytes that are present in the sample eluting from the column at different times. Retention time can be used to identify analytes, and the area under a peak is proportional to the amount of the analyte present. The concentration of the analyte in the original sample can be determined by calculating the area of the peak using a calibration curve that can be created by determining the response for a series of concentrations of the analyte. A calibration curve for carbon monoxide and hydrogen was prepared, and the amounts of carbon monoxide and hydrogen were determined using the integrated values for carbon monoxide and hydrogen (17.409, 5.393 min) and the calibration curve.

2.3.4 Photochemistry Liquid Product Analysis

The liquid products from the photocatalytic reactions were analyzed using ^{1}H NMR and ^{13}C NMR when appropriate. In all cases, the only product observed was formic acid, HCOOH. A formic acid calibration curve was constructed with deuterated water (D_2O) as an internal standard employing dimethyl sulfone. A standard solution containing 0.15 g dimethyl sulfone (DMS) in 15 mL of D_2O is prepared. A small portion (100 μL) was then taken from the irradiated samples and placed in an NMR tube together with 400 μL of D_2O to which a known quantity of dimethyl sulfone had been added. The sample was mixed well, and the ^{1}H NMR spectra were collected. The amount of formic acid was determined using the integrated values for the formic acid ($\delta \approx 8.1$ ppm) and a calibration curve.

2.3.5 Actinometer Results

Figures (2.3 and 2.5) explain that the volume of the irradiated sample and the molar extinction coefficient (ε) for DPA is 11,107 M^{-1} cm^{-1}. Hence, it is possible to calculate the number of moles of DPA consumed during the irradiation using equation (1).

$$\text{\# of moles DPA consumed} = \left(\frac{AINITIAL - AFINAL}{\varepsilon 372\ nm\ \iota}\right) \times V \quad (1)$$

$$\text{\# of moles DPA consumed} = \left(\frac{2.609871149 - 1.883626461}{11{,}107\ M^{-1}\ cm^{-1} \times 1\ cm}\right) \times 0.005\ L$$

$$\text{\# of moles DPA consumed} = 0.00000033\ \text{mole} = 3.3 \times 10^{-7}\ \text{mole}$$

As seen in equation (1), AINITIAL and AFINAL represent the absorbance of the solution at 372 nm before irradiation and after, respectively; $\varepsilon_{372\ nm}$ is the extinction coefficient of DPA at 372 nm in acetonitrile. The symbol l is used for the cuvette path length, and V for the sample volume on which absorption measurements have been taken. Applying standard volumetric dilution factors is necessary in cases where a dilution was made before the measurement.

The actinometer's quantum yield (Φ) is 0.019, as already determined. At this point, the number of moles of DPA consumed can be used to determine the number of moles of photons absorbed by our sample per unit time $\left(\frac{Nh\nu}{t}\right)$ by applying equation (2).

$$\frac{Nh\nu}{t} = \frac{moles\ of\ DPA\ consumed}{\Phi\ t} \quad (2)$$

$$\frac{Nh\nu}{t} = \frac{3.3 \times 10^{-7}\text{mole}}{0.019 \times 60\ \text{second}}$$

$$\frac{Nh\nu}{t} = 2.9 \times 10^{-8}\ \text{mole/second} \sim 3 \times 10^{-8}\ \text{mole/second}$$

In this equation, Φ represents the quantum yield of DPA consumption, and t represents irradiation time in seconds.

To find the quantum yield (Φ) of the reaction, the sample was exposed to light using the same setup as the actinometer. After irradiation, the number of moles of product formed or substrate used over time was measured with a suitable analytical method. Then, the quantum yield was calculated using Equation (3).

$$\Phi = \frac{\#\ of\ moles\ consumed\ or\ produced}{t} \times \left(\frac{Nh\nu}{t}\right)^{-1} \quad (3)$$

$$\Phi = \frac{3.3\times 10^{-7}\ \text{mole}}{60\ \text{second}} \times \left(3.0 \times 10^{-8}\ \frac{\text{mole}}{\text{second}}\right)^{-1}$$

$$\Phi = 0.01896285 \sim 0.019$$

Where $\left(\frac{Nh\nu}{t}\right)^{-1}$ is the reciprocal of the number of photons absorbed by the sample per unit time, and t is the irradiation time.

In many cases, the actinometer and the reaction of interest were performed multiple times on different time scales, and the results were corrected for the time of exposure, as seen in **Figures** 2.6 and 2.7.

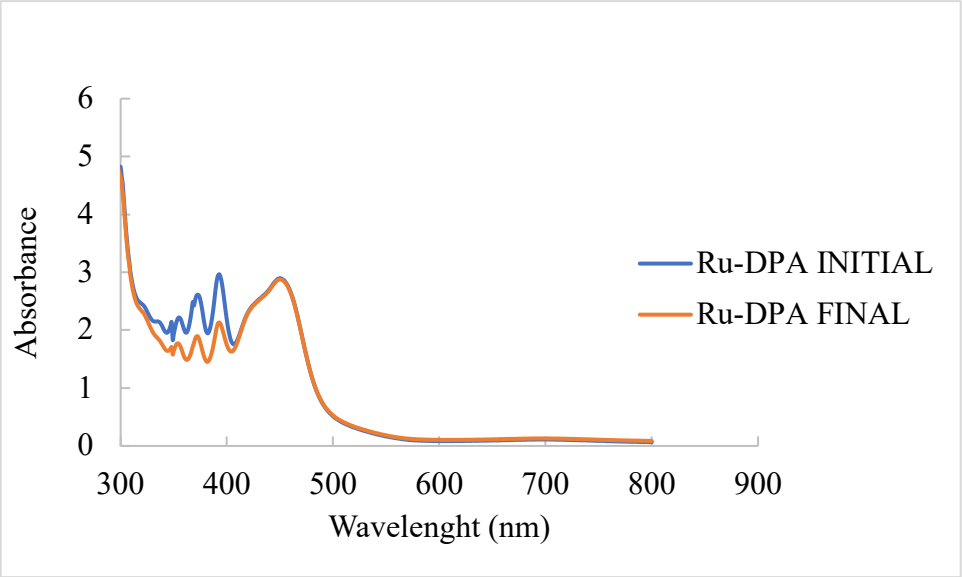

Figure 2.3. *Absorption spectra of a typical actinometry experiment performed with $Ru(bpy)_3(PF_6)_2$ (0.19 mM) and DPA (0.10 mM) in acetonitrile and irradiated with a 450 nm LED. AINITIAL is before irradiation, and AFINAL is after 1 minute of irradiation*

2.3.5.1 Calibration of a $Ru(bpy)_3(PF_6)_2$ Based Actinometer.

Measurement of the number of molecules consumed or produced and the number of photons absorbed by the system (in the case of metabolism) during the exposure period is required for the calculation of the photochemical reaction quantum yield (Φ). The distinction between incident and absorbed photons is essential; absorbed photons incite chemical transformation, while incident photons do not. Thus, the definition of quantum yield (Φ) of a photochemical reaction is given in Equation (4).

$$\text{Quantum Yield } (\Phi) = \frac{\#\text{ of molecules (or moles)consumed or produced per unit time}}{\#\text{ of photons (or einstein)absorbed per unit time}}\ \text{X } 100 \qquad (4)$$

For our $Ru(bpy)_3(PF_6)_2$ actinometer, we applied a well-documented process of singlet oxygen consumption in the oxidation of DPA, involving the photochemical conversion of 1,9-diphenylanthracene (DPA) to diphenyl anthracene endoperoxide (DPAO). The reaction involving DPA in the endoperoxide form is readily monitored by UV-Vis spectrophotometry, so that the concentration changes can be tracked by absorption changes at 372 nm, which is its distinct peak as seen in **Figures** 2.4 and 2.5.

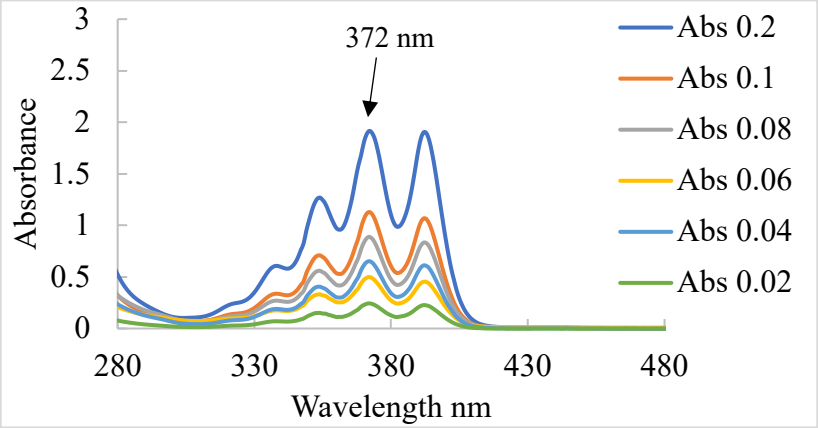

Figure 2.4. *UV-Vis Spectrum of DPA in acetonitrile at different concentrations.*

2.3.5.2 Absorbance @ 372 nm as a function of [DPA] for determination of ε of DPA:

By determining the ε for DPA in acetonitrile at 372 nm, we can correlate the change in absorption with the number of moles of DPA consumed, as seen in Figure 2.5.

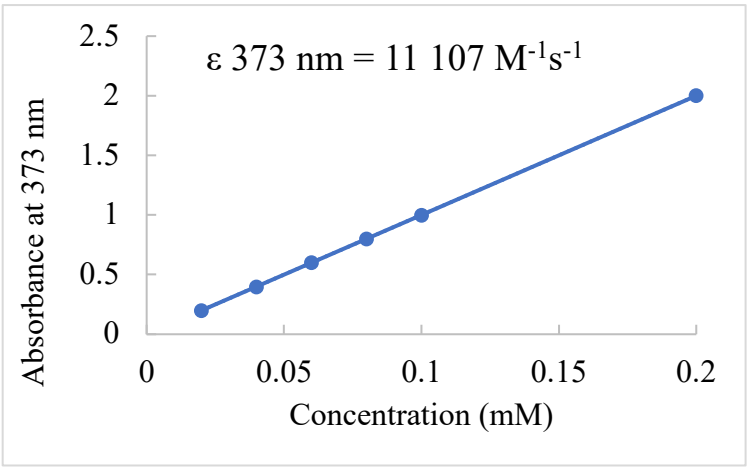

Figure 2.5. *Absorbance @ 373 nm as a function of [DPA] for determination of ε of DPA*

A typical experiment with our $Ru(bpy)_3(PF_6)_2$ actinometer system is shown in Fig. 2.6. As demonstrated, the consumption of DPA through its oxidation by $^1O_2$ generated from $Ru(bpy)_3(PF_6)_2$ can be easily monitored at 372 nm. By using the extinction coefficient (ε) at 372 nm, which we measured to be 11,107 M^{-1} cm^{-1} (see Figures 2.4 and 2.5), one can calculate the quantity of DPA present in the sample at any point in time by applying the Beer-Lambert law to make calculations for quantifying the conversion of DPA to its respective endoperoxide during a specified irradiation time.

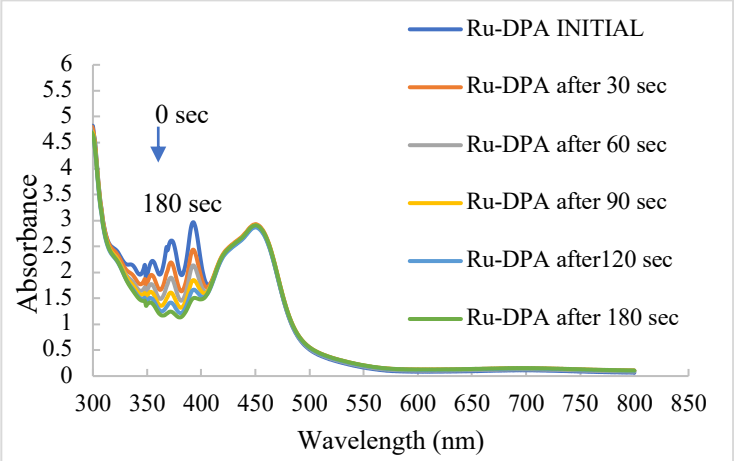

Figure 2.6. *Absorption spectra of a typical actinometry experiment performed with $Ru(bpy)_3(PF_6)_2$ (0.19 mM) and DPA (0.10 mM) in acetonitrile and irradiated with a 450 nm LED equipped*

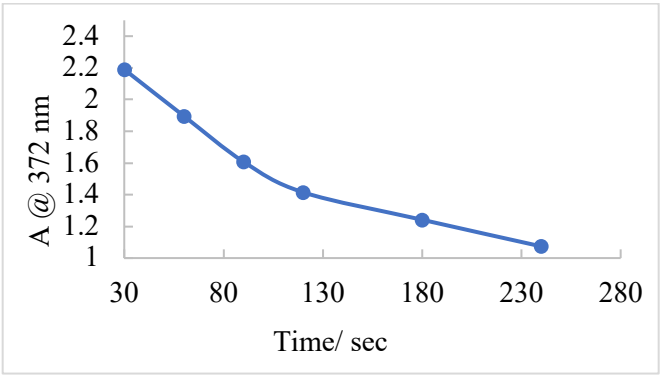

Figure 2.7. *Absorption at 372 nm vs. irradiation time corresponding to data from (fig.2.6)*

2.3.6 Photocatalytic CO_2 Reduction Results

The photocatalytic reduction of carbon dioxide was carried out in the glovebox in a glass reactor at room temperature using $[Ru\{\kappa^2\text{-}(Ph_2P)NMe(NC_5H_4)\}(CO)_2Cl_2]$ **(1)** or $[Ru\{\kappa^2\text{-}(Ph_2P)NH(NC_5H_4)\}(CO)_2Cl_2]$ **(2)** combined $\kappa^2$with $[Ru(bpy)_3](PF_6)_2]$ (PS) and TEOA-DMF (1:4

v/v) under a CO_2 atmosphere. The reaction mixture was exposed to 450 nm visible light from LEDs (1050 mW, 700 mA, $3.4x10^{-8}$ mol photons/sec). The gaseous product from this reaction was identified as CO and H_2 and quantified by gas chromatography (GC), thus confirming that under these conditions, (**1)** was a visible-light photoredox catalyst for the selective production of HCOOH, with other detected by-products CO and H_2 (Table 2.1). The molar ratio of HCOOH produced to catalyst **1** defined the turnover number for HCOOH (TON_{HCOOH} 1880) and a quantum yield of **6.4%**, and with 0.02 mM catalyst (1) and 0.02 mM $[Ru(bpy)_3]^{2+}$, the TON_{H2} of 900 was obtained (Table 2.1).

Catalyst (**2)**, as seen in Table 2.5, was also found to be a highly active catalyst for visible-light-induced CO_2 reduction. The system exhibits the maximum activity when DMF and TEOA are used, generating 318 μmol of formic acid (HCOOH) over 24 hours of irradiation with a turnover number (TON_{HCOOH}) of 3180 and a turnover frequency (TOF) of 132. Selectivity toward HCOOH reaches 89%, while the quantum yield (Φ%) is very high, 11%.

2.3.6.1 Photochemistry of $[Ru\{\kappa^2\text{-}(Ph_2PNMe)NC_5H_4\}(CO)_2(Cl)_2]$ Catalyst (1) at different conditions under CO_2 irradiation for 24 h.

A series of control experiments unequivocally demonstrated both the necessity and functions of the respective constituents of this catalytic system in HCOOH preparation. Reactions without a catalyst (**1**) under the same conditions did not form observable HCOOH. The entire photocatalytic reaction process was conducted under an N_2 atmosphere, such that HCOOH was not formed, and thus HCOOH must have come from CO_2 and not from the catalyst (**1**) disintegration or from the photosensitizer or from the electron donor. Catalyst (**1**) was a visible-light photoredox catalyst for selective HCOOH production along with other observed by-products as H_2 and traces of CO (Table 2.1). The mole ratio of HCOOH formed to catalyst (**1**) formulated the turnover number for HCOOH (TON_{HCOOH}), and with 0.02 mM (**1**), 0.02 mM $[Ru(bpy)_3]^{2+}$ and (DMF: TEOA, 4:1 v/v), the TON_{HCOOH} was found to be 1880 (Table 2.1).

Table 2.1. Effect of solvent and electron donor on the photocatalytic reduction of CO_2 with [Ru{κ^2-(Ph_2PNMe) NC_5H_4}$(CO)_2(Cl)_2$] (**1**) and [$Ru(bpy)_3(PF_6)_2$] as the photosensitizer (PS) (0.02 mM). In DMF, CH_3CN and DMA (4 mL) and different electron donors, TEOA, TEA, BNAH, AA and NaAA (1mL). Turnover number (TON) = (moles of product)/ (moles of catalyst). Irradiation with 450 nm light for 24 h.

Cat (**1**) (mM)	Solvent 4ml	e-donor 1ml	Amount of H_2 (μmol)	TON_{H2}	Amount of CO μmol	TON CO	Amount of HCOOH μmol	TON $_{HCOOH}$	(Φ%) $_{HCOOH}$	CS (%) $_{HCOOH}$
0.02	DMF	TEOA	90	900	11	110	188	1880	6.4	65
0.02	CH_3CN	TEOA	13	130	0	0	67	670	2.3	84
0	CH_3CN	TEOA	9	90	2	20	46	460	1.6	81
0.02	DMA	TEOA	20	200	5	50	82	820	2.8	77

-The photocatalytic reaction was performed using a Ru complex (**1**) (0.02 mM), $[Ru(bipy)_3]^{2+}$ as PS (0.02 mM), and CO_2-saturated different solvents and electron donors (4:1, v/v) solution, λ = 450 nm, 25 °C irradiation for 24 h.
-Turnover number based on the catalyst used and calculated: $5x10^{-3}$L x $0.02x10^{-3}$moles/L OR 0.1 micromoles of catalyst.

Photocatalytic CO_2 reduction reactions with a 1:1 photosensitizer-to-catalyst ratio ensured that all reactants are vital for catalytic activity. Reaction between $[Ru(ppy)_3(PF_6)_2]$ and catalyst (**1**) in DMF/TEOA (4:1, v/v) provided extensive formic acid (188 μmol) and hydrogen (90 μmol) production and minor CO (11 μmol) formation with strong activity and selectivity. Optimal electron donor choice was recognized as critical: other donors such as TEA, BNAH, AA, and Na AA could not produce products, highlighting optimum TEOA performance by virtue of strong reduction ability coupled with dual role as electron and proton provider.

The turnover number (TON) was defined in Chapter 1, Section 1.4.5, and was calculated using Equation (**5**). The same methodology was consistently applied to all results presented in this thesis.

$$\text{Turnover Number (TON)} = \frac{\mu\text{moles of } CO_2 \text{ reduction product formed}}{\mu\text{moles of catalyst used}} \qquad (\mathbf{5})$$

$$\text{TON(HCOOH)} = \frac{188\ \mu\text{mol}}{0.1\ \mu\text{mol}} = 1880$$

In general, amines are known for their electron-donating properties, and in the case of the photoreduction of CO_2, triethanolamine (TEOA) has a long history of application in photocatalytic CO_2 reduction and is a popular sacrificial electron donor for photosensitizer excited-state reductive

quenching. Although N, N-Dimethylformamide (DMF) is often chosen as a solvent in CO_2 reduction reactions because it has good solvation properties for CO_2 and metal complexes, it is not an utterly inert solvent in both reaction and analysis. Under visible light irradiation, particularly in the presence of photosensitizers and reduced metal catalysts, DMF may decompose through photochemistry or with metals to form CO and formic acid. Because these are among the products already sought after for the reduction of CO_2, their appearance as byproducts from the solvent makes it problematic to assign reliable quantification values to these products.[23]

The lower selectivity in DMF likely stems from enhanced H_2 evolution competing with CO_2 reduction, possibly due to DMF's coordinating ability or its effect on proton availability and reaction kinetics. DMF may facilitate proton reduction pathways more readily than CO_2 reduction, thus increasing H_2 generation and reducing overall selectivity for formic acid. In contrast, solvents like CH_3CN and DMA may better suppress hydrogen evolution, allowing for more selective CO_2 conversion.

Table 2.2 and Figure 2.8 depict how CO_2 photocatalytic reduction is affected by different concentrations of $[Ru(bipy)_3]^{2+}$ (photosensitizer) and catalyst (**1**) in **DMF**/TEOA solution, wherein formic acid (HCOOH) is recognized as the predominant product and hydrogen (H_2) and carbon monoxide (CO) recognized as side products with their respective turnover numbers (TON), quantum yields (Φ%), and HCOOH selectivity.

Table 2.2. Photocatalytic CO_2 reduction experiments with complexes $[Ru\{\kappa^2\text{-}(Ph_2PNMe)NC_5H_4\}(CO)_2(Cl)_2]$ (**1**) at different concentrations of $[Ru(bpy)_3(PF_6)_2]$ [PS] and catalyst. In **DMF** (4mL) as the solvent and **TEOA** (1 mL) as the electron donor (ED). Irradiation with 450 nm light for 24 h.

$[Ru(bipy)_3]^{2+}$ (mM)	Cat (**1**) (mM)	Amount of H_2 µmol	Amount of CO µmol	Amount of HCOOH µmol	TON_{HCOOH}	$(\Phi\%)_{HCOOH}$	Selectivity $(\%)_{HCOOH}$
0.02	0.02	90	11	188	1880	6.4	65
0	0.02	13	0	115	1150	3.9	90
0.02	0.01	115	9	192	3840	6.5	61
0.02	0.005	33	5	171	6840	5.8	81
0.02	0.001	78	6	153	30,600	5.2	65
0.02	0	32	2	115	1150	4.0	77
0.01	0.02	49	3	170	1700	5.8	77
0.005	0.02	33	1	150	1500	5.1	82
0.001	0.02	25	0	95	950	3.2	79

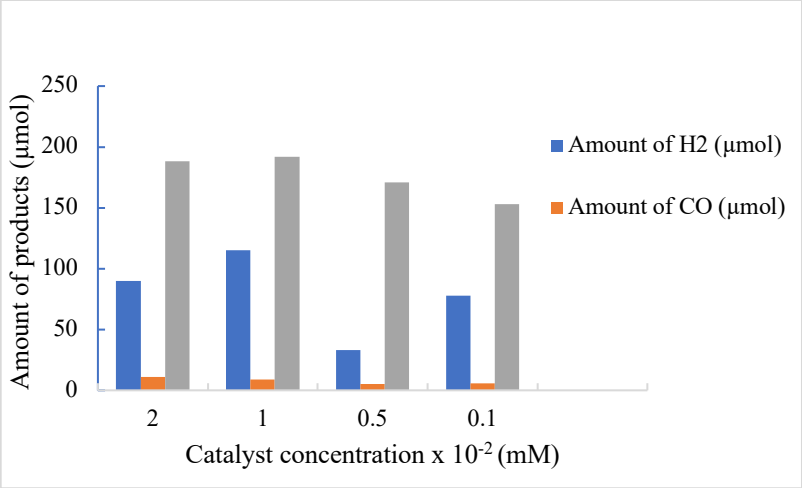

Figure 2.8. *Effect of the concentration of the catalyst (**1**) on the amount of products/ PS (0.02mM)*

The activities of the catalyst (**1**) and $[Ru(bpy)_3]^{2+}$ photosensitizer for photocatalytic reduction of CO_2 strongly depend on both components' loadings (see Table 2.2 and Figure 2.8). Optimal combined product amounts are achieved at high loadings of both the catalyst and photosensitizer, 0.02 mM, resulting in considerable amounts of HCOOH (188 µmol), H_2 (90 µmol), and CO (11 µmol). However, turnover numbers are reduced under these conditions. Lowering the catalyst loading slightly results in an improvement of formic acid selectivity and quantum efficiency, owing to the inhibition of the unwanted hydrogen evolution reaction. Without the photosensitizer, there is an affected lowering of product amount, confirming its essential function to drive photocatalysis. In conclusion, whereas the greatest values are realized at high loadings of both the catalyst and photosensitizer, a moderate loading of the catalyst provides a better compromise of activity and selectivity, and the trend of formic acid quantum efficiency corresponds to this trend.[26]

Despite being widely used in photochemical CO_2 reduction, $[Ru(bpy)_3]^{2+}$-type photosensitizers have a significant disadvantage in that they are prone to photo-induced dissociation of one N^N ligand during the catalytic process (Fig. 2.9). The resulting decomposed species, such as $[Ru(bpy)_2(solvent)_2]^{2+}$, can still act as active catalysts for CO_2 reduction. Consequently, photocatalytic activity without an intentionally added catalyst may influence product distribution. For instance, irradiation of a CO_2-saturated DMF-TEOA solution with only $[Ru(bpy)_3]^{2+}$ present produced formate as the primary product, due to the catalytic activity of the degraded Ru complex.[27-30]

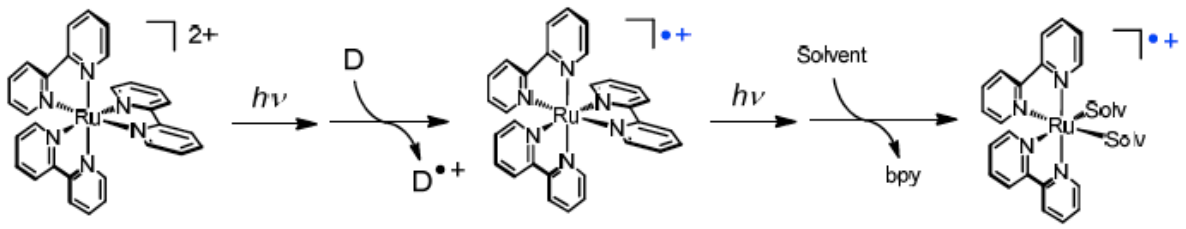

Figure 2.9. *Photo-labialization of the bpy ligand from the OERS of $[Ru(bpy)_3]^{2+}$.[28] Reproduced from reference number 28 with permission by the Coordination Chemistry Reviews.*

Table 2.3 reports comparative results obtained under identical conditions using DMA instead of DMF as the solvent, highlighting the photocatalytic efficiency of CO_2 reduction with the $[Ru(bpy)_3]^{2+}$ photosensitizer and catalyst (1), particularly for the formation of formic acid (HCOOH), as well as H_2 and CO.

Table 2.3. Photocatalytic CO_2 reduction experiments with complexes $[Ru\{\kappa^2\text{-}(Ph_2PN\mathbf{Me})NC_5H_4\}(CO)_2(Cl)_2]$ (**1**) at different concentrations of $[Ru(bpy)_3(PF_6)_2]$ [PS] and catalyst. In **DMA** (4 mL) as the solvent and **TEOA** (1 mL) as the electron donor (ED). Irradiation with 450 nm light for 24 h.

$[Ru(bipy)_3]^{2+}$ (mM)	Cat (**1**) (mM)	Amount of H_2 µmol	Amount of CO µmol	Amount of HCOOH µmol	TON $_{H2}$	TON_{HCOOH}	TOF_{HCOOH} (24h)	(Φ%) $_{HCOOH}$	Selectivity (%) $_{HCOOH}$
0.02	0.02	20	5	82	200	820	34	3.1	80
0	0.02	18	1	40	180	400	17	1.5	69
0.02	0	11	0	53	110	530	22	1.8	83
0.02	0.01	17	1	58	340	1160	48	2.2	77
0.02	0.005	13	0	53	520	2120	88	2	80
0.02	0.001	12	0	51	2400	10,200	425	1.9	81
0.01	0.02	14	0	57	140	570	24	2.1	80
0.005	0.02	13	0	49	130	490	20	1.8	79
0.001	0.02	13	0	42	130	420	18	1.6	76

The results reveal that HCOOH production strictly depends on catalyst (**1**), with zero formation of HCOOH without catalyst addition. Maximum turnover number (TON = 10,200) and turnover frequency (TOF = 425) of HCOOH are obtained at the lowest concentrations of catalyst and photosensitizer examined, consistent with high catalytic efficiency and low deactivation at low loadings. Quantum yield of Φ = 3.1% and selectivity of HCOOH of up to 80% are also high and confirm the system efficiency. Lack of $[Ru(bpy)_3]^{2+}$ leads to zero HCOOH production. General dependence of the reaction efficiency on the synergistic interaction of catalyst and photosensitizer is essential; their ratio optimization is paramount for an optimal HCOOH production.

Photocatalytic reactions are heavily reliant on light absorption and hence show a change in activity depending on the wavelength of the incident light, the concentration of the catalyst, and the intensity of the light. Quantum yield (Φ), defined in Chapter **1**, Section 1.4.8 and calculated using Equation (**4**), measures the efficiency of converting absorbed photons to chemical products such as formic acid, and the experimental details about photon flux are provided in Section 2.3.4. This method was consistently applied to all photocatalytic results in this thesis.

$$\text{Quantum Yield } (\Phi) = \frac{\text{\# of molecules (or moles) consumed or produced per unit time}}{\text{\# of photons (or einstein)absorbed per unit time}} \text{ X } 100 \qquad (4)$$

To calculate the quantum yield (Φ) for formic acid (HCOOH) production in a photocatalytic reaction, two important values must be determined during the specified irradiation period:

1. The number of HCOOH molecules produced
2. The number of photons absorbed by the system

Quantum Yield Equation

$$(\Phi) = \frac{\text{Number of molecules of HCOOH produced}}{\text{Number of photons absorbed}}$$

a. Calculate the moles of formic acid produced:

$$n_{HCOOH} = C_{HCOOH} \times V$$

b. Calculate the moles of photons absorbed

$$n_{photons} = \Phi_{light} \times t$$

The calculations can be summarized by following the steps below:

Measure Photon Flux

- Calculate the light intensity (photon flux) in mol photons/s by using chemical actinometry. Actinometers used are:
- Ferrioxalate actinometer for UV light
- $Ru(bpy)_3^{2+}$/DPA system for visible light

Φ_{light} = mol photons·s^{-1}

Determine Irradiation Time

Measure and record the time for which the sample will be exposed to light with a timer to note the time (in seconds), represented by the variable (t).

Calculate the Number of Photons Absorbed

Assuming 100% absorption (ideal case):

$n_{\text{photons}} = \Phi_{\text{light}} \times t$

Calculate Quantum Yield

$$\Phi = \frac{n\ \text{HCOOH}}{n\ \text{photons absorbed}}$$

An example of calculating the quantum yield from **Table 2.4** in the first row

- HCOOH produced: 188.0×10^{-6} mol
- Photon flux: 3.4×10^{-8} mol photons/s
- Irradiation time: 24 × 3600 s = 86400s

$n_{\text{photons}} = 3.4 \times 10^{-8} \times 86400 = 2.9 \times 10^{-3}$ mol photons

$$\Phi = \frac{188 \text{ x } 10^{-6}}{3.4 \text{ x } 10^{-8} \text{ x } 24 \text{ x } 3600} = 0.064\ (or\ 6.4\%)$$

Photocatalytic reduction of CO_2 is an emerging approach towards transforming carbon dioxide into value-added chemicals by utilizing light energy. Early experiments with 450 nm four-LED lamp irradiation and a $[Ru(bpy)_3]^{2+}$ photosensitizer displayed effective production of formic acid up to 188 μmol after a 24-hour exposure with a quantum yield of 6.4% (Table 2.2). Upon replacing the solvent from DMF to DMA, the production of formic acid fell to 82 μmol with a lower quantum yield of 3.1%, while hydrogen evolution also declined markedly from 90 μmol to 20 μmol (Tables 2.2& 2.3).

Uplifted by the above discoveries, we opted for greener, non-noble metal substitutes, specifically organic photosensitizers such as methyl orange, phenazine, and purpurin. However, purpurin has previously been reported as an effective photosensitizer in combination with Fe and Co catalysts [1,8]. Its use as a photosensitizer with catalyst (**1**) in the present study resulted in photocatalytic CO_2 reduction with markedly reduced activity, yielding only 8 μmol of formic acid. Methyl orange

proved inactive with any of the examined complexes (Table 2.4). These results highlight the setback of substituting noble metal sensitizers while ensuring high photocatalytic efficiency.

Table 2.4. Photocatalytic CO_2 reduction experiments with complexes [Ru{κ^2-(Ph_2PNMe)NC_5H_4}$(CO)_2(Cl)_2$] (**1**) at different types of [PS] (0.02 mM) and catalyst 1 (0.02 mM). In **DMF** (4 mL) as the solvent and **TEOA** (1 mL) as the electron donor (ED). Irradiation with 450 nm light for 24 h.

PS	Catalyst	Amount of H_2 µmol	Amount of CO µmol	Amount of HCOOH µmol	TON_{HCOOH}	Selectivity (%) $_{HCOOH}$
$[Ru(bpy)_3]^{2+}$	(**1**)	**90**	**11**	**188**	**1880**	**65**
Purpurin	(**1**)	0	0	**8**	**80**	**100**
Methyl orange	(**1**)	0	0	0	0	0

-The photocatalytic reaction was performed using a Ru complex (0.02 mM), $[Ru(bipy)_3]^{2+}$, Purpurin and Methyl orange as PS (0.02 mM), and CO_2-saturated different solvents and electron donors (4:1, v/v) solution, λ = 450 nm, 25 °C for 24 h.
-Turnover number based on the catalyst used and calculated: $5x10^{-3}$L x $0.02x10^{-3}$moles/L OR 0.1 micromoles of catalyst.
-Selectivity is calculated as µmol HCOOH/ (µmol HCOOH + µmol H_2) x 100

2.3.6.2 Photochemistry of [Ru{κ^2-(Ph_2PNH)NC_5H_4}$(CO)_2(Cl)_2$] Catalyst (2) at different conditions under CO_2 and irradiation with 450 nm light for 24 h.

In catalyst (**2**), where the N–Me group has been replaced with N–H, successful photocatalytic reduction was observed, albeit with higher TON_{HCOOH}, using the same conditions used in catalyst (**1**). The ruthenium catalysts all selectively produced HCOOH as a CO_2 reduction product. The catalyst bearing an N-H group yields a higher TON than the analogous catalyst bearing an N-Me group.

The influence of both the solvent and the choice of electron donor was also investigated. For instance, substituting DMF with CH_3CN or DMA as the reaction solvent led to a decrease in photocatalytic CO_2 reduction activity. Moreover, alternative electron donors, including TEA and BNAH, resulted in significantly lower performance (Table 2.5). As a result, the H_2, CO and HCOOH amounts are presented in the tables below. For each catalyst, a table including the amount of products, turnover number (TON), turnover frequency (TOF), catalytic selectivity (CS), and quantum efficiency (Φ) will be presented. All of these parameters were explained in Chapter 1.

Table 2.5. Selective HCOOH formation in photochemical CO_2 reduction using (0.02 mM) of [Ru{κ^2-$(Ph_2PNH)NC_5H_4$}$(CO)_2(Cl)_2$](**2**) and (0.02 mM) of [Ru$(bpy)_3(PF_6)_2$] as photosensitizer (PS) with different electron donors (1 mL) and different solvents (4 mL). Irradiation with 450 nm light for 24 h.

Solvent (4 mL)	e-donor (1 mL)	Amount of H_2 µmol	Amount of CO µmol	Amount of HCOOH µmol	TON_{HCOOH}	TOF $_{HCOOH\ (24h)}$	$(\Phi\%)_{HCOOH}$	Selectivity $(\%)_{HCOOH}$
DMF	TEOA	26	12	318	3180	133	11	89
DMF	TEA	5	0	0	0	0	0	0
DMF	BNAH	5	0	0	0	0	0	0
CH_3CN	TEOA	11	0	143	1430	60	5	93
CH_3CN	TEA	0	0	0	0	0	0	0
CH_3CN	BNAH	4	5	0	0	0	0	0
DMA	TEOA	48	4	62	620	26	2.1	54

-The photocatalytic reaction was performed using a Ru complex (2) (0.02 mM), $[Ru(bipy)_3]^{2+}$ as PS (0.02 mM), and CO_2-saturated different solvents and electron donors (4:1, v/v) solution, λ = 450 nm, 25 °C for 24 h.
-Turnover number based on the catalyst used and calculated: $5x10^{-3}$L x $0.02x10^{-3}$moles/L OR 0.1 micromoles of catalyst
-Selectivity is calculated as µmol HCOOH/ (µmol HCOOH + µmol H_2) x 100

The photocatalytic reduction of CO_2 of the $[Ru(bpy)_3]^{2+}$/complex (2) system strongly depends on the solvent and electron donor. The optimum activity is obtained by use of DMF with TEOA, yielding 318 µmol of HCOOH (TON 3180; TOF 133; Φ% = 11%; 89% selectivity). CH_3CN with TEOA also exhibits satisfactory activity (143 µmol; TON 1430; Φ% = 5), while DMA yields moderate activity (62 µmol; TON 620; Φ% = 2.1). Notably, no product is obtained by use of TEA or BNAH as the electron donors, irrespective of the solvent used, proving that TEOA is crucial for effective electron transfer. These findings prove that, by choice of solvent as well as electron donor, high photocatalytic efficiency as well as selectivity require crucial roles.

Table 2.6. Photocatalytic CO_2 reduction experiments with complexes [Ru{κ^2-(Ph_2PN**H**)NC_5H_4}$(CO)_2(Cl)_2$] (**2**) at different concentrations of [$Ru(bpy)_3(PF_6)_2$] [PS] and catalyst. In **DMA** (4 mL) as the solvent and **TEOA** (1 mL) as the electron donor (ED). Irradiation with 450 nm light for 24 h.

$[Ru(bipy)_3]^{2+}$ (mM)	Cat (**2**) (mM)	Amount of H_2 µmol	Amount of CO µmol	Amount of HCOOH µmol	TON $_{H2}$	TON $_{HCOOH}$	$TOF_{HCOOH\ (24h)}$	(Φ%) $_{HCOOH}$	Selectivity (%) $_{HCOOH}$
0.02	0.02	48	4	62	480	620	26	2.1	54
0	0.02	0	0	39	0	390	16	1.3	100
0.02	0	17	0	48	170	480	20	1.6	74
0.02	0.01	21	1	51	420	1020	43	1.7	71
0.02	0.005	15	1	54	600	2160	90	1.8	78
0.02	0.001	25	0	47	5000	9400	392	1.6	65
0.01	0.02	15	0	49	150	490	20	1.7	77
0.005	0.02	11	0	44	110	440	18	1.5	80
0.001	0.02	10	0	41	100	410	17	1.4	80

Table 2.6. assesses the performance of the $[Ru(bipy)_3]^{2+}$ (PS) and catalyst (**2**) system in the field of photocatalytic CO_2 reduction at different concentrations of the photosensitizer (PS) and the catalyst. The combination of 0.02 mM PS and 0.02 mM Ru-PN-H reaches the highest overall product formation, i.e., 48 µmol H_2, 4 µmol CO, and 62 µmol HCOOH, with a turnover number (TON) for HCOOH of 620 and a TOF of 26 after 24 hours. Lowering PS or catalyst concentrations influences both TON and selectivity. Notably, the 0.02 mM PS and 0.001 mM Ru-PN-H system shows a very high TON of 9400 and TOF of 392 for HCOOH with moderate HCOOH formation (47 µmol), indicating high catalyst efficiency at low loading. In contrast, the system without the PS or catalyst is found to yield zero or negligible product. Selectivity to HCOOH varies from 54% to 100%, the highest selectivity being in the absence of PS, showing that side reactions are suppressed, but catalytic activity is sacrificed. Overall efficiency of the system is highly dependent on the optimum ratio of PS to catalyst.

Table 2.7. Photocatalytic CO_2 reduction experiments with complexes [Ru{κ^2-(Ph_2PNH)NC_5H_4}$(CO)_2(Cl)_2$] (**2**) at different concentrations of [Ru$(bpy)_3(PF_6)_2$] [PS] and catalyst (**2**) constant (0.02 mM). In **DMA** (4 mL) as the solvent and **TEOA** (1 mL) as the electron donor (ED). Irradiation with 450 nm light for 24 h. photon flux = 3.4 x 10^{-8} photons/sec.

$[Ru(bipy)_3]^{2+}$ (mM)	Cat (**2**) (mM)	Amount of H_2 µmol	Amount of CO µmol	Amount of HCOOH µmol	TON_{H2}	TON_{HCOOH}	$TOF_{HCOOH\ (24h)}$	$(\Phi\%)_{HCOOH}$	Selectivity (%) HCOOH
0.02	0.02	48	4	62	480	620	26	2.1	54
0.01	0.02	15	0	49	150	490	20	1.7	77
0.005	0.02	11	0	44	110	440	18	1.5	80
0.001	0.02	10	0	41	100	410	17	1.4	80
0	0.02	0	0	39	0	390	16	1.3	100

Table 2.7 is a summary of the effects of varying concentrations of photosensitizer (PS) on the photocatalytic CO_2 reduction by (**2**). As PS decreases, the yield of formic acid (HCOOH) is reduced slightly from 62 to 47, but the selectivity is raised to 100% when there is no PS present, albeit with low yield. Reduced PS also reduces TON, quantum yield, and TOF, meaning that sufficient PS is necessary in order to get high catalytic efficiency and effective electron transfer. Reduction of the $[Ru(bpy)_3]^{2+}$ concentration from 0.02 to 0.001 mM led to less HCOOH production (TON was reduced from 26 to 17) because of presumably less light absorption.

Table 2.8. Photocatalytic CO_2 reduction experiments with complexes [Ru{κ^2-**(**Ph_2PNH)NC_5H_4}$(CO)_2(Cl)_2$] at different concentrations of catalyst (**2**) and [Ru$(bpy)_3(PF_6)_2$] [PS] constant (0.02 mM). In **DMA** (4 mL) as the solvent and **TEOA** (1 mL) as the electron donor (ED). Irradiation with 450 nm light for 24 h. photon flux = 3.4 x 10^{-8} photons/sec.

$[Ru(bipy)_3]^{2+}$ (mM)	Cat (**2**) (mM)	Amount of H_2 µmol	Amount of CO µmol	Amount of HCOOH µmol	TON_{H2}	TON_{HCOOH}	$TOF_{HCOOH\ (24h)}$	$(\Phi\%)_{HCOOH}$	Selectivity (%) HCOOH
0.02	0.02	48	4	62	480	620	26	2.1	54
0.02	0.01	21	1	51	420	1020	43	1.7	71
0.02	0.005	15	1	54	600	21600	90	1.8	78
0.02	0.001	25	0	47	5000	9400	392	1.6	65
0.02	0	17	0	48	0	480	20	1.6	74

Table 2.8 shows the photocatalytic activity of (**2**) towards CO_2 reduction, varying the catalyst concentration in a systematic manner with the photosensitizer (PS) being fixed at 0.02 mM. When the catalyst (**2**) concentration is decreased from 0.02 mM to 0.001 mM, the yield of HCOOH generated is relatively consistent (47–62 μmol), whereas the turnover numbers (TON_{HCOOH}) and turnover frequencies (TOF_{HCOOH}) increase exponentially with a maximum of 9400 and 392, respectively, at 0.001 mM catalyst. Such a high rise in TON and TOF at low catalyst concentration is due to the increased number of product molecules generated per unit of catalyst. In parallel with this, quantum yield (Φ%) decreases slightly from 2.1% to 1.6%, while HCOOH selectivity rises to a maximum of 78% before decreasing slightly. Overall, the data reveal falling catalyst concentration with increasing efficiency per molecule of catalyst, with similar absolute yields, thus pointing toward a compromise between catalyst economy and reaction kinetics. The trend seen is that decreasing the catalyst concentration can enhance the catalytic turnover, perhaps due to less interaction or aggregation effects among the catalysts.[1]

2.4 Proposed Mechanisms for Photocatalytic CO_2 Reduction

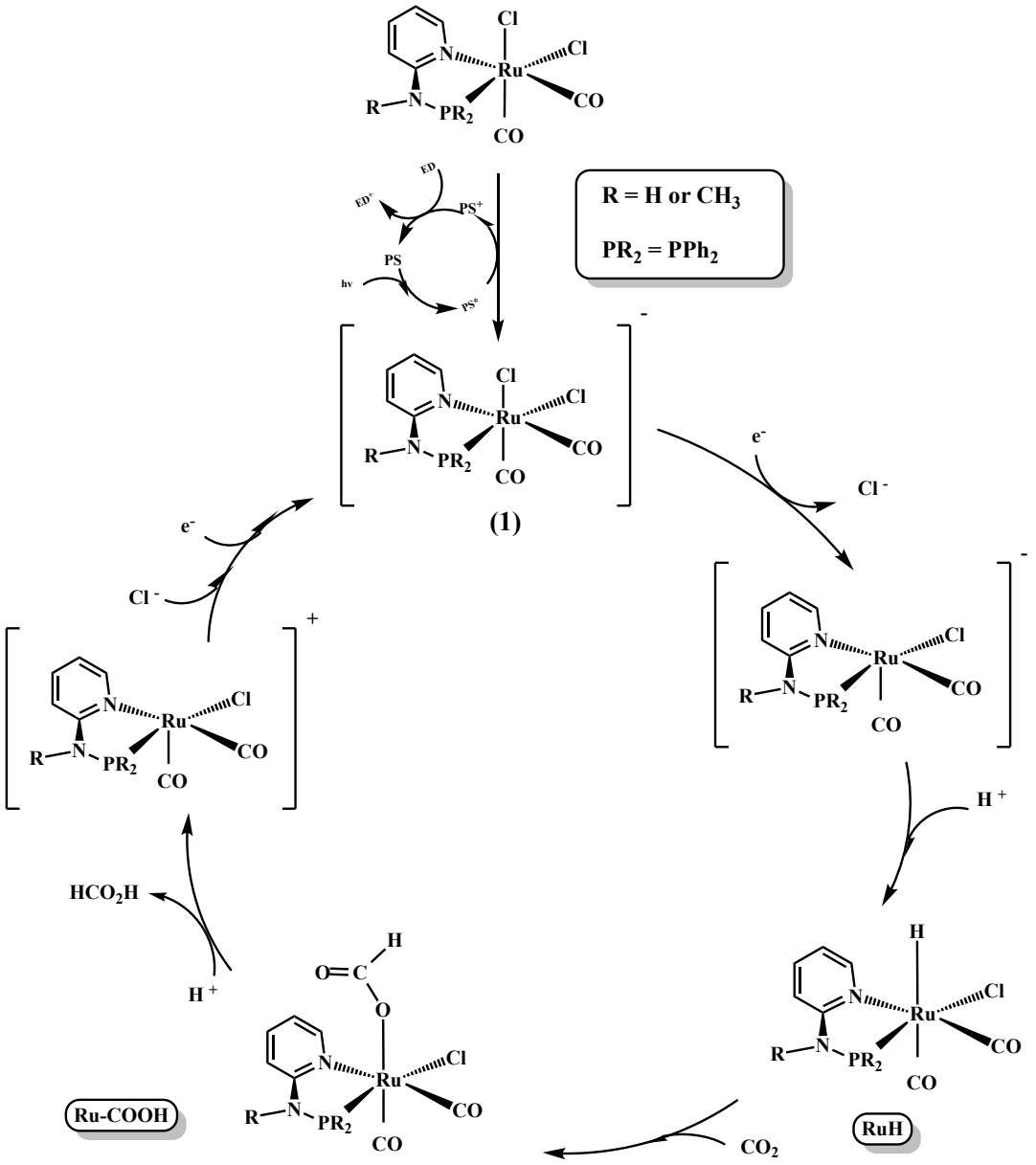

Figure 2.10. *Proposed Catalytic Cycle for the Reduction of CO_2 to HCOOH using complexes [Ru{k²-(Ph₂P)N**Me**(NC₅H₄)}(CO)₂Cl₂] or complexes [Ru{k²-(Ph₂P)N**H**(NC₅H₄)}(CO)₂Cl₂].*

Beginnings of the catalytic cycle mark the reduction of (**1**), which, during the optimizing routine, spontaneously dissociates a chloride anion with formation of a distorted square-pyramidal species,

designated as Ru^0 (Figure 2.10). Protonation of the resulting electron pair results in the formation of the hydride complex, Ru–H.

The conversion of CO_2 to formate is typically posited to proceed via a transition-metal hydride intermediate capable of assimilating CO_2 to generate a metallacarboxylic acid complex. Interaction of CO_2 with the Ru–H bond results in the creation of the metallacarboxylic acid compound, Ru–COOH, which then gets reduced and suffers proton transfer to yield the release of formic acid and the formation of a Ru(I) species (Ru^+). The catalytic cycle is then finally finished when Ru^+ gets reduced back to Ru^0 by the reduced photosensitizer (PS^-).

This hypothetical catalytic pathway also offers a competitive pathway to the formation of H_2. As shown in Figure 2.10, protonation of the hydride intermediate species (Ru–H) or coupling of two Ru–H species has the potential to evolve molecular hydrogen and hence circumvent the formic acid formation pathway. In reality, protonation of the hydride intermediate is typically challenging to prevent, implying that the reaction medium, especially the pK_a of the potential proton sources, has an enormous effect on the competition involving the formation of H_2 and the formation of formate.[26,31]

2.5 Electrochemistry Experiment

Figure 2.11 displayed is a cyclic voltammogram (CV) for the complex (**1**), obtained under a nitrogen (N_2) atmosphere. The following graph illustrates the response current (in μA) dependence on the applied potential (in V vs. Fc/Fc^+) from 0 V to -2.7 V. The CV curves reveal three principal cathodic (reduction) peaks at ca. -1.66 V, -2.03 V, and -2.3 V, indicating that Ru-PN-Me undergoes a sequence of electron transfer events under the experimental conditions. Reduction reactions are more likely to be connected with stepwise electron addition to the metal centre or the ligands of the complex. The use of a nitrogen atmosphere guarantees that such redox behaviour is characteristic of the inherent properties of the complex, free from any contribution from oxygen or other reactive species. The voltammogram shape, with its fairly broad and asymmetric peaks, indicates that some of the redox processes are quasi-reversible or chemically coupled with follow-up reactions.

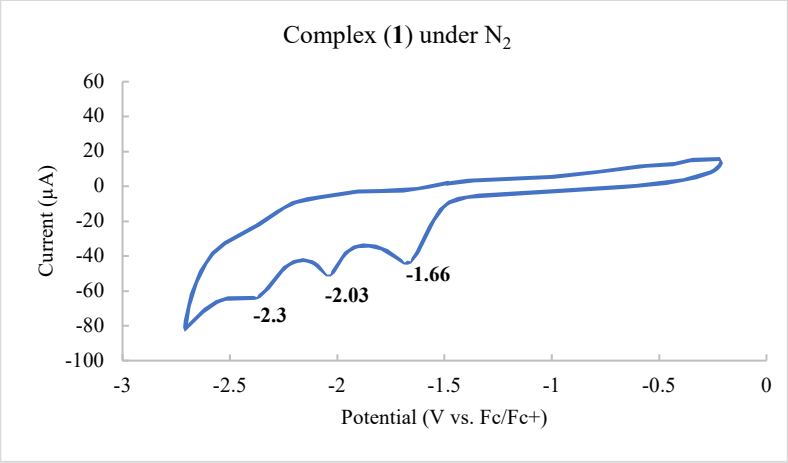

Figure 2.11. *Cyclic voltammograms of 0.02 mM catalyst (**1**) under N_2 in CH_3CN with 0.1 M $(n\text{-}Bu)_4NPF_6$ supporting electrolyte at 100 mV/s.*

Figure 2.12 is a cyclic voltammogram (CV) of the complex (**2**) measured in a nitrogen (N_2) atmosphere, with current (µA) displayed versus the applied potential (V vs. Fc/Fc^+). The voltammogram indicates multiple redox processes, as labelled by the consecutive cathodic and anodic peaks. Two split reduction peaks at −1.06 and −2.24 V vs. Fc/Fc^+ are observed, indicating sequential reduction processes that are probably linked to the metal centre, corresponding to the reduction processes of Ru^{II}/Ru^{I} and Ru^{I}/Ru^{0}, respectively.

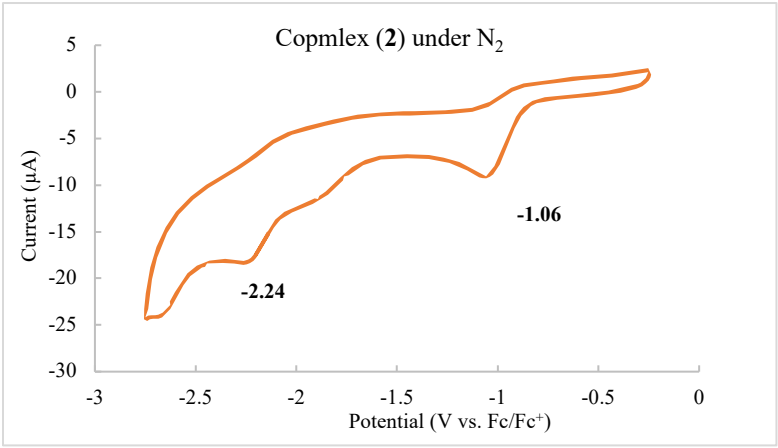

Figure 2.12. *Cyclic voltammograms of 0.02 mM of complex (**2**) under N_2 in CH_3CN with 0.1 M $(n\text{-}Bu)_4NPF_6$ supporting electrolyte at 100 mV/s.*

The lack of catalytic current in the presence of N_2 demonstrates that these effects are inherent to the complex when free of CO_2 or a proton source, providing a background against which comparisons may be made in electrocatalytic experiments. This kind of electrochemical characterization is significant to gain insight into the redox properties and possible catalytic activity of transition-metal complexes, e.g., Complex (**2**). The same methods are routinely applied to establish the electrochemical characteristics of complexes before examining their activity in carbon dioxide reduction or hydrogen evolution.

2.6 Conclusion

In this thesis, we have synthesized new Ru-based catalysts, complexes **1** and **2,** bearing PN ligands (R = H or CH_3) and investigated their catalytic performance for the selective production of formic acid (HCOOH).

The present work describes a photochemical dielectronic selectivity, reduction of carbon dioxide to a catalytic formic acid system performed with high efficiency, giving a maximum quantum yield of 11% and selectivity around 89%. used complex (**2**) with DMF-TEOA.

The purpurin catalytic systems are also applied in complex (**1)**, generating a small amount of formic acid, approximately 8 micromoles, and no detectable CO and H_2.

We have shown that dimethylacetamide (DMA) is an effective substitute for dimethylformamide (DMF) in the photocatalytic reduction of carbon dioxide (CO_2), in which complex (**1**), $[Ru(bpy)_3]^{2+}$, and triethanolamine (TEOA) serve respectively as the photosensitizer, catalyst, and sacrificial electron donor. The photoreduction of CO_2 occurred efficiently in the DMA/TEOA (4:1, v/v) solution system and exhibited catalytic activities comparable with those in DMF/TEOA. Furthermore, DMA does not lead to contamination of formic acid, whereas DMF is decomposed partially to yield formic acid. The utilization of DMA as a solvent instead of DMF allows the analysis of formic acid even with more forcing analytical conditions. Even after the quantities of formic acid yielded by the decomposition of DMF under N_2 are subtracted from the quantities of formic acid yielded in the CO_2 reduction in DMF/TEOA (4:1, v/v), the quantities are larger than those in the CO_2 reduction in DMA/TEOA (4:1, v/v). The precise origin of the difference in H_2/formic acid selectivity between DMF and DMA is uncertain, and the focus of current research.

Experiments were carried out to better understand the factors that cause the catalysis to stop. The loss of catalytic activity is mainly due to the decomposition of the catalyst and photosensitizer, as well as the consumption of TEOA. Quantum yields for HCOOH production (Φ_{HCOOH}) were determined by ferrioxalate actinometry. When $[Ru(bpy)_3]^{2+}$ was used as the sensitizer, the quantum yields for the overall photocatalytic reduction of CO_2 to HCOOH were 6.4% for complex (**1**) and 11% for complex (2) after irradiation for 24 h at 450 nm with DMF-TEOA.

A comparison between the two novel ruthenium catalysts presented in this study, complex (**2**) recorded the highest TON, at 3180, followed by Catalyst (**1**), at 1880. Even though these two novel Ru catalysts had high selectivity and good Φ%. These results are important in that they also demonstrate the impact that changing ligand substituents has on the catalytic reactivity. Comparing these two catalysts, the optimal catalyst has R = H and R' = phenyl and yields formic acid with a greater TON than the second catalyst, which has R = CH_3 and R' = phenyl. One reason for this activity is the electron-donating nature of the R groups. The methyl R group is more electron-donating than the hydrogen R group, placing more electron density on the ligand and metal. The greater electron density can render the catalyst more resistant to reduction, thus resulting in a lower TON with the methyl R substituent.

Homogeneous catalysis of transition metal complexes can find application in the generation of products, namely formic acid and CO. Formic acid can indeed be considered as an intriguing intermediate or, straightforwardly, as energy storage. In most cases, formic acid is thought to be generated by the reaction of a hydride donor intermediate with CO_2. In-depth studies to establish the variables that affect the specific generation of formic acid, carbon monoxide, and hydrogen would certainly be beneficial.

2.7 References

1. Guo, Z.; Cheng, S.; Cometto, C.; Anxolabéhère-Mallart, E.; Ng, S.-M.; Ko, C.-C.; Liu, G.; Chen, L.; Robert, M.; Lau, T.-C. *Highly Efficient and Selective Photocatalytic CO_2 Reduction by Iron and Cobalt Quaterpyridine Complexes*. J. Am. Chem. Soc. **2016**, *138* (30), 9413–9416.

2. Benson, E. E.; Kubiak, C. P.; Sathrum, A. J.; Smieja, J. M. *Electrocatalytic and Homogeneous Approaches to Conversion of CO_2 to Liquid Fuels*. Chem. Soc. Rev. **2009**, *38* (1), 89–99.

3. Aresta, M.; Dibenedetto, A.; Angelini, A. *Catalysis for the Valorization of Exhaust Carbon: From CO_2 to Chemicals, Materials, and Fuels. Technological Use of CO_2*. Chem. Rev. **2014**, *114* (3), 1709–1742.

4. Hawecker, J.; Lehn, J.-M.; Ziessel, R. *Efficient Photochemical Reduction of CO_2 to CO by Visible Light Irradiation of Systems Containing $Re(bipy)(CO)_3X$ or $Ru(bipy)_3^{2+}$–Co^{2+} Combinations as Homogeneous Catalysts*. J. Chem. Soc., Chem. Commun. **1983**, (9), 536–538.

5. Takeda, H.; Koike, K.; Inoue, H.; Ishitani, O. *Development of an Efficient Photocatalytic System for CO_2 Reduction Using Rhenium(I) Complexes Based on Mechanistic Studies*. J. Am. Chem. Soc. **2008**, *130* (6), 2023–2031.

6. Takeda, H.; Ishitani, O. *Development of Efficient Photocatalytic Systems for CO_2 Reduction Using Mononuclear and Multinuclear Metal Complexes Based on Mechanistic Studies*. Coord. Chem. Rev. **2010**, *254* (3–4), 346–354.

7. Hawecker, J.; Lehn, J.-M.; Ziessel, R. *Photochemical Reduction of Carbon Dioxide to Formate Mediated by Ruthenium Bipyridine Complexes as Homogeneous Catalysts*. J. Chem. Soc., Chem. Commun. **1985**, (2), 56–58.

8. Ishida, H.; Terada, T.; Tanaka, K.; Tanaka, T. *Photochemical Carbon Dioxide Reduction Catalyzed by Bis(2,2'-bipyridine)dicarbonylruthenium(2^+) Using Triethanolamine and 1-Benzyl-1,4-dihydronicotinamide as an Electron Donor*. Inorg. Chem. **1990**, *29* (5), 905–911.

9. Lehn, J.-M.; Ziessel, R. *Photochemical Generation of Carbon Monoxide and Hydrogen by Reduction of Carbon Dioxide and Water under Visible Light Irradiation*. Proc. Natl. Acad. Sci. U.S.A. **1982**, *79* (2), 701–704.

10. Tinnemans, A. H. A.; Koster, T. P. M.; Thewissen, D. H. M. W.; Mackor, A. *Tetraaza-Macrocyclic Cobalt(II) and Nickel(II) Complexes as Electron-Transfer Agents in the Photo(electro)chemical and Electrochemical Reduction of Carbon Dioxide*. Recl. Trav. Chim. Pays-Bas **1984**, *103* (10), 288–295.

11. Morris, A. J.; Meyer, G. J.; Fujita, E. *Molecular Approaches to the Photocatalytic Reduction of Carbon Dioxide for Solar Fuels*. *Acc. Chem. Res.* **2009**, *42* (12), 1983–1994.

12. Thoi, V. S.; Kornienko, N.; Margarit, C. G.; Yang, P.; Chang, C. J. *Visible-Light Photoredox Catalysis: Selective Reduction of Carbon Dioxide to Carbon Monoxide by a Nickel N-Heterocyclic Carbene–Isoquinoline Complex*. *J. Am. Chem. Soc.* **2013**, *135* (38), 14413–14424.

13. Takeda, H.; Ohashi, K.; Sekine, A.; Ishitani, O. *Photocatalytic CO_2 Reduction Using Cu(I) Photosensitizers with a Fe(II) Catalyst*. *J. Am. Chem. Soc.* **2016**, *138* (13), 4354–4357.

14. Fei, H.; Sampson, M. D.; Lee, Y.; Kubiak, C. P.; Cohen, S. M. *Photocatalytic CO_2 Reduction to Formate Using a Mn(I) Molecular Catalyst in a Robust Metal–Organic Framework*. *Inorg. Chem.* **2015**, *54* (14), 6821–6828.

15. Cohen, K. Y.; Nedd, D. G.; Evans, R.; Bocarsly, A. B. *Mechanistic Insights into CO_2 Conversion to CO Using Cyano Manganese Complexes. Dalton Trans.* **2023**, *52* (22), 7524–7537.

16. Li, A.; Cao, Q.; Zhou, G.; Schmidt, B. V. K. J.; Zhu, W.; Yuan, X.; Huo, H.; Gong, J.; Antonietti, M. *Three-Phase Photocatalysis for the Enhanced Selectivity and Activity of CO_2 Reduction on a Hydrophobic Surface. Angew. Chem., Int. Ed.* **2019**, *58* (41), 14549–14555.

17. Nakajima, T.; Tamaki, Y.; Ueno, K.; Kato, E.; Nishikawa, T.; Ohkubo, K.; Yamazaki, Y.; Morimoto, T.; Ishitani, O. *Photocatalytic Reduction of Low Concentration of CO_2. J. Am. Chem. Soc.* **2016**, *138* (42), 13818–13821.

18. Reithmeier, R. O.; Meister, S.; Siebel, A.; Rieger, B. *Synthesis and Characterization of a Trinuclear Iridium (III) Based Catalyst for the Photocatalytic Reduction of CO_2. Dalton Trans.* **2015**, *44* (14), 6466–6472.

19. Tamaki, Y.; Koike, K.; Ishitani, O. *Highly Efficient, Selective, and Durable Photocatalytic System for CO_2 Reduction to Formic Acid. Chem. Sci.* **2015**, *6* (12), 7213–7221.

20. Yang, Y.; Gurnham, J.; Liu, B.; Duchateau, R.; Gambarotta, S.; Korobkov, I. *Selective Ethylene Oligomerization with Chromium Complexes Bearing Pyridine–Phosphine Ligands: Influence of Ligand Structure on Catalytic Behavior. Organometallics* **2014**, *33* (20), 5749–5757.

21. Yang, Y.; Gurnham, J.; Liu, B.; Duchateau, R.; Gambarotta, S.; Korobkov, I. Selective ethylene oligomerization with chromium complexes bearing pyridine-phosphine ligands: influence of ligand structure on catalytic behavior. *Organometallics*. **2014**, 33, 5749–5757.

22. Hameed, Y.; Rao, G. K.; Ovens, J. S.; Gabidullin, B.; Richeson, D. Visible-Light Photocatalytic Reduction of CO_2 to Formic Acid with a Ru Catalyst Supported by N,N′-

Bis(diphenylphosphino)-2,6-diaminopyridine Ligands. *ChemSusChem* **2019**, *12* (15), 3453–3457.

23. Pitre, S. P.; McTiernan, C. D.; Vine, W.; DiPucchio, R.; Grenier, M.; Scaiano, J. C. *Visible-Light Actinometry and Intermittent Illumination as Convenient Tools to Study Ru(bpy)₃Cl₂-Mediated Photoredox Transformations*. Sci. Rep. **2015**, *5*, 16397.

24. Akbar, H.; Javed, M. S.; Iqbal, S. T.; Khan, M. I.; Anwar, T.; Anjum, F.; Ahmad, A.; Muneeb, M.; Ali, A.; Oh, W.-C. *A Review of Photocatalytic CO_2 Reduction: Exploring Sustainable Carbon Emission Mitigation from Thermodynamics to Kinetics and Strategies for Enhanced Efficiency*. Catal. Surv. Asia **2024**, 61 (3), 367–390.

25. Gong, K.; Fang, Q.; Gu, S.; Li, S. F. Y.; Yan, Y. *Nonaqueous Redox-Flow Batteries: Organic Solvents, Supporting Electrolytes, and Redox Pairs. Energy Environ*. Sci. **2015**, *8* (11)

26. Ḥamīd, Y. *Exploring New Catalysts for Photocatalytic Carbon Dioxide Reduction Using Homogeneous Transition Metal Complexes*; Ph.D. Thesis, University of Ottawa, Department of Chemistry, Ottawa, **2019**.

27. Fujita, E.; Grills, D. C.; Manbeck, G. F.; Polyansky, D. E. *Understanding the Role of Inter and Intramolecular Promoters in Electro- and Photochemical CO_2 Reduction Using Mn, Re, and Ru Catalysts*. *Acc. Chem. Res.* **2022**, *55* (5), 616–628.

28. Kuramochi, Y.; Ishitani, O.; Ishida, H. *Reaction Mechanisms of Catalytic Photochemical CO_2 Reduction Using Re(I) and Ru (II) Complexes*. *Coord. Chem. Rev.* **2018**, *373*, 333–356.

29. Lehn, J.-M.; Ziessel, R. *Photochemical Reduction of Carbon Dioxide to Formate Catalyzed by 2,2'-Bipyridine- or 1,10-Phenanthroline-Ruthenium (II) Complexes.* J. Organomet. Chem. **1990**, 382 (1), 157–173.

30. Hawecker, J.; Lehn, J.-M.; Ziessel, R. *Photochemical Reduction of Carbon Dioxide to Formate Mediated by Ruthenium Bipyridine Complexes as Homogeneous Catalysts.* J. Chem. Soc., Chem. Commun. **1985**, (2), 56–58.

31. Taheri, A.; Berben, L. A. Making C–H Bonds with CO_2: *Production of Formate by Molecular Electrocatalysts. Chem. Commun.* **2016**, *52* (9), 1768–1777.

Chapter 3: Photocatalytic Activity of Ruthenium (II) Complex with Isopropyl Phosphinoaminopyridine Ligand and Generation of Formic Acid and Hydrogen through Reduction of Carbon Dioxide and Water Splitting under Visible Light Irradiation.

3.1 Introduction

With the backdrop of global warming and the need for a shift from fossil fuels to green energy sources, research into effective energy-storing technologies must take center stage quickly.[1-3] Chemical storage, as in the chemical bonds of an energy-dense substance such as hydrogen from water splitting, yields better gravimetric densities.[4] In the last few years, energy storage by the reduction of the CO_2 molecule has had renewed popularity.[5,6] Even though this reduction of the CO_2 molecule into energy-dense liquid or gaseous fuels constitutes a highly intriguing fundamental problem, the technological implementation thereof into devices (electrolyzer connected to photovoltaics or photoelectrochemical cells) proves highly difficult due to the excellent stability of the CO_2 molecule and, accordingly, the endergonic character of the transformation. In addition, the reactions involve several electron/proton pairs and thus require effective catalysts to mediate these transformations. Lastly, a persistent problem consists of the competition with the proton reduction into dihydrogen, which requires the conception of selective catalysts and suitable adjustment of the reaction conditions (temperature, pressure, solvent…).[1]

As for catalysts for reducing CO_2, significant research exists for two classes of compounds: solid materials and homogeneous metal complexes (organometallic and coordination complexes). Though respecting the first strategy, special attention will be given herein to the advantages of molecular catalysts, which tend to be ideal for the fine-tuning of their reactivity by means of ligand synthetic modifications.[1]

Photocatalytic water splitting, producing hydrogen (H_2), has attracted increasing attention, because H_2 is a clean energy source for the future to reduce dependence on fossil fuels and emissions of greenhouse gases in the long term.[3,7,8] Extensive efforts have explored the development of photocatalytic H_2 evolution systems, which consist of an electron donor, a photosensitizer, and a catalyst. Photosensitizers (PSs) for HER can be ruthenium- or iridium-type complexes, organic dyes, or inorganic semiconducting materials.[9]

Ruthenium-containing photosensitizers, particularly $[Ru(bpy)_3]^{2+}$ and its structural counterparts, have been given widespread attention, and these molecules are applied extensively in many relevant photochemical technologies.[10]

There have also been strategies used to investigate photosynthetic approaches toward hydrogen production through the reduction of water, including semiconductor devices[11] as transition-metal complexes functioning in heterogeneous [12,13] or homogeneous phases.[13-16] For molecular catalytic systems featuring transition-metal complexes, the process generally depends on more than one component; a significant benefit of such an approach is that each component may be synthetically designed and optimized for its role in the photocatalytic cycle.[9]

Several sacrificial reductants are also applicable, including triethylamine (TEA), triethanolamine (TEOA), and ascorbic acid (AA), among many others. In evaluating the performance of the photocatalytic hydrogen evolution catalyst, TON, the Φ for hydrogen, and the catalyst selectivity are critical parameters as previously described in sections 1.4.5 and 1.4.8, Chapter 1.[9]

Sacrificial agents, also generally referred to as electron donors, play an integral part in the synthesis of hydrogen (H_2) by photocatalysis due to the thermodynamically unfavorable nature of the water split reaction (ΔH_0 = 286 kJ mol^{-1}).[17] TEOA, TEA, and AA are some sacrificial agents for the enhancement of photocatalysts for the reduction of water. In acidic conditions, ascorbic acid acts as both a proton and electron donor, which results in the creation of dehydroascorbic acid as a secondary product.[18] Use of triethylamine and triethanolamine as sacrificial agents becomes more effective in more alkaline conditions. Oxidative reactions with either triethylamine or triethanolamine lead to the creation of radical cations, which then decompose to produce protons, electrons, and some byproducts, such as aldehydes and secondary amines.[19]

This chapter aims to widen the scope of this thesis from the photoreduction of carbon dioxide (CO_2), which mainly produces carbon-based products with hydrogen (H_2) as a byproduct, to the intentional production of hydrogen through photocatalytic water splitting. Water splitting as a process driven by visible-light irradiation constitutes a promising means for the production of clean energy since it not only mitigates the emission of CO_2 by alleviating the dependence on fossil fuels but also produces high-grade H_2 as a green energy vector. This study draws focus towards the

development of a photocatalytic system aimed principally at two tasks: (i) enhancing the yield of hydrogen production and (ii) achieving the selective production of high-grade H_2. Towards these ends, a ruthenium-based homogeneous compound, [Ru{κ²-(iPr_2PNMe)NC_5H_4}$(CO)_2(Cl)_2$] (**3**), serves as a potential catalyst. This compound not only serves as a test for the suitability of facilitating visible-light-driven water splitting but also for playing a binary role of reducing the CO_2 by enhancing the formation of formic acid (HCOOH) as well as H_2.

3.2 The Synthesis and Characterization of the Complex (3)

3.2.1 Experimental procedures

All chemicals, solvents, and reagents employed in the current study were of analytical quality and were utilized as received. All NMR spectra (^1H, ^{13}C and ^{31}P) were recorded on 300 or 400 MHz spectrometers at 25 °C with chemical shifts reported in ppm using the residual protons of the NMR solvent as internal standards.

"PNMe" (iPr_2P)NMe(NC_5H_4) ligand was synthesized using the literature-described procedure.[20] The reaction of $[Ru(CO)_3Cl_2]_2$ and N-(diisopropylphosphino)-2-methyl aminopyridine ligand directly provided the complex [Ru{κ²-(iPr_2P)NMe(NC_5H_4)}$(CO)_2Cl_2$] (R= Me) in 69% yield.[21] The catalyst's (**3**) identity was established by matching the results of the literature and our independent NMR, and UV-Vis spectroscopy. Photochemical procedures used within this chapter have been previously established in section 2.2.6 of Chapter 2, and the electrochemical methods have also been presented in section 2.6 of Chapter 2.

3.2.2 Synthesis and characterization of N-(diisopropylphosphino)-2-(methylamino) pyridine ligands (iPr_2P)NMe(NC_5H_4)

This ligand was synthesized following the procedure described in the literature (Scheme 3.1).[20] In the glovebox, a mixture of 1.08g (10.0 mmol, 1.026 ml) of 2-(methylamino) pyridine in 25 ml of diethyl ether. The flask was sealed before being removed from the glovebox. The flask was chilled to -78°C with a dry ice and acetone bath. n-BuLi (10 mmol, 1.6 M in hexane, 6.25 ml) was added dropwise. After 30 minutes of stirring, the reaction mixture was allowed to warm to room temperature and was stirred for an additional 3 hours. $[(CH_3)_2CH]_2PCl$] (chlorodiisopropylphosphine) (11 mmol, 1.9 ml) was then added dropwise at 0°C, and the reaction mixture was stirred overnight at room temperature. The reaction mixture was filtered twice using

diethyl ether (2 × 15 ml), and the solvent was removed to give a yellow oil. Yield: 1.89 g (65%). ^{1}HNMR (400 MHz, $CDCl_3$, 25 ºC): δ= 8.10 (1H, d), 7.10-7.25 (2H, m), 6.50-6.73 (1H, t), 3.15 (3H, s), 2.19 (2H, s), 1.09-1.38 (6H, q), 0.9-1.05 (6H, q).

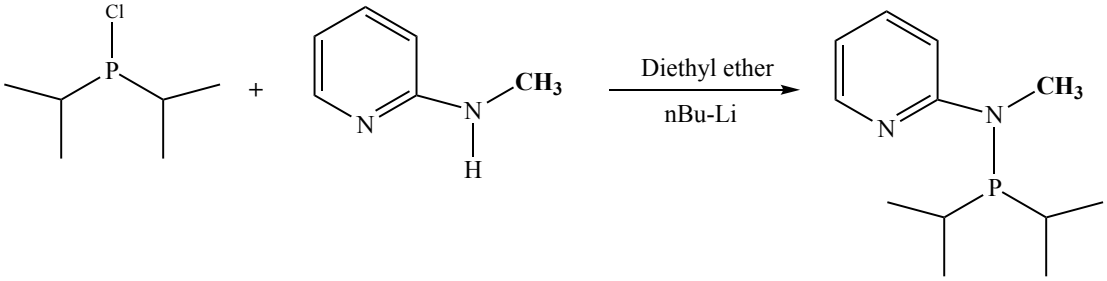

Scheme 3.1. Synthetic scheme for the preparation of $([(CH_3)_2CH]_2P)NMe(NC_5H_4)$ ligand.

3.2.3 Synthesis and Characterization of $[Ru\{\kappa^2\text{-}(iPr_2PNMe)NC_5H_4\}(CO)_2(Cl)_2]$ (3)

This complex was synthesized following the procedure described in the literature (Scheme 3.2).[21] In a glove box, a mixture was prepared by dissolving 0.2 g (0.8 mmol) of the ligand (diisopropylphosphino)-2-(methylamino) pyridine ligand in 30 mL of toluene. To this solution was added $[Ru\ (CO)_3Cl_2]_2$ (0.204 g, 0.4 mmol). The flask was removed from the glovebox and connected to a Schlenk line via a reflux condenser. The reaction mixture was stirred and heated to 110 °C under N_2 for over 16 h. The solution was cooled to room temperature. The reaction mixture was filtered, and the precipitate was washed with hexane to give the complex (**3**). Yield 0.3847 g (69%). Single crystals were grown by slow diffusion of hexane and DCM. ^{1}HNMR (400 MHz, DMSO, 25 ºC): δ= 9.11 (1H, d), 7.85-8.02 (1H, t), 7.05-7.12 (2H, m), 3.2 (3H, d), 2.8-3.17 (2H, m), 1.35-1.40 (3H, q), 1.21-1.30 (6H, q), 0.98 (3H, q). ^{31}P{^{1}H} NMR (400 MHz, DMSO, 25 ºC): δ = 147.

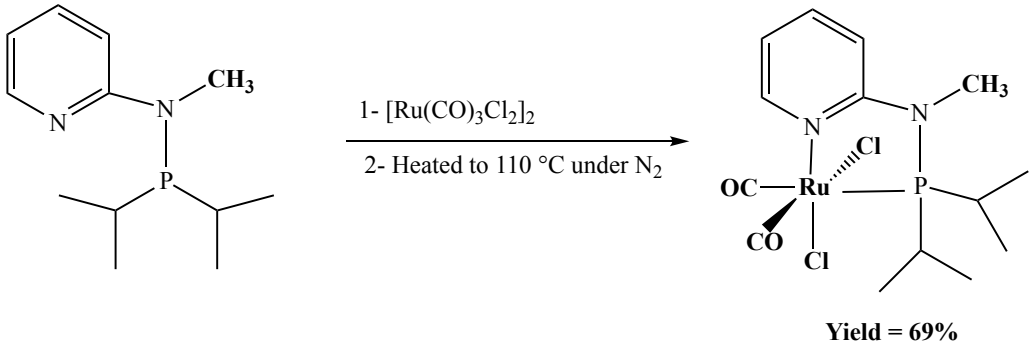

Scheme 3.2. The reaction scheme for the preparation of catalyst (**3**)

3.3 Photocatalytic CO_2 Reduction Experiment

Photocatalytic reduction was performed in a 20 mL glass vial (i.d. = 10 mm) fitted with a magnetic stirrer bar. A mixed solution comprising DMA–TEOA (4:1, v/v, 5 mL) containing 0.02 mM of catalyst (**3**) and 0.02 mM of $[Ru(bpy)_3]^{2+}$ as a photosensitizer was introduced into the vial, sealed, extracted from the nitrogen-filled glovebox, and purged with CO_2 for a minimum of 20 minutes. The vials were subsequently positioned on a magnetic stirrer, along with a four-reaction vial sample holder and four blue-light LEDs (a 450 nm LED with a radiant flux of 1050 mW at 700 mA) for 24 hours, set approximately 10 cm from the reaction vials as the excitation source. Formate was quantified using NMR, while the gaseous products, CO and H_2, were analyzed through gas chromatography (GC-TCD).

3.4 Electrocatalytic CO_2 Reduction Experiment

In order to further investigate the catalytic conduct of the catalysts, an analysis of the electrochemical study has also been carried out. The samples were initially prepared in a glovebox, then sealed, and finally removed from the glovebox. The electrochemical experiments were conducted in a 25 mL gas-impermeable three-neck flask containing a three-electrode assembly, including a glassy carbon working electrode (diameter = 0.3 cm), a platinum wire working as an auxiliary electrode, and a silver wire working as the pseudo-reference electrode. The electrodes were contained in a supporting electrolyte solution of 0.1 mM tetrabutylammonium hexafluorophosphate $[(n\text{-}Bu)_4N]PF_6$ (TBAHFP) and 15 mL of CH_3CN. The solution was degassed for 20 minutes with CO_2 before each experiment started. Scanning speed was 100 mV s^{-1}. All potential results were referred against the internal standard of ferrocenium/ferrocene (Fc^+/Fc).

3.5 Results and Discussions

3.5.1 UV-vis Spectroscopy

UV-vis absorption spectra for catalyst (**3**) were recorded at room temperature in a solution of CH_3CN (Figure 3.1). The ultraviolet-visible (UV–Vis) absorption spectrum of the complex (**3**) was recorded from 200 to 800 nm. Two major absorption bands appear in the spectrum: a sharp absorption from 200 to 250 nm and a second distinct peak near 300 nm. The deep UV region absorption (≈201–250 nm) of high intensity may be due to ligand-centred $\pi \rightarrow \pi^*$ electronic transitions of the phosphine and aromatic ligands.[22] Comparatively, the band at 300 nm is ascribed

to the d → d, π → π*, n → π*, and charge-transfer transitions due to the interaction of π electrons of the metal and ligands involving a metal-to-ligand (MLCT) or ligand-to-metal (LMCT) electron transfer characteristic of Ru (II) polypyridyl or phosphine complexes.[23,24] At wavelengths greater than 350 nm, the absorption spectrum is weakly absorbing, and hence Ru-PN-Me(iPr) does not efficiently absorb visible light. This implies that, whereas the complex is photoreactive at the ultraviolet level, its application as a photocatalytic system for visible light is restricted unless in conjunction with a photosensitizer, for instance, $[Ru(bpy)_3]^{2+}$.

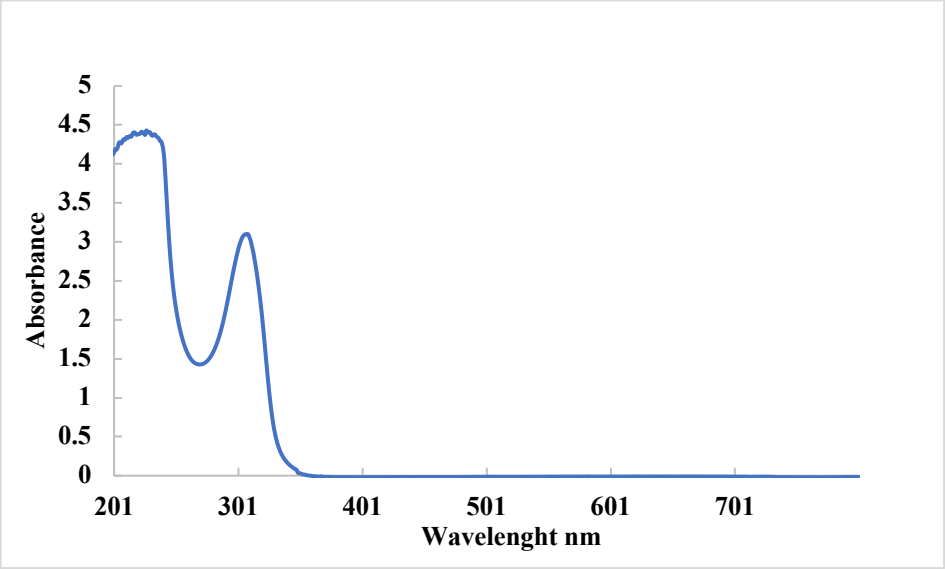

Figure 3.1. *UV-VIS Spectra in CH_3CN for Catalyst (3)*

3.5.2 Photochemistry Gaseous Product Analysis

The assessment of CO_2 reduction and H_2 generation from water necessitates the employment of dependable methodologies for quantifying the yield of each respective reduction product. An Agilent 7820A gas chromatograph (GC), equipped with an Agilent Select permanent gases column and utilizing a thermal conductivity detector (TCD), is employed to quantify the production of CO and H_2. Gas chromatography represents a straightforward, rapid, and adaptable technique for measuring the evolution of gaseous products, wherein the thermal conductivity detector (TCD) is typically utilized to ascertain yields of gaseous products through the integration of the area beneath the peak. Typically, chromatographic data are presented as a graph displaying the detector response in relation to the retention time, resulting in a spectrum of peaks corresponding to the sample that will be injected to characterize the substance analytes present in the sample as they

elute from the column at varying times. Retention time serves as a means to identify analytes, while the area under a peak is directly proportional to the quantity of the analyte present. The concentration of the analyte within the original sample can be ascertained by calculating the peak area through a calibration curve established by measuring the detector response across a range of analyte concentrations.

3.5.2.1 Hydrogen calibration curve results

The quantification of hydrogen was carried out using a calibration curve prepared from pure H_2 gas. The chromatographic possibility was elected since it allows detection and quantification of hydrogen, avoiding misinterpretations of the quantity of hydrogen evolved during the photocatalytic experiments. This is particularly important, considering that under real reaction conditions, there are other gases present with hydrogen. A 250 µL sample was then taken to the GC-TCD system, and the procedure was repeated by injecting different amounts of H_2. Every point was duplicated three times, as can be seen in Figure 3.2.

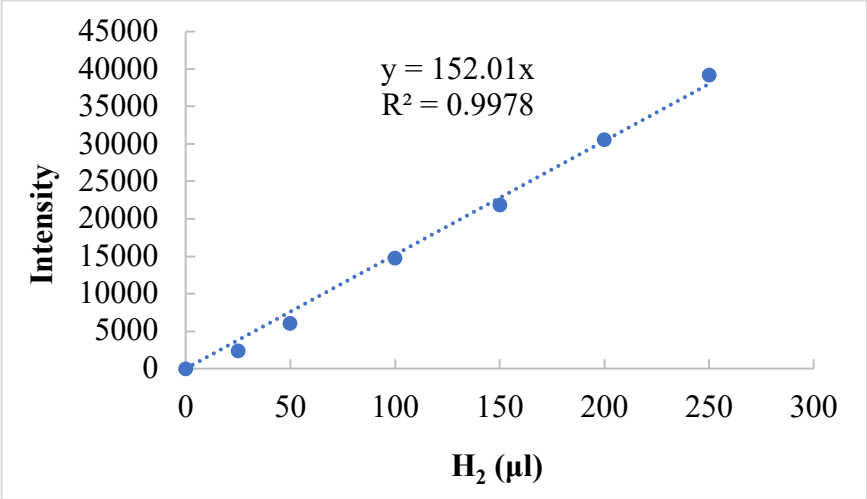

Figure 3.2. *Calibration curve for calculating the amount of H_2 in the injected aliquot*

The calculation of the number of moles of H_2 is according to the ideal gas law, and through simplifications, taking into consideration that the operating pressure is 1 atm, the ambient temperature is 25°C (298 K), at which the gas is extracted from the gas burette that contains it and introduced into the reaction system, then the moles of H_2 in the system are determined from the volume of gas injected into the system:

$$n = \frac{P \times V}{R \times T} \quad (1)$$

Where n, P, V, R, T represent the moles of H_2, the working pressure (1 atm), the volume of the gas injected in the system, the universal gas constant 0.082 (L x atm)/ (K x mol), and the temperature of the H_2 when withdrawn from its reservoir, respectively. Also, the concentration of H_2 in the headspace of the reactor, assuming that the headspace volume remains constant:

$$C = \frac{n}{Vh} \quad (2)$$

Here, C is the concentration of H_2, and Vh is the volume of the headspace.

The calibration curve above shows the H_2 concentration on the x-axis and the peak area obtained from the chromatogram on the y-axis. Consequently, the calibration curves were made by plotting peak area against hydrogen concentration, and the regression parameters were obtained by employing a standard least-squares linear regression model.[25]

3.5.2.2 Photochemistry Liquid Product Analysis

The liquid products from the photocatalytic reactions were analyzed using ^{1}H NMR. In all cases, the only product observed was formic acid, HCOOH. A formic acid calibration curve was constructed with dimethyl sulfone as an internal standard. A standard solution containing 0.15 g dimethyl sulfone (DMS) in 15 mL of D_2O is prepared. A small portion (100 µL) was then taken from the irradiated samples and placed in an NMR tube, together with 400 µL of the standard solution. The sample was thoroughly mixed, and the ^{1}H NMR spectra were collected. The amount of formic acid was determined using the integrated values for the formic acid ($\delta \approx 8.1$ ppm) and a calibration curve that was prepared by a member of our group.

3.5.3 Photocatalytic CO_2 Reduction Results

The findings are validated in Table 3.1 that both the photosensitizer and the catalyst are necessary for photocatalytic activity since no notable products were formed with either component in either N_2 or CO_2 environments individually. Although some formic acid was formed with the photosensitizer alone with CO_2 present, maximum yields of H_2, CO, and in particular HCOOH were noted with the simultaneous use of $[Ru(bpy)_3]^{2+}$ and of catalyst (**3**). This shows the system's synergy with the combined system, with formic acid being the predominant product.

The role of solvents and various electron donors was also evaluated similarly (Table 3.2). The reaction solvent DMA was replaced with acetonitrile; however, it was shown that the photocatalytic activity of this system was decreased for the reduction of CO_2. Even though TEA was less active, BNAH and ascorbic acid did not show any catalytic activity in this experiment.

Table 3.1. Photocatalytic CO_2 Reduction Performance Using $[Ru(bpy)_3]^{2+}$ as a photosensitizer and $[Ru\{\kappa^2\text{-}(iPr_2PNMe)NC_5H_4\}(CO)_2(Cl)_2]$ (**3**) as a catalyst under Various Reaction Conditions.

$[Ru(bpy)_3]^{2+}$ (mM)	Cat (3) (mM)	Solvent 4ml	E-donor 1ml	H_2 (µmol)	CO (µmol)	HCOOH (µmol)
0.02 mM (N_2)	0	DMA	TEOA	0	0	0
0 mM (CO_2)	0.02 mM	DMA	TEOA	0	0	0
0.02 mM (CO_2)	0	DMA	TEOA	0	0	61
0.02 mM (CO_2)	0.02 mM	DMA	TEOA	54	5	123

Table 3.2. Effect of different electron donors and solvents on the photocatalytic reduction of CO_2 with $[Ru\{\kappa^2\text{-}(iPr_2PNMe)NC_5H_4\}(CO)_2(Cl)_2]$ as the catalyst (**3**) (0.02 mM) and $[Ru(bpy)_3(PF_6)_2]$ as the photosensitizer (PS) (0.02 mM). Turnover number (TON) = (moles of product)/ (moles of catalyst). Irradiation with 450 nm light for 24 h.

$[Ru(bpy)_3]^{2+}$ (mM)	Cat (3) (mM)	Solvent 4ml	E-donor 1ml	H_2 (µmol)	CO (µmol)	HCOOH (µmol)	TON $_{HCOOH}$	(Φ%) $_{HCOOH}$	CS % $_{HCOOH}$
0.02	0.02	DMA	TEOA	54	5	123	1230	4.2	68
0.02	0	DMA	TEOA	0	0	61	610	2.1	100
0.02	0.02	DMA	TEA	9	2	46	460	1.6	81
0.02	0	DMA	TEA	14	0	38	380	1.3	73
0.02	0.02	CH_3CN	TEOA	12	0	50	500	1.7	81
0.02	0	CH_3CN	TEOA	42	0	44	440	1.5	51
0.02	0.02	CH_3CN	TEA	10	0	44	440	1.5	81
0.02	0	CH_3CN	TEA	11	0	0	0	0	0

In Table 3.2, the Ru catalyst (**3**), in conjunction with the $[Ru(bpy)_3]^{2+}$ photosensitizer in DMA, possesses predominantly efficient photocatalytic activity for the reduction of CO_2 by utilizing TEOA as an electron source, yielding 123 µmol of HCOOH with superior turnover number, quantum yield, and selectivity, while TEA possesses low efficacy. The electron donors BNAH and ascorbic acid were evaluated in this experiment and showed no catalytic activity. This highlights the increasingly significant roles of both the selection of the catalyst and the selection of electron source in optimizing efficiency (with TEOA-mediated systems superior to those of other donors) of processes of Ru-photosensitized reductions of CO_2.[26]

The turnover number (TON), quantum yield (Φ%), and the selectivity (CS%) were defined in Chapter 1 and determined using equations **4**, **5** and **6** and the same methodology used throughout for all results presented in this thesis:

Turnover number based on the catalyst used and calculated:

$$n = \mathrm{C} \times \mathrm{V} \qquad (4)$$

Where n represents the moles (or µmol) of the catalyst, C is the concentration of the catalyst (0.02 mM), and V is the total volume comprising DMA–TEOA (4:1, v/v, 5 mL),

$n = 0.02\ x\ 10^{-3}\ moles/L \times 5\ x\ 10^{-3}\mathrm{L} = 0.0000001\ moles$ **OR** 0.1 $\mu mols$ of catalyst

The formation of 123 µmol HCOOH corresponds to a TON = $\frac{123}{0.1} = 1230$

The quantum yield (Φ%) based on the catalyst used and calculated:

$$\text{Quantum Yield } (\Phi) = \frac{\#\text{ of molecules (or µmoles)consumed or produced per unit time}}{\#\text{ of photons (or einstein)absorbed per unit time}} \times 100 \qquad (5)$$

$$\Phi = \frac{123 \times 10^{-6}}{3.4 \times 10^{-8} \times 24 \times 3600} = 0.042\ (or\ 4.2\%)$$

The selectivity (CS%) is based on the catalyst used and calculated:

$$\mathrm{CS} = \frac{\text{Amount of one specific product}}{\text{Total amount of all products}} \times 100 \qquad (6)$$

$$\mathrm{CS} = \frac{123}{54 + 5 + 123} \times 100 = 68\%\ \mathrm{HCOOH}$$

Comparative Photocatalytic CO_2 Reduction Activity of Three Ru-Based Catalysts (1–3)

The comparative photocatalytic efficiencies concerning the reduction of carbon dioxide among the three ruthenium-based catalysts, namely [Ru{κ²-(Ph_2PNMe)NC_5H_4}$(CO)_2Cl_2$] (**1**), [Ru{κ²-

$(Ph_2PNH)NC_5H_4\}(CO)_2Cl_2]$ (**2**), and $[Ru\{\kappa^2\text{-}(iPr_2PNMe)NC_5H_4\}(CO)_2Cl_2]$ (**3**), are illustrated in Table 3.3 and Figure 3.3. The experiments were performed using $Ru(bpy)_3(PF_6)_2$ as the photosensitizer solubilized in DMA, and comparing the electron donors triethanolamine (TEOA) and triethylamine (TEA).

Table 3.3. A comparison of the photocatalytic CO_2 reduction experiments with complexes (**1**, **2** and **3**) (0.02 mM). In DMA (4mL) with $[Ru(bpy)_3(PF_6)_2]$ as photosensitizer (PS) (0.02 mM), (TEOA and TEA) as the electron donors (ED). Turnover number (TON) = (moles of product)/ (moles of catalyst). Irradiation with 450 nm light for 24 h.

Catalysts (0.02 mM)	PS (0.02 mM)	Solvent 4 mL	E-donor 1 mL	H_2 (µmol)	HCOOH (µmol)	TON_{HCOOH}/ Φ % $_{HCOOH}$
Cat (1)	Ru(bpy)	DMA	TEOA	20	82	820/ 3.1
Cat (1)	Ru(bpy)	DMA	TEA	0	0	0
Cat (2)	Ru(bpy)	DMA	TEOA	48	62	620/ 2.1
Cat (2)	Ru(bpy)	DMA	TEA	0	0	0
Cat (3)	Ru(bpy)	DMA	TEOA	54	123	1230/ 4.2
Cat (3)	Ru(bpy)	DMA	TEA	9	46	460/ 1.6

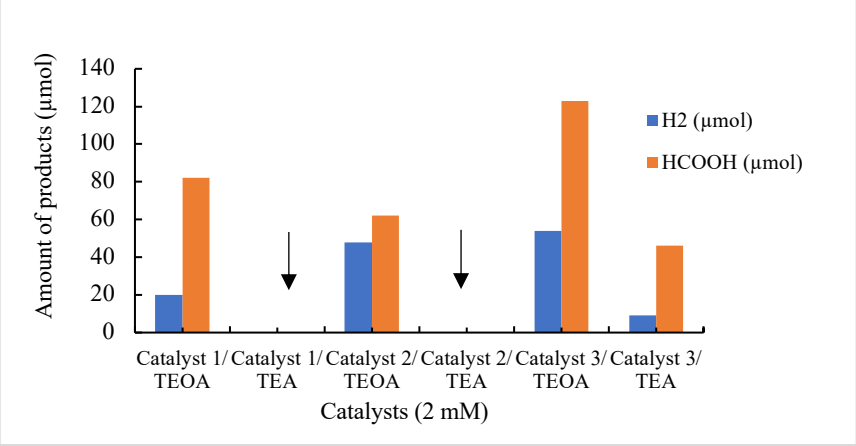

Figure 3.3. *Comparison between the catalysts 1, 2 and 3 with TEOA and TEA in DMA*

Catalyst (**3**) showed the highest photocatalytic activity, producing 54 µmol H_2 and 123 µmol HCOOH with a TON of 1230 and a quantum yield of 4.2%, significantly outperforming catalysts (**1** and **2**). It appears that replacing the phenyl groups on the phosphorus centers with larger isopropyl groups results in superior activity. The origin may be enhanced electron donation and/or steric protection at the Ru center to improve activation of CO_2 and reduction of protons. For all three Ru catalysts, triethanolamine (TEOA) gave higher product yield than triethylamine (TEA), evidenced by larger TON and Φ values as shown in Table 3.3 and Figure 3.3. Catalyst design

(ligand environment) and selection of electron donors are of utmost importance for high efficiency in photocatalytic reduction of CO_2.

Product selectivity for the conversion of CO_2 is excellent; however, the selectivity concerning the reducing equivalents used in this reaction is diminished due to the appearance of H_2 (Table 3.4). Taking into account the H_2, the selectivity of the reduction reaction is higher for catalyst (**1**) than for the others.

Table 3.4. Effect of different catalysts (**1**), (**2**), and (**3**) on the photocatalytic reduction of CO_2 with $[Ru(bpy)_3(PF_6)_2]$ as the photosensitizer (PS). In DMA (4 mL) and TEOA as an electron donor (ED). Turnover number (TON) = (moles of product)/ (moles of catalyst). Irradiation with 450 nm light for 24 h.

Catalysts (0.02 mM)	**H_2 (µmol)**	**CO (µmol)**	**HCOOH (µmol)**	**TON_{H2}**	**TON_{HCOOH}**	**TOF_{HCOOH} (24h)**	**(Φ%) H2**	**(Φ%) HCOOH**	**Selectivity (%) HCOOH**
Cat (1)	20	5	82	200	820	34	0.68	2.8	80
Cat (2)	48	4	62	480	620	26	1.6	2.1	54
Cat (3)	54	5	123	540	130	51	1.8	4.2	68

-The photocatalytic reaction was performed using a Ru complex (0.02 mM), $[Ru(bipy)_3]^{2+}$ as PS (0.02 mM), and CO_2- saturated different solvents and electron donors (4:1, v/v) solution, λ = 450 nm, 25 °C for 24 h.
-Turnover number based on the catalyst used and calculated: $5x10^{-3}$L x $0.02x10^{-3}$moles/L OR 0.1 micromoles of catalyst.
-Selectivity is calculated as µmol HCOOH/ (µmol HCOOH + µmol H_2) x 100
-Photon flux = 3.4 x 10^{-8} photons/sec.

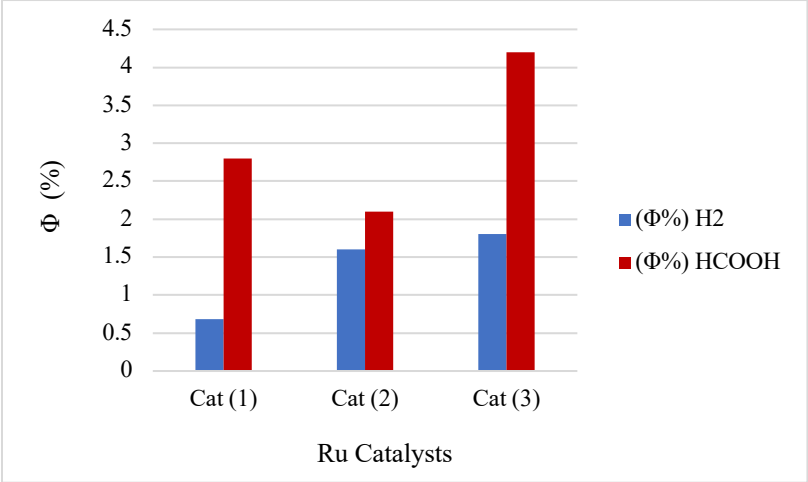

Figure 3.4. *Φ values for HCOOH (blue) and H_2 (red) formation in Ru catalysts **1**,**2**, and **3**.*

The bar chart describes the significant impact of phosphine substituents upon ruthenium photoredox complex photocatalytic efficiency. Complex (**3**), with its bulky iPr_2PNMe ligands, achieves the maximum quantum yield of formic acid (HCOOH) of 6%, together with measurable hydrogen (H_2) production. In contrast, complex (**1**) possesses only modest activity towards HCOOH and shows next to no H_2 production, while complex (**2**) shows the lowest overall efficiency. These results suggest that strong steric and electron-donating effects of iPr substituents of complex (**3**) give rise to reaction intermediate stabilization and increased orbital interactions to preferentially drive carbon dioxide (CO_2) reduction over other competing processes. Overall, such a comparative study highlights critically the fundamental role of ligand design to enhance both selectivity and quantum efficiency of ruthenium-centred photoreduction schemes for converting CO_2.

3.5.4. Hydrogen Production Via Photocatalytic Water Splitting Results

Hydrogen (H_2) is a clean energy carrier that has received significant attention due to the depletion of natural energy sources, such as petroleum and coal.[27,28] One of the effective pathways for H_2 production is photocatalytic water splitting, which exploits solar energy as an unlimited and free energy source available globally. Thus, H_2 would be an attractive clean energy source in the coming era, as it is non-toxic and can generate energy from natural sources like water and sunlight. These are clean and long-term renewable sources.[29,30]

Chapter **1** provides a general overview of the key components and parameters that need to be attended to and considered in an effort to investigate the photocatalytic capacity of this series of second-row metal complexes for CO_2 reduction. Two essential parts of a photocatalytic system, for example, are the catalyst and the photosensitizer.

This photoreduction requires an electron donor, and a range of electron donors was tested under standard conditions. The three electron donors are amines that have been observed to be effective in photocatalytic reduction reactions. TEOA is the most common ED.[31] Observe that the $[Ru(bpy)_3]^{2+}$ is acting as a photosensitizer, with the DMA being our solvent for this experiment. Tables (3.5 and 3.6) summarize the data for the different electron donors. TEA was the most effective of the three electron donors employed in this study, and therefore, TEA was chosen as the electron donor for optimization.

Table 3.5. Photocatalytic H_2 Production with [Ru{κ²-(iPr₂PNMe)NC₅H₄}(CO)₂(Cl)₂] (**3**) in **DMA** using $[Ru(bpy)_3]^{2+}$ as Photosensitizer, Various Electron Donors, and H_2O as Proton Source under 450 nm Irradiation.

$[Ru(bpy)_3]^{2+}$ (mM)	Catalyst (3) (mM)	Solvent (4 mL)	E-donor (1 mL)	Additive (1 mL)	H_2 (µmol)	TON_{H2}	$(\Phi\%)_{H2}$
0.02	0.02	DMA	TEOA	H_2O	100	1000	3.4
0.02	0	DMA	TEOA	H_2O	17	170	0.58
0.02	0.02	DMA	TEA	H_2O	177	1770	6.0
0.02	0	DMA	TEA	H_2O	58	580	2.0
0.02	0.02	DMA	BNAH	H_2O	25	250	0.85
0.02	0	DMA	BNAH	H_2O	12	120	0.4

The table shows the impact of the choice of electron donor on H_2 evolution from the Ru-centered photocatalytic system. TEA was best with 177 µmol H_2 yield for TON of 1770 and a Φ of 6.0%, TEOA exhibited moderate activity, and BNAH exhibited low activity. Control experiments without a catalyst confirmed its pivotal role, and superior activity with TEA is attributed to its superior redox capabilities. In conclusion, results highlight the importance of the selection of the donor and of catalyst design to improve photocatalytic hydrogen production.

Table 3.6. Photocatalytic H_2 Production with [Ru{κ²-(iPr₂PNMe)NC₅H₄}(CO)₂(Cl)₂] (**3**) in **CH3CN** using $[Ru(bpy)_3]^{2+}$ as Photosensitizer, Various Electron Donors, and H_2O as Proton Source under 450 nm Irradiation.

$[Ru(bpy)_3]^{2+}$ (mM)	Catalyst (3) (mM)	Solvent (4 mL)	E-donor (1 mL)	Additive (1 mL)	H_2 (µmol)	TON_{H2}	$(\Phi\%)_{H2}$
0.02	0.02	CH_3CN	TEOA	H_2O	29	290	1.0
0.02	0	CH_3CN	TEOA	H_2O	0	0	0
0.02	0.02	CH_3CN	TEA	H_2O	90	900	3.0
0.02	0	CH_3CN	TEA	H_2O	10	100	0.34
0.02	0.02	CH_3CN	BNAH	H_2O	10	100	0.34
0.02	0	CH_3CN	BNAH	H_2O	10	100	0.34

The TEA is the most efficient electron donor for hydrogen evolution (H_2) for the Ru-based photocatalytic system in CH_3CN, producing 90 µmol of H_2, as seen in Table 3.6. TEOA shows mediocre activity with 29 µmol of production, while BNAH is largely ineffective. Control

experiments eliminating the catalyst confirm its essential role, and water incorporation through its role as a proton source plays a superior role. These results confirm the importance of donor redox properties and their conformity with the system of catalyst–photosensitizer to define photocatalytic hydrogen generation efficacy.

Figure 3.5 shows that choosing appropriate solvents and electron donors has a remarkable effect on the efficiency of hydrogen evolution photocatalytic activity.

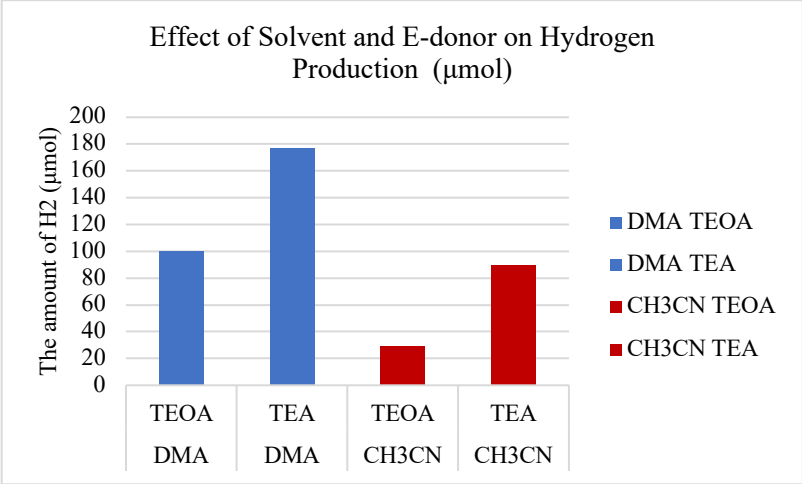

Figure 3.5. *Comparison of H_2 production from water splitting using different solvents and electron donors.*

TEA is the most effective donor, yielding 177 µmol H_2 in DMA (TON = 1770, Φ = 6.0%) and 90 µmol in CH_3CN (TON = 900, Φ = 3.0%), whereas TEOA shows lower activity, with 100 µmol in DMA (TON = 1000, Φ = 3.4%) and only 29 µmol in CH_3CN (TON = 290, Φ = 1.0%). These results underline the superior efficiency of TEA and the favorable role of DMA as a solvent in enhancing H_2 production.

Table 3.7. Comparative Study of Photocatalytic H_2 Generation from CO_2 Reduction and Water Splitting: Influence of Solvent and Electron Donor Choice

$[Ru(bpy)_3]^{2+}$ (mM)	Catalyst (3) (mM)	Solvent (4mL)	E-donor (1mL)	H_2 (µmol) from (1 mL) H_2O addition	H_2 (µmol) from CO_2 injection
0.02	0.02	DMA	TEOA	100	**54**
0.02	0.02	DMA	TEA	177	**9**
0.02	0.02	DMA	BNAH	25	**0**
0.02	0.02	CH_3CN	TEOA	29	**12**
0.02	0.02	CH_3CN	TEA	90	**10**
0.02	0.02	CH_3CN	BNAH	10	**0**

The data in Table 3.7 show that solvent, electron donor, and proton source strongly affect H_2 evolution in the Ru-based photocatalytic system. The highest H_2 yield from water is achieved in DMA with TEA (177 µmol), while the most effective CO_2-derived H_2 production occurs with TEOA in DMA (54 µmol). BNAH gives the lowest activity, with no detectable H_2 from CO_2, confirming its poor suitability as a donor. Overall, DMA consistently outperforms CH_3CN, and the choice of donor determines whether water or CO_2 serves more effectively as the proton source, highlighting the importance of matching solvent–donor conditions to reaction selectivity.

3.6 Electrocatalytic CO_2 Reduction Results

Electrocatalytic activities of such a complex were investigated under a wide range of conditions. As explained in Section 1.7 of Chapter 1, the electrochemistry experiments were conducted at a single-compartment cell with CH_3CN as solvent and supporting electrolyte as tetrabutylammonium hexafluorophosphate $[(n\text{-}Bu)_4N]PF_6$ (TBAHFP). Measurements were conducted in a nitrogen and a carbon dioxide atmosphere and with the aid of acetic acid. Figures below are presented as an illustration of the electrocatalytic behavior towards the reduction of CO_2 of the complex.

For complex (**3**), the cathodic scan of the cyclic voltammogram carried out under N_2 exhibited two irreducible reduction waves at –0.80 and –1.52 V relative to Fc/Fc^+ (Figure 3.6). Introduction of a CO_2 atmosphere (Figure 3.7) produced a gradual increase at the second peak of reduction. With the addition of acetic acid (Figure 3.8), the peak exhibited a significant current increment, as a confirmation of the fact that the catalyst can electrocatalytically promote CO_2 reduction.

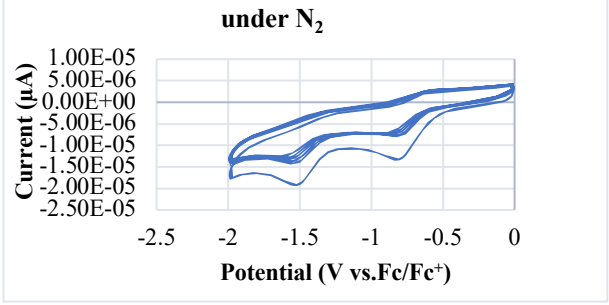

Figure 3.6. *Cyclic voltammograms of (**3**) under N_2*

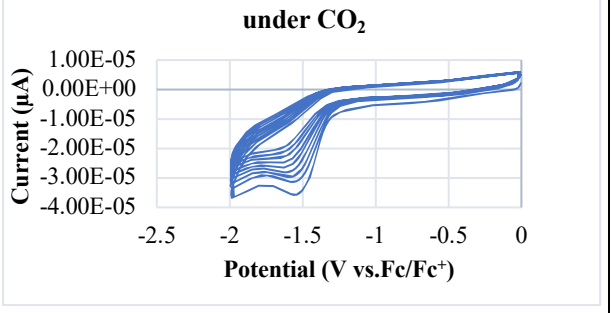

Figure 3.7. *Cyclic voltammograms of (**3**) under CO_2*

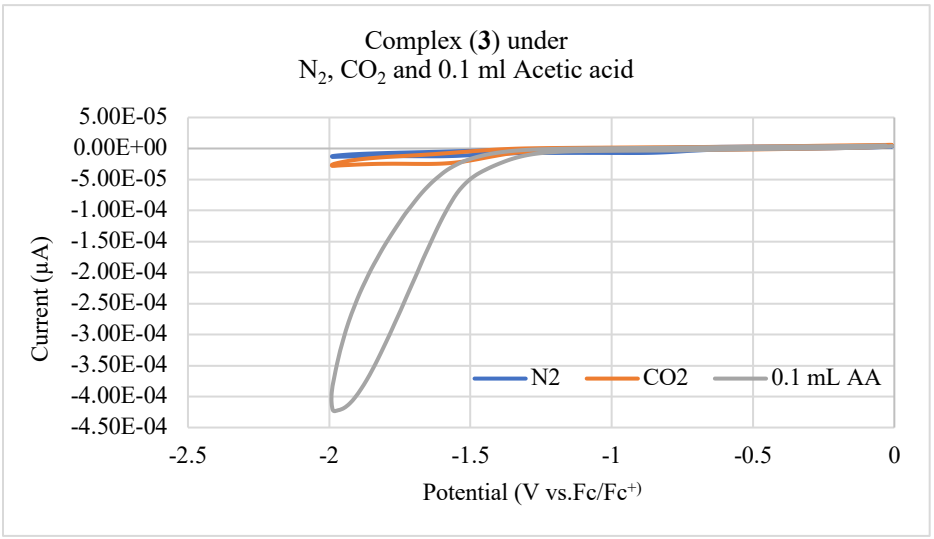

Figure 3.8. *Cyclic voltammograms of 0.02 mM complex (**3**) under N_2 (blue), CO_2 (orange) and CO_2/ 0.1mL AA (gray) in CH_3CN with 0.1 M $(n\text{-}Bu)_4NPF_6$ supporting electrolyte at 100 mV/s*

3.7 Conclusion

Three second-row transition metal complexes containing PN ligands were synthesized, and a preliminary assessment of their ability to reduce CO_2 and to bring about the evolution of hydrogen by using water as the source of H_2 revealed that all the complexes could perform this chemical transformation, but with varying activities.

The analysis of quantum yield reveals that modifications to the ligand have a significant influence on photocatalytic outcomes. Of the three investigated Ru-based complexes, complex **(3)**, with the bulky iPr_2PNMe ligand substitution, exhibits the highest efficacy in the HCOOH formation (about 6%) with accompanying detectable H_2 evolution, while complexes (**1** and **2)** reveal greatly diminished activity. These results confirm that the steric as well as electronic effects caused by the ligand design play an imperative role in enhancing selectivity as well as quantum efficacy in the Ru-based CO_2 photoreduction systems.

The findings also verify that the selection of the electron donor has a critical influence on photocatalytic H_2 yield. TEA exhibits the best activity (177 μmol H_2, TON = 1770, Φ = 6.0%), medium-level TEOA yields, but poor performance for BNAH. These data illustrate the pivotal importance of the Ru catalyst support as well as the beneficial redox capability of TEA required for high-efficiency hydrogen evolution.

All the solvents tested in the present study proved to be effective, with the best performance among them for dimethylacetamide (DMA). Since the polarity for DMA is 6.5, which is larger than that for acetonitrile (CH_3CN), 5.8, the solvent polarity could play a crucial role in the dynamics of the reaction.

3.8 References

1. Elgrishi, N.; Chambers, M. B.; Wang, X.; Fontecave, M. Molecular Polypyridine-Based Metal Complexes as Catalysts for the Reduction of CO_2. *Chem. Soc. Rev.* 2017, *46* (3), 761–796.

2. Ager, J. W.; Shaner, M. R.; Walczak, K. A.; Sharp, I. D.; Ardo, S. Experimental Demonstrations of Spontaneous, Solar-Driven Photoelectrochemical Water Splitting. *ChemInform* 2015, *46* (3).

3. Lewis, N. S.; Nocera, D. G. Powering the Planet: Chemical Challenges in Solar Energy Utilization. *Proc. Natl. Acad. Sci. U.S.A.* 2006, *103* (43), 15729–15735.

4. Cook, T. R.; Dogutan, D. K.; Reece, S. Y.; Surendranath, Y.; Teets, T. S.; Nocera, D. G. Solar Energy Supply and Storage for the Legacy and Nonlegacy Worlds. *Chem. Rev.* 2010, *110* (11), 6474–6502.

5. Qiao, J.; Liu, Y.; Hong, F.; Zhang, J. A Review of Catalysts for the Electroreduction of Carbon Dioxide to Produce Low-Carbon Fuels. *ChemInform* 2014, *45* (17).

6. Costentin, C.; Robert, M.; Savéant, J.-M. Catalysis of the Electrochemical Reduction of Carbon Dioxide. *Chem. Soc. Rev.* 2013, *42* (6), 2423–2436.

7. Fukuzumi, S.; Kobayashi, T.; Suenobu, T. Photocatalytic Production of Hydrogen by Disproportionation of One-Electron-Reduced Rhodium and Iridium–Ruthenium Complexes in Water. *Angew. Chem., Int. Ed.* 2011, *50* (3), 728–731.

8. Esswein, A. J.; Nocera, D. G. Hydrogen Production by Molecular Photocatalysis. *Chem. Rev.* 2007, *107* (10), 4022–4047.

9. Du, P.; Eisenberg, R. Catalysts Made of Earth-Abundant Elements (Co, Ni, Fe) for Water Splitting: Recent Progress and Future Challenges. *Energy Environ. Sci.* 2012, *5* (3), 6012–6021.

10. Bock, C. R.; Connor, J. A.; Gutierrez, A. R.; Meyer, T. J.; Whitten, D. G.; Sullivan, B. P.; Nagle, J. K. Estimation of Excited-State Redox Potentials by Electron-Transfer Quenching. Application of Electron-Transfer Theory to Excited-State Redox Processes. *J. Am. Chem. Soc.* **1979,** *101* (17), 4815–4824.

11. Bock, C. R.; Connor, J. A.; Gutierrez, A. R.; Meyer, T. J.; Whitten, D. G.; Sullivan, B. P.; Nagle, J. K. Estimation of Excited-State Redox Potentials by Electron-Transfer Quenching. Application of Electron-Transfer Theory to Excited-State Redox Processes. *J. Am. Chem. Soc.* **1979,** *101* (17), 4815–4824.

12. Khaselev, O.; Bansal, A.; Turner, J. A. High-Efficiency Integrated Multijunction Photovoltaic/Electrolysis Systems for Hydrogen Production. *Int. J. Hydrogen Energy* **2001**, *26* (2), 127–132.

13. Junge, H.; Rockstroh, N.; Fischer, S.; Brückner, A.; Ludwig, R.; Lochbrunner, S.; Kühn, O.; Beller, M. Light to Hydrogen: Photocatalytic Hydrogen Generation from Water with Molecularly Defined Iron Complexes. *Inorganics* **2017**, *5* (1), 14.

14. Cline, E. D.; Adamson, S. E.; Bernhard, S. Homogeneous Catalytic System for Photoinduced Hydrogen Production Utilizing Iridium and Rhodium Complexes. *Inorg. Chem.* **2008**, *47* (22), 10378–10388.

15. Queyriaux, N.; Jane, R. T.; Massin, J.; Artero, V.; Chavarot-Kerlidou, M. Recent Developments in Hydrogen Evolving Molecular Cobalt (II)–Polypyridyl Catalysts. *Coord. Cem. Rev.* **2015**, *304–305* (SI), 3–19.

16. Brewer, K. J.; Murphy, W. R.; Moore, K. J.; Eberle, E. C.; Petersen, J. D. Visible-Light Production of Molecular Hydrogen by Sensitization of a Cobalt Dihydride Complex. *Inorg. Chem.* **1986**, *25* (14), 2470–2472.

17. Goldsmith, J. I.; Hudson, W. R.; Lowry, M. S.; Anderson, T. H.; Bernhard, S. Discovery and High-Throughput Screening of Heteroleptic Iridium Complexes for Photoinduced Hydrogen Production. *J. Am. Chem. Soc.* **2005**, *127* (20), 7502–7510.

18. Kumaravel, V.; Imam, M. D.; Badreldin, A.; Chava, R. K.; Do, J. Y.; Kang, M.; Abdel-Wahab, A. Photocatalytic Hydrogen Production: Role of Sacrificial Reagents on the Activity of Oxide, Carbon, and Sulfide Catalysts. *Catalysts* **2019,** *9* (3), 276.

19. Krishnan, C. V.; Sutin, N. Homogeneous Catalysis of the Photoreduction of Water by Visible Light. 2. Mediation by a Tris(2,2′-Bipyridine) ruthenium (II)-Cobalt (II) Bipyridine System. *J. Am. Chem. Soc.* **1981,** *103* (8), 2141–2142.

20. Chan, S. F.; Chou, M.; Creutz, C.; Matsubara, T.; Sutin, N. Mechanism of the Formation of Dihydrogen from the Photoinduced Reactions of Poly(Pyridine)ruthenium(II) and Poly(Pyridine)rhodium(III) Complexes. *J. Am. Chem. Soc.* **1981,** *103* (2), 369–379.

21. Yang, Y.; Gurnham, J.; Liu, B.; Duchateau, R.; Gambarotta, S.; Korobkov, I. Selective ethylene oligomerization with chromium complexes bearing pyridine-phosphine ligands: influence of ligand structure on catalytic behavior. *Organometallics*. **2014**, 33, 5749–5757.

22. Hameed, Y.; Rao, G. K.; Ovens, J. S.; Gabidullin, B.; Richeson, D. Visible-Light Photocatalytic Reduction of CO_2 to Formic Acid with a Ru Catalyst Supported by N,N′-Bis(diphenylphosphino)-2,6-diaminopyridine Ligands. *ChemSusChem* **2019**, *12* (15), 3453–3457.

23. Mostafa, S. H.; Khorassani, M.; Maghsoodlou, M.; Nassiri, M.; Zakarianezhad, M.; Fattahi, M. Synthesis of Stable Phosphorus Ylides from 3,5-Dimethylpyrazole and Kinetic Investigation of the Reactions by UV Spectrophotometry. *Arkivoc* **2006**, *2006*, 168.

24. van Wyk, P.-H.; Gerber, W. J.; Koch, K. R. A Robust Method for Speciation, Separation and Photometric Characterization of All $[PtCl_{6-n}Br_n]^{2-}$ (n = 0–6) and $[PtCl_{4-n}Br_n]^{2-}$ (n = 0–4) Complex Anions by Means of Ion-Pairing RP-HPLC Coupled to ICP-MS/OES, Validated by High Resolution ^{195}Pt NMR Spectroscopy. *Anal. Chim. Acta* **2011**, *704*, 154–161.

25. Cox, L. E.; Peters, D. G.; Wehry, E. L. Photoaquation of Hexachloroplatinate(IV). *J. Inorg. Nucl. Chem.* **1972**, *34*, 297–305.

26. Nevárez Martínez, M. C.; Cavdar, O.; Haliński, Ł. P.; Miodyńska, M.; Parnicka, P.; Bajorowicz, B.; Kobylański, M.; Lewandowski, Ł.; Zaleska-Medynska, A. Hydrogen Detection during Photocatalytic Water Splitting: A Tutorial. *Int. J. Hydrogen Energy* **2022**, *47* (35), 15783–15788.

27. Li, Z.; Yang, C.; Su, Y.; Cheng, Y.; Cui, Y.; Liu, S.; Fang, Y. Photochemical Reduction of CO_2 into CO Coupling with Triethanolamine Decomposition. RSC Adv. 2023, 13, 31616–31621.

28. Ahmad, H.; Kamarudin, S. K.; Minggu, L. J.; Kassim, M. Hydrogen from Photocatalytic Water Splitting Process: A Review. *Renew. Sustain. Energy Rev.* **2015**, *43*, 599–610.

29. Gupta, N. M. Factors Affecting the Efficiency of a Water Splitting Photocatalyst: A Perspective. *Renew. Sustain. Energy Rev.* **2017**, *71*, 585–601.

30. Fajrina, N.; Tahir, M. A Critical Review in Strategies to Improve Photocatalytic Water Splitting towards Hydrogen Production. *Int. J. Hydrogen Energy* **2019**, *44* (2), 540–577.

31. Aḥmadī, S. Exploring Simple Catalyst for Transfer Hydrogenation of Ketones and Photocatalytic Hydrogen Production Using Homogeneous Metal Complexes. M.Sc. Thesis, University of Ottawa, Ottawa, 2019.

Chapter 4: Photocatalytic Activity of Co (II) Complex with Isopropyl Phosphinoaminopyridine Ligand and Generation of Formic Acid

4.1 Introduction

Artificial photosynthesis of renewable fuels using solar power and abundant resources, such as H_2O and CO_2, is the most promising approach toward addressing the energy crises and environmental pollution resulting from the use of fossil fuels. Photocatalytic CO_2 reduction to renewable fuels of use, like CO and CH_3OH, is an appealing method of producing renewable fuels and, simultaneously, cleaning up the environment of the CO_2 molecules.[1,2] CO may then be converted into liquid fuels by the Fischer−Tropsch synthesis. [3,4] As the CO_2 reduction is an uphill process possessing a large energy barrier, proper catalysts need to be used for bringing this reaction about at a tolerable rate. A typical homogeneous photocatalytic system for reducing CO_2 comprises a photosensitizer, a sacrificial donor, and a molecular catalyst. A large number of systems utilizing noble metals like Re [5−7] and Ru [8,9] as catalysts, owing to their superior activity and durability, do exist; however, in order to make the process economical, there is a need for developing catalytic systems utilizing earth-abundant elements. Although there have been quite a few reports of catalytic CO_2 reduction by complexes of Co,[10,11] Ni,[12,13] Fe,[12,14] and Mn, [15,16] most of these systems suffer from a lack of adequate efficiency and selectivity.

An applicable catalyst needs to meet the following requirements: 1) The photocatalytic CO_2 reduction should be achieved in the visible-light, matching the solar spectrum, with a high catalytic activity under low-intensity light, as the average solar intensity is only around 136.6 mW cm^{-2}.
2) The catalyst needs to show high selectivity for CO_2 reduction to get a single carbon atom-based product. 3) The catalyst should be inexpensive and highly efficient.[17]

Herein, we report a noble-metal-free photocatalytic CO_2 reduction using three components: $[Ru(bpy)_3]^{2+}$ as the photosensitizer, $[Co\{\kappa^2\text{-}(iPr_2PNMe)NC_5H_4\}(Br)_2]$ as the catalyst (**4**), and TEOA as an electron donor. Our system exhibits high activity with a TON of 10,500 in DMA/TEOA (4:1, v/v). Compared to the system with CH_3CN as a solvent and TEOA as an electron donor, the TON of 8,200.
Complex $[Co\{\kappa^2\text{-}(iPr_2PNMe)NC_5H_4\}(Br)_2]$ was obtained through the use of cobalt (II) (d^7). Because of its coordination environment, defined by two bromide ligands and one bidentate phosphino-pyridine ligand, it is foreseen that it will be a distorted tetrahedral geometry, although

steric effects can also permit the presence of a slight square-pyramidal distortion. However, definitive structure verification was not obtained. An attempt at collecting single-crystal X-ray diffraction data was unsuccessful, and ^{1}H NMR spectroscopy was not employed by virtue of the Co (II) center's paramagnetic nature.

Spectroscopic analysis revealed little toward the structure of the complex. The UV–Vis spectrum showed diagnostic absorption features of ligand-to-metal charge transfer (LMCT) and d–d transitions that are expected for Co (II) complexes. However, the IR spectrum was unable to be routinely obtained by virtue of the marked air sensitivity of the complex that caused it to quickly incorporate atmospheric moisture, thus obliterating diagnostic vibrational bands and hindering reliable analysis.

Regarding the aspect of reactivity, the photocatalytic reduction of the CO_2 was demonstrated by the complex (4). No noticeable electrocatalytic reduction of the CO_2 was observable under the tested conditions, presumably owing to instability of the catalyst under test potential conditions or owing to the need for extra optimization of electrochemical parameters.

Briefly, although detailed structural and spectroscopic identification was not feasible, initial identification of photocatalytic activity points to the promise of the cobalt-based system. Future research needs to address first stabilizing the Co (II) (e.g., handling under inert atmosphere), crystallographic data acquisition, and extension of studies of the photochemical and electrochemical properties.

4.2 The Synthesis and Characterization of the Complex (4)

4.2.1 Experimental Procedures

All chemicals, solvents, and reagents employed in the current study were of analytical quality and were utilized as received. All NMR spectra (^{1}H, ^{13}C and ^{31}P) were recorded on 300 or 400 MHz spectrometers at 25 °C with chemical shifts reported in ppm using the residual protons of the NMR solvent as internal standards.

4.2.2 Synthesis and Characterization of [Co{κ^2-(iPr_2PNMe) NC_5H_4}$(Br)_2$] (4)

This complex was prepared according to the literature procedure.[18] In a glove box, $CoBr_2$ powder (30 mg, 0.137 mmol) was added to a clear orange oil ligand ($[(CH_3)_2CH]_2P)NMe(NC_5H_4)$ (0.481

g, 48.1 mg, 0.206 mmol) in 15 mL toluene. The reaction mixture was stirred for 14 hours and gave an opaque blue precipitate. The solution was cooled at -20°C overnight. The precipitate turned blue, and it was isolated by the filtration method and then washed with 5 x 2 mL hexane and dried in a vacuum. No crystals were obtainable to grow to be studied by single-crystal X-ray analysis. The ^{1}H NMR spectrum also did not display the desired peaks.

4.3 Photocatalytic Experiments

Experimental procedures of the photoreaction are described in section 2.2.6 of (Chapter 2).

4.4 Results and Discussion

Before Catalyst (**4**) could be tested in photoreduction, crucial physical chemistry experiments were performed using cyclic voltammetry and UV–vis spectroscopy; however, under the tested conditions, no detectable electrocatalytic CO_2 reduction activity was observed.

4.2.1 The UV-Vis Spectroscopy

The UV–Vis absorption spectrum of the compound $[Co\{\kappa^2\text{-}(iPr_2PNMe)NC_5H_4\}(Br)_2]$ in CH_3CN solution is shown in Figure 4.1. Broad absorption bands at 217 and 257 nm arise from ligand-centered $\pi\rightarrow\pi^*$ and $n\rightarrow\pi^*$ transitions of the phosphino-pyridine unit, while weaker absorptions at 584 and 686 nm correspond to Co(II) d–d transitions (d^7, high-spin) and bear witness to an elongated tetrahedral/square-pyramidal geometry. The presence of both ligand-centered and metal-centered features signifies the duality of the complex's ability in light absorption and redox activity, which is crucial in photocatalytic CO_2 reduction.

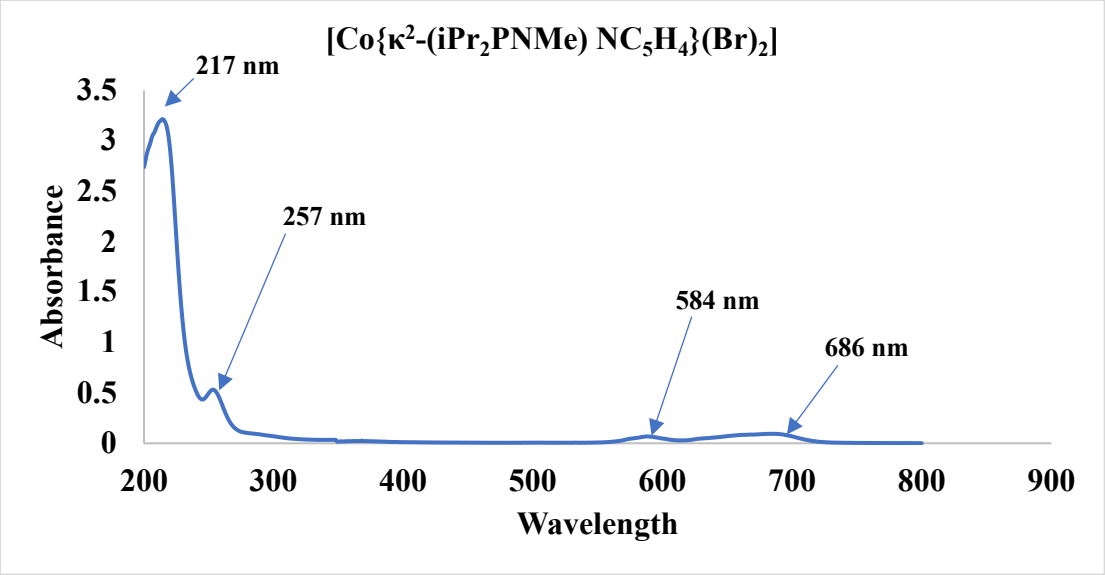

Figure 4.1. *UV-vis spectra in CH_3CN for complex (4)*

4.4.2 Photocatalytic CO_2 Reduction Results

The initial experiments on photocatalytic reduction of CO_2 employed (0.02 mM) of complex (**4**) in dimethylacetamide (DMA) and acetonitrile (CH_3CN), supported by (0.02 mM) of $[Ru(bpy)_3]^{2+}$ photosensitizer and TEOA and TEA as electron donors. This reaction medium was irradiated at ambient CO_2 pressure in visible light generated by blue LEDs (450 nm, 1050 mW at 700 mA, 3.4 x 10^{-8} mol photons/sec) for 24 hours. Analysis by gas chromatography of the reaction headspace demonstrated the evolution of hydrogen gas but no carbon monoxide. The reaction solution ^1H NMR analysis identified the product to be formic acid (HCOOH), quantified by NMR analysis. These observations confirmed that the complex Co-complex was a photoredox catalyst for the selective reduction of CO_2 to formic acid and H_2 (Table 4.1, Table 4.2). Control experiments highlighted the crucial role of the electron donor (TEOA) and demonstrated the photocatalytic effectiveness of the Co catalyst to be critically impaired when an electron donor of TEA was used and zero when CH_3CN was employed as a solvent.

Calculation details of TON, TOF, CS, and quantum yield are elaborated in chapters **2** and **3**.

Table 4.1. Summary of results for the photocatalytic CO_2 reduction with the Co-complex (**4**) in **DMA**. Irradiation with 450 nm light was conducted on the solution under a CO_2 atmosphere for 24 h. The electron donors used were triethanolamine (TEOA) and triethylamine (TEA).

$Ru(bpy)_3]^{2+}$ (mM)	Cat (4) (mM)	e-donor (1mL)	H_2 (µmol)	HCOOH (µmol)	TON_{H2}/ TOF_{H2}	TON_{HCOO}/ TON_{HCOOH}	(Φ%) $_{H2}$	(Φ%) $_{HCOOH}$	CS % $_{HCOOH}$
0.02	0	TEOA	41	63	410/ 17	630/ 26	1.4	2.1	61
0.02	0.002	TEOA	238	88	23800/ 991	8800/ 367	8.1	3	27
0.02	0.02	TEOA	331	105	3310/ 138	1050/ 44	11.3	3.6	24
0.02	0	TEA	0	46	0	460/ 19	0	1.6	100
0.02	0.02	TEA	0	79	0	790/ 33	0	2.7	100

Among the myriad conditions tested, the highest overall effectiveness was achieved using 0.002 mM catalyst (**4**) and TEOA as the electron donor, resulting in an optimum TON_{H_2} (23,800) and TOF_{H_2} (991 h^{-1}), with significantly enhanced H_2 production (238 µmol). Production of the H_2 and HCOOH in the absence of a catalyst is an outcome of $[Ru(bpy)_3]^{2+}$ acting simultaneously as a photosensitizer and photocatalyst for transforming CO_2 to the products H_2 and formic acid (HCOOH).[5] An increase in the concentration of the catalyst to 0.02 mM increases the overall product turnover, but at a penalty in site performance, indicating that higher catalyst concentrations are less efficient at turnover number. However, replacing TEOA with TEA abolishes hydrogen production and results in exclusive production of the formic acid analog HCOOH (CS = 100%), demonstrating significant product selectivity by the choice of electron donor in this photocatalytic system.[19]

Table 4.2. Summary of results for the photocatalytic CO_2 reduction with the Co-complex (**4**) in **CH_3CN**. Irradiation with 450 nm light was conducted on the solution under a CO_2 atmosphere for 24 h. The electron donors used were triethanolamine (TEOA) and triethylamine (TEA).

$[Ru(bpy)_3]^{2+}$ mM	Cat (**4**) (mM)	e-donor (1ml)	H_2 (µmol)	HCOOH (µmol)	TON_{H2}/ TOF_{H2}	TON_{HCOOH}/ TOF_{HCOOH}	(Φ%) $_{HCOOH}$	CS % $_{HCOOH}$
0.02	0	TEOA	20	44	200/ 8	440/ 18	1.5	69
0.02	0.02	TEOA	35	82	350/ 15	820/ 34	2.8	75
0.02	0	TEA	2	0	20/ 0.8	0	0	0
0.02	0.02	TEA	19	48	190/ 8	480/ 20	1.6	72

The photocatalytic results point to the crucial role of catalyst (**4**) in raising the efficiency of the reduction of CO_2. Experimental outcomes realized for reactions that were conducted in CH_3CN under illumination by light of wavelength 450 nm indicated that the addition of catalyst (**4**) strongly enhanced H_2 and HCOOH production compared to the control system, with concomitant enhancements of TON, TOF, quantum yield, and selectivity. Whilst TEOA was by far the best electron donor, TEA demonstrated markedly reduced activity, yielding only moderate product

amounts even in the presence of the addition of the catalyst. These results validate that the choice of cobalt catalyst and electron donor is of pivotal significance to attaining higher activity and selectivity for HCOOH synthesis.

4.5 Conclusion

The construction of earth-abundant, noble-metal-free catalysts and photosensitizers is still a primary challenge to the sustainable reduction of CO_2. Much has already been achieved, but further priority is required for optimization of quantum yields, assessments of excited-state redox attributes, and utilization of greener sacrificial donors. In this work, we demonstrated for the first time that a Co complex is an extremely efficient and selective homogeneous photocatalyst for the conversion of CO_2 to HCOOH and present a possible route to economic and practical photocatalytic systems. The future direction will be to design new first-row metal complexes to further improve the photocatalytic reduction of useful products from CO_2.

In summary, we introduced here a photocatalytic system of noble metal-free reduction of CO_2 utilizing $[Ru(bpy)_3]^{2+}$ as the photosensitizer, $[Co\{\kappa^2\text{-}(iPr_2PNMe)NC_5H_4\}(Br)_2]$ (**4**) as the photocatalyst, and TEOA as the electron donor. The system was remarkably active, achieving a turnover number (TON) of 1050 in DMA/TEOA (4:1, v/v) and 820 in CH_3CN/TEOA, thus emphasizing its efficacy in the photoreduction of CO_2 to HCOOH. Although definitive structural characterization of complex 4 was limited due to its paramagnetic nature, sensitivity to air, and failed attempts at crystallographic determination, UV–Vis spectroscopy indeed verified features typical of Co (II) complexes. Notably, photocatalytic activity was clearly observed, thus qualifying this complex (**4**) photocatalyst for the photoreduction of CO_2 despite its lack of electrocatalytic activity under test conditions. Future studies should be focused on stabilizing the Co (II) center, collecting crystallographic data, and extending the examination of its photochemical as well as electrochemical behavior.

4.6 References

1. Riplinger, C.; Carter, E. A. Influence of Weak Brønsted Acids on Electrocatalytic CO_2 Reduction by Manganese and Rhenium Bipyridine Catalysts. *ACS Catal.* **2015**, *5* (2), 900–908.

2. Aresta, M.; Dibenedetto, A.; Angelini, A. Catalysis for the Valorization of Exhaust Carbon: From CO_2 to Chemicals, Materials, and Fuels. Technological Use of CO_2. *Chem. Rev.* **2014**, *114* (3), 1709–1742.

3. Guo, Z.; Cheng, S.; Cometto, C.; Anxolabéhère-Mallart, É.; Ng, S.-M.; Ko, C.-C.; Liu, G.; Chen, L.; Robert, M.; Lau, T.-C. Highly Efficient and Selective Photocatalytic CO_2 Reduction by Iron and Cobalt Quaterpyridine Complexes. *J. Am. Chem. Soc.* **2016**, *138* (30), 9413–9416.

4. Chen, W.; Filot, I. A. W.; Pestman, R.; Hensen, E. J. M. Mechanism of Cobalt-Catalyzed CO Hydrogenation: 2. Fischer–Tropsch Synthesis. *ACS Catal.* **2017**, *7* (12), 8061–8071.

5. Hawecker, J.; Lehn, J.-M.; Ziessel, R. Efficient Photochemical Reduction of CO_2 to CO by Visible Light Irradiation of Systems Containing $Re(bipy)(CO)_3X$ or $Ru(bipy)_3^{2+}$–Co^{2+} Combinations as Homogeneous Catalysts. *J. Chem. Soc., Chem. Commun.* **1983**, 536–538.

6. Takeda, H.; Koike, K.; Inoue, H.; Ishitani, O. Development of an Efficient Photocatalytic System for CO_2 Reduction Using Rhenium(I) Complexes Based on Mechanistic Studies. *J. Am. Chem. Soc.* **2008**, *130* (6), 2023–2031.

7. Takeda, H.; Ishitani, O. Development of Efficient Photocatalytic Systems for CO_2 Reduction Using Mononuclear and Multinuclear Metal Complexes Based on Mechanistic Studies. *Coord. Chem. Rev.* **2010**, *254* (3–4), 346–354.

8. Kuramochi, Y.; Ishitani, O.; Ishida, H. Reaction Mechanisms of Catalytic Photochemical CO_2 Reduction Using Re(I) and Ru(II) Complexes. *Coord. Chem. Rev.* **2018**, *373*, 333–356.

9. Ishida, H.; Terada, T.; Tanaka, K.; Tanaka, T. Photochemical Carbon Dioxide Reduction Catalyzed by Bis(2,2′-bipyridine) dicarbonylruthenium(2+) Using Triethanolamine and 1-Benzyl-1,4-dihydronicotinamide as an Electron Donor. *Inorg. Chem.* **1990**, *29* (5), 905–911.

10. Fisher, B. J.; Eisenberg, R. Electrocatalytic Reduction of Carbon Dioxide by Using Macrocycles of Nickel and Cobalt. *J. Am. Chem. Soc.* **1980**, *102* (24), 7361–7363.

11. Lehn, J.-M.; Ziessel, R. Photochemical Generation of Carbon Monoxide and Hydrogen by Reduction of Carbon Dioxide and Water under Visible Light Irradiation. *Proc. Natl. Acad. Sci. U.S.A.* **1982**, *79* (2), 701–704.

12. Takeda, H.; Cometto, C.; Ishitani, O.; Robert, M. Electrons, Photons, Protons and Earth-Abundant Metal Complexes for Molecular Catalysis of CO_2 Reduction. *ACS Catal.* **2017**, *7* (1), 70–88.

13. Beley, M.; Collin, J.-P.; Ruppert, R.; Sauvage, J.-P. Electrocatalytic Reduction of Carbon Dioxide by Nickel Cyclam^{2+} in Water: Study of the Factors Affecting the Efficiency and the Selectivity of the Process. *J. Am. Chem. Soc.* **1986**, *108* (24), 7461–7467.

14. Yamazaki, Y.; Takeda, H.; Ishitani, O. Photocatalytic Reduction of CO_2 Using Metal Complexes. *J. Photochem. Photobiol. C: Photochem. Rev.* **2015**, *25*, 106–137.

15. Takeda, H.; Koizumi, H.; Okamoto, K.; Ishitani, O. Photocatalytic CO_2 Reduction Using a Mn Complex as a Catalyst. *Chem. Commun.* **2014**, *50* (12), 1491–1493.

16. Torralba-Peñalver, E.; Luo, Y.; Compain, J.-D.; Chardon-Noblat, S.; Fabre, B. Selective Catalytic Electroreduction of CO_2 at Silicon Nanowires (SiNWs) Photocathodes Using Non-Noble Metal-Based Manganese Carbonyl Bipyridyl Molecular Catalysts in Solution and Grafted onto SiNWs. *ACS Catal.* **2015**, *5* (10), 6138–6147.

17. Ouyang, T.; Huang, H.-H.; Wang, J.-W.; Zhong, D.-C.; Lu, T.-B. A Dinuclear Cobalt Cryptate as a Homogeneous Photocatalyst for Highly Selective and Efficient Visible-Light Driven CO_2 Reduction to CO in CH_3CN/H_2O Solution. *J. Am. Chem. Soc.* **2015**, *137* (46), 14870–14873.

18. Ḥamīd, Y. *Exploring New Catalysts for Photocatalytic Carbon Dioxide Reduction Using Homogeneous Transition Metal Complexes*; Ph.D. Thesis, University of Ottawa, Department of Chemistry: Ottawa, 2019.

19. Ouyang, T.; Huang, H.-H.; Wang, J.-W.; Zhong, D.-C.; Lu, T.-B. A Dinuclear Cobalt Cryptate as a Homogeneous Photocatalyst for Highly Selective and Efficient Visible-Light Driven CO_2 Reduction to CO in CH_3CN/H_2O Solution. *Angew. Chem., Int. Ed.* **2017**, *56* (3), 738–743.

Chapter 5: Conclusion and Future Work

5.1 Conclusion

This study investigated the photocatalytic reduction of CO_2 using ruthenium catalysts containing bidentate phosphinoaminopyridine ligands. Chapter **1** provides the background of the introduction on photocatalytic CO_2 reduction, including examples of varied catalysts, electron donors, and solvents that were efficient for reducing CO_2.

New Ru-based catalysts have been prepared, characterized, and studied for the CO_2 reduction under photocatalytic conditions in Chapter **2**, and more work needs to be done on the electrochemical behavior of the two catalysts in order to totally characterize these new compounds. All of the catalysts exhibited good TON and good selectivity. Although varying levels of success have been seen, most of the catalysts in this thesis exhibit their potential towards the photocatalytic CO_2 reduction. Although these two new Ru catalysts exhibited good selectivity and good Φ%. These findings are significant in the sense that they also show the effect that varying ligand substituents have on the catalytic reactivity. Comparing the two catalysts, the best catalyst has R= H and R'= phenyl and produces formic acid with a higher TON than the second catalyst, which has R= CH_3 and R'= phenyl. It is partly due to the electron-donating capability of the R groups that this activity is seen. When R is a methyl R group, it is more electron-donating than R= H, thus putting more electron density on the ligand and on the metal. The increased electron density may make the catalyst harder to reduce, thus lowering the resulting TON of the catalyst with the R=CH_3 R substituent.

In Chapter **3**, the ligand [PNMe(iPr)], presented as $([(CH_3)_2CH]_2P)NMe(NC_5H_4)$, was successfully utilized as a supporting ligand for catalysts involved in carbon dioxide reduction. The third new ruthenium catalyst was successful under a suite of photocatalytic tests. Additionally, since some of these catalysts produce hydrogen (H_2) among their byproducts while reducing CO_2, examining these catalysts for future application in water splitting for the creation of H_2 is important. Studies on water splitting, which was undertaken concurrently with CO_2 reduction in Chapter **3**, generated spectacular findings on the creation of hydrogen from water. All three ruthenium catalysts demonstrated superior turnover number (TON) and formic acid (HCOOH) selectivity. There was also a change in R and R' substituents of the phosphinoaminopyridine ligands, and it was found that these altered the level of activity of the catalysts. These findings are promising since they

indicate that deviation from standard diimine ligand backbones generates extremely selective photoreduction catalysts of respectable TONs.

In Chapter **4**, I proceeded further and introduced divalent first-row transition metal catalysts, wherein cobalt would be a potentially most promising candidate toward CO_2 reduction. Towards this, a cobalt (II) complex, synthesized from the ligand ($[(CH_3)_2CH]_2P)NMe(NC_5H_4$), was then characterized and utilized in the CO_2 reduction reaction. Briefly, the Co complex is a highly efficient and selective molecular photocatalyst for reducing CO_2 into HCOOH. While the catalyst exhibits remarkable selectivity for the formation of HCOOH over H_2 evolution, further detailed mechanistic studies of the important intermediates will be required for a comprehensive understanding of the processes of the catalysis. Other syntheses of longer-life photosensitizers will facilitate the enhancement of the long-time stability and efficiencies of this system, but they remain waiting for more experiments to document their electrocatalytic ability toward CO_2 reduction.

5.1 Future Work

This thesis presents four new catalysts for the photocatalytic reduction of carbon dioxide, each in support of different ligands. Further research to be conducted within this project encompasses an analysis of the electrochemical characteristics of these four catalysts to provide complete characterization, the identification of the crystal structure of one of these catalysts, and DFT calculations to be carried out. Prospective research would, therefore, include the re-synthesis of some catalysts under different methodologies to reach an appropriate catalyst. Practical initiatives include the introduction of support substituents onto both phosphorus and nitrogen in the phosphonaminopyridine ligand, which would enable us to better understand the role of these substituents in photocatalytic activity. The investigation of different photosensitizers and new electron donors also features in future research proposals. Future studies should include an investigation of these catalysts' efficiencies in water splitting, considering most of these catalysts pump out H_2 as a byproduct in reaching an equilibrium in the reduction process of CO_2. Evaluation of their activity in direct H_2 production from H_2O could provide valuable information regarding potential wider roles in solar fuel production. Additionally, exploration of more accessible earth-abundant first-row transition metal catalysts (e.g., Fe, Co, and Ni), which can be less costly than noble metal catalysts, also features as another focus of future research.

From an experimental outlook, reactor design and irradiation conditions are factors that may improve reproducibility and accuracy in future studies of CO_2 reduction through photocatalytic reactions. For sources, larger or flat-bottomed reaction vessels would guarantee a more homogeneous light distribution and efficient CO_2 diffusion; a punched photoreactor or collimated light would offer better control of photon flux as calibrated. Shorter or intermittent irradiation was desirable to follow the kinetics of the reaction and the photodegradation of the photocatalyst, and direct measurements of the light intensity in the reaction vials were shown to be better for accurate photon flux determination. Under such conditions, systematic errors could be greatly reduced, and the evaluation of CO_2 photocatalytic reduction efficiency would be both more uniform and accurate.